Modeling and Optimization of a Standalone Photovoltaic System supplying an alternative Load

Yassine Chaibi

جامعة مولاي إسماعيل
UNIVERSITÉ MOULAY ISMAÏL

ENSAM
المدرسة الوطنية العليا للفنون و المهن
ÉCOLE NATIONALE SUPÉRIEURE D'ARTS ET MÉTIERS

Université Moulay Ismail
Ecole Nationale Supérieure d'Arts et Métiers, Meknès

Centre d'études doctorales
Recherche et innovation pour les sciences de l'ingénieur

THESE

Présentée et soutenue le 10 Juillet 2019
pour l'obtention du Diplôme de

DOCTORAT

Discipline : **Sciences de l'ingénieur**
Spécialité : **Génie Électrique et Énergies Renouvelables**

Par :

CHAIBI Yassine

Titre :

Modeling and Optimization of a Standalone Photovoltaic System supplying an alternative Load

AL MARS Ahmed	PES, ENSAM/UMI/Meknès	Président
ECHCHATBI Abdelwahed	PES, FST/UH1/Settat	Rapporteur
ELGOURI Rachid	PH, ENSAK/UIT/Kénitra	Rapporteur
BROURI Adil	PH, ENSAM/UMI/Meknès	Rapporteur
TISSIR El Houssaine	PES, FSDM/USMBA/Fès	Examinateur
SALHI Mohamed	PH, ENSAM/UMI/Meknès	Directeur de thèse
EL JOUNI Abdeslam	PH, CRMEF/UAE/Tanger	Co-directeur de thèse
CHOUDER Aissa	HDR, FT/UMB/M'Sila - Algérie	Invité

To my beloved parents Abdellah, Drissia and Assia

To my sisters Sarra, Fatima Zahrae and Khansae

Abstract

In this thesis, two efficient control strategies are proposed to optimize the performances of a single-phase double stage standalone Photovoltaic (PV) system. The first controller allows tracking instantly the maximum power point (MPP) of the PV module regarding any sudden change of atmospheric conditions. Furthermore, the second control strategy consists of forcing the output current of the inverter to follow a generated reference. Thanks to its advantages, Both control strategies are based on the sliding mode approach due to its accuracy and robustness under external perturbations. Accordingly, the developed controllers require the availability of a high-quality database that describes the standalone PV system behavior under the different variations of climate condition. To deal with this concern, a MATLAB simulation is developed to elaborate a trusted standalone PV system. This latter requires the use of a PV module to supply two converters in order to feed a resistive load with an alternative current. The PV panel modelling necessitates the use of the electrical parameters of the equivalent-circuit model. For this, an efficient and simple strategy based on the shunt resistance measure and the datasheet manufacturer is developed to extract the single-diode model (SDM) parameters. Finally, the SDM identified parameters are implemented in the PV module to build the standalone PV system. The efficiency of the developed controllers is assessed by simulation under different climate variations.

Keywords: Photovoltaic module; Standalone PV system; maximum power point; DC to DC converter; Inverter; Single-diode model.

Résumé

Dans cette thèse, deux stratégies de contrôle efficaces sont proposées pour optimiser les performances d'un système photovoltaïque (PV) monophasé à double étage. Le premier contrôleur permet de suivre instantanément le point de puissance maximale (PPM) du module PV indépendamment de tout changement brusque des conditions atmosphériques. De plus, la deuxième stratégie de contrôle consiste à forcer le courant de sortie de l'onduleur à suivre une référence générée. Grâce à ses avantages, les deux stratégies de contrôle sont basées sur l'approche des modes glissants en raison de sa précision et de sa robustesse face aux perturbations externes. En conséquence, les contrôleurs développés nécessitent la disponibilité d'une base de données de haute qualité décrivant le comportement du système PV autonome en fonction des différentes variations des conditions climatiques. Pour résoudre ce problème, une simulation MATLAB est développée afin d'élaborer un système PV autonome fiable. Cette dernière nécessite l'utilisation d'un module PV pour alimenter une charge résistive alternative via deux convertisseurs DC/DC et DC/AC. La modélisation du panneau photovoltaïque nécessite la détermination des paramètres électriques du modèle de circuit équivalent. Pour cela, une méthode simple et efficace basée sur la mesure de la résistance shunt et les données du fabricant est développée pour extraire les paramètres du modèle à une seule diode (MSD). Enfin, les paramètres identifiés du MSD sont implémentés dans le module PV pour construire le système PV autonome. L'efficacité des contrôleurs développés est évaluée par simulation sous différentes variations climatiques.

Mots-clés : Module photovoltaïque; Système PV autonome; point de puissance maximale; Convertisseur continu-continu; Onduleur; Modèle à une seule diode;

Acknowledgements

In the name of ***ALLAH***, the Most Gracious and the Most Merciful; and prayers and peace be upon ***Mohamed*** His servant and messenger.

First and foremost, I should acknowledge my infinite thanks to ***ALLAH*** for giving me opportunity, guidance and strength to accomplish this thesis.

This project has been elaborated the **National School of Arts and Crafts of Meknes** at **Moulay Ismail University**, and it took us nearly five years of hard and continuous work. It was an unforgettable period in which I have made very precious relationships with several inspired, supportive and kindly persons. Without them, this project would not have been established.

Firstly, I would like to express my deepest thanks to my thesis supervisors, Professor ***Mohamed SALHI*** and Professor ***Abdeslam EL-JOUNI***, who gave me the great support during the elaboration of this project. I am sincerely grateful for their presence in my side at times of doubts, for their valuable pieces of advice, help and support.

My deepest gratitude is also addressed to the reading committee members: Professor ***AL MARS Ahmed***, Professor ***ECHCHATBI Abdelwahed***, Professor ***ELGOURI Rachid,*** Professor ***BROURI Adil*** Professor ***TISSIR El Houssaine*** for their extremely precious comments and suggestions.

Also, I should thank my best friends: ***Mohammed EL MBARKI***, ***Amine BASSLI***, ***Zakariae EL-IDRISSI***, ***Saad MOTAHHIR*** and ***Mohamed Amine RAZZOUK*** for their friendship, sympathy and support. My dear friends, I will never forget our memories.

At the end, I would like to express my very grateful gratitude to my parents ***Abdellah***, ***Drissia*** and ***Assia***, to my sisters ***Sarra***, ***Fatima zahrae***, and ***Khansae*** for all sacrifices and patience they ever made so that I succeed in my life.

Yassine CHAIBI

10/07/2019

List of symbols

$\mathbf{A_m}$	module surface [m^2]
$\mathbf{C, C_i}$	input capacitor of the DC-DC converter [F]
$\mathbf{C_o, C_{DC}}$	output capacitor of the DC-DC converter [F]
$\mathbf{E_{GO}}$	band gap [=1.22 eV]
$\mathbf{E_{pv}}$	produced energy [Wh]
$\mathbf{I, I_{pv}}$	output current of the PV module [A]
$\mathbf{I_{sol}}$	light-generated current [A]
$\mathbf{I_D}$	current of the diode [A]
$\mathbf{I_{pvg}}$	current of the PV generator [A]
$\mathbf{I_{Rsh}}$	current following in shunt resistance [A]
$\mathbf{I_{os}}$	cell saturation current [A]
$\mathbf{I_{or}}$	reverse current of the cell [A]
$\mathbf{I_{sc}}$	short-circuit current [A]
$\mathbf{i_L}$	input current of the boost converter [A]
$\mathbf{i_o}$	output current of the inverter [A]
$\mathbf{I_{ref}}$	reference current [A]
$\mathbf{I_m}$	maximal current at optimal operating point [A]
$\mathbf{k}$	Boltzmann constant [1.381 10^{-23} J/K]
$\mathbf{K_i}$	temperature coefficient of I_{sc} [A/K]
$\mathbf{K_v}$	temperature coefficient of V_{oc} [V/K]
$\mathbf{L}$	input inductance of the DC-DC converter [H]
$\mathbf{L_o}$	inductance of the output filter [H]
$\mathbf{N_{cell}}$	number of cells in series
$\mathbf{N_s}$	the number of modules in series
$\mathbf{N_p}$	the number of modules in parallel
$\mathbf{P_{MPP}}$	maximum power of the PV module [W]
$\mathbf{q}$	electron charge [=1.602 10^{-19} C]
$\mathbf{R_c}$	load resistance [Ω]
$\mathbf{R_o}$	resistance of the output filter [Ω]
$\mathbf{R_s}$	series resistance [Ω]
$\mathbf{R_{sh}}$	shunt resistance [Ω]
$\mathbf{T_a}$	ambiant temperature [K]

$\mathbf{T, T_{cell}}$	cell temperature [K]
$\mathbf{T_{NOCT}}$	the nominal operating cell temperature [K]
$\mathbf{T_r}$	reference temperatures [K]
$\mathbf{V_{1,2}}$	Lyapunov function
$\mathbf{V_m}$	maximum voltage of the PV module [V]
$\mathbf{V_{oc}}$	open-circuit voltage [V]
$\mathbf{v_{DC}}$	output-voltage of the boost converter [V]
$\mathbf{V, V_{pv}}$	output voltage of the PV module [V]
$\mathbf{v_w}$	wind velocity [m/s]

List of Greek letters

$\boldsymbol{\alpha\tau}$	the transmittance-absorbance product
$\boldsymbol{\gamma}$	ideality factor
$\boldsymbol{\omega}$	the pulsation [rad/s]
$\boldsymbol{\lambda}$	solar irradiances [W/m^2]
$\boldsymbol{\lambda_{ref}}$	reference solar irradiances [= 1000 W/m^2]
$\boldsymbol{\sigma}$	sliding surface
$\boldsymbol{\eta}$	module efficiency
$\boldsymbol{\eta_{ref}}$	reference module efficiency

List of Abbreviations

AC: alternative current

DC: direct current

DDM: double-diode model

IC: incremental conductance

MPP: maximum power point

MPPT: maximum power point tracking

NOCT: normal operating condition test

P&O: perturb and observe

PI: proportional integrator

PV: photovoltaic

SDM: single-diode model

SMC: sliding mode control

STC: standard test conditions

THD: total harmonic distortion

List of Figures

List of Tables

Table of Contents

General introduction

Due to the increasing fuel prices and related environmental concerns, renewable energies become an important source to supply electricity to the buildings and industrial sectors. Power generation from these sources possesses many outcomes such as clean and limitless behavior. Wind, hydro, geothermal and solar energies have been available since the birth of our planet and have been used by the first human generation in different ways. Nowadays, the exploitation of these energies knows a remarkable improvement taking profit from the accelerated technological advances. Solar energy is considered among the fast-developing technologies and experiences a considerable drop in equipment costs. More specifically, photovoltaic-based power source has already proved its merit when used in grid-connected and stand-alone systems. In addition, it is considered as one of the promising solutions for solving greenhouse gas emissions problems. Thus, its eco-friendly nature, abundance and the continuous cost decreasing have given additional advantages that motivated its worldwide deployment. Despite the inherent advantages of the photovoltaic power generation, the information provided by several specialized agencies on deployed PV plants indicates that several factors can affect the overall performance of the installed photovoltaic systems.

Due to the nonlinearity of the current-voltage (I-V) characteristic of the photovoltaic (PV) module, accurate modeling and optimization of the PV panel are substantial in order to improve the conversion chain efficiency. For this reason, maximum power point tracking (MPPT) algorithms have been developed using different approaches. These techniques allow the tracking of the maximum power point (MPP) regarding the variation of solar irradiance and temperature. In the literature, we found many published works about MPPT techniques, each one differs based on many aspects such as the complexity degree, the number of sensors required, the cost and the tracking efficiency. For these reasons, the choice of adequate MPPT is related to the field of applications and must represent a good balance between the efficiency and the cost.

In the last decades, the use of MPPT controllers has known an important growth in grid-connected and standalone PV systems. However, most of the PV installations are dedicated to grid-connected, which makes the application of standalone PV systems neglected despite its important role in feeding isolated areas where the grid utility is unavailable. Accordingly, the main objective of this thesis is to model and optimize a standalone PV system that could be very useful for different utilizations such us underground car parks, the cellar of a hospital and

of course the isolated sites. Thus, a control unit of the proposed standalone PV system is mainly composed of two controllers:

The first controller consists in achieving the maximum power point of the PV module with a high level of accuracy regarding the weather conditions variations (solar irradiance and temperature) that affects the nonlinearly the I-V output characteristic, resulting a permanent change in the locus of the MPP, which makes its tracking very hard. For these reasons, the proposed MPPT technique must respect the conditions of robustness and accuracy.

The second controller ensures feeding a sinusoidal output current of high quality to supply the AC load. This current must respect the requirements imposed by standards. Because it is necessary to have low levels of Total Harmonic Distortion (THD) at the inverter output.

To achieve the objectives of this thesis, good modeling and simulation of the standalone PV system are required. For this, an accurate process of PV panel modeling is adopted. accordingly, parameters extraction of the PV cell equivalent circuit model has been established in order to have a simulated PV generator that reflects the same results as the real one. Then, the developed PV module is used with a boost DC to DC converter and an inverter to build the conversion chain of the proposed standalone PV system.

This thesis is organized as follows:

Chapter 1: This chapter deals with the different topologies used in PV systems applications. In addition, the Objectives, the contributions and the organizations of this thesis are presented in this chapter.

Chapter 2: In this chapter, a modelling of the PV panel is discussed. Thus, section 2.2 is dedicated to a parameters extraction process. Section 2.3 gives a performances analysis of the different PV cell equivalent circuit models according to the climate variation.

Chapter 3: This chapter focuses on an evaluation of various MPPT technique. A review of diverse MPPT methods is presented in section 3.2, followed by the modelling and the examined MPPT techniques in section 3.3 and 3.4 respectively. Finally, section 3.5 gives the results and discussion.

Chapter 4: This chapter presents the modelling and control of a standalone PV system. The mathematical modeling of the proposed PV system is discussed in section 4.3. then, the used controllers are presented in section 4.4 and 4.5. Finlay, the results and discussion.

Appendix A: This appendix contains the manufacturer datasheets of the different PV modules used in this thesis.

Appendix B: This appendix presents the extracted (from datasheet) and the calculated values of short-circuit current, open-circuit voltage and maximum power.

Appendix C: This appendix gives the calculated values of different time derivatives of the PV current equation.

CHAPTER1 : Photovoltaic System Topologies

1.1 Introduction

In the last decades, according to statistic (BP, 2017), the world energy need exhibits a rapid growth, which caused a huge production of electricity with different polluting sources as natural gas, oil and coal (Kousksou et al., 2015). Nowadays, the excessive use of these fossil sources has a negative effect on both economic and environmental point of views. In fact, the economic consequence is presented by the high increase in petroleum's price which leads directly to a rise of the electricity tariff. For the environmental impact, the emission of CO_2 accentuating the damaging effects of climate change remains the major issue (Kumar and Kandpal, 2005; Sadorsky, 2009). In order to overcome these complications, leader countries in energy production have imposed a new policy that encourages the use of renewable energies due to its clean behavior and limitless quantity (Ellabban et al., 2014).

Today, diverse renewable energy sources are developed, such as solar, wind, hydro and geothermal. Due to their huge potential, these sources of energy are being used increasingly in industrial and buildings sectors. Solar energy at the top of renewable energy sources is believed to cover a significant part of energy needs in several countries. More specifically, photovoltaic systems due to their simple implementation and low maintenance cost (Kumar and Kandpal, 2005), can provide clean and sustainable electricity. Power generated from photovoltaic modules can be used in grid-connected and stand-alone systems (Kaundinya et al., 2009). Grid-connected PV systems are developed to operate with the electric utility grid and offer the possibility of covering energy requirements of the structure with the capability of selling the rest of produced energy to electricity supplier (Del Fabbro et al., 2016; Kumar and Kandpal, 2005). Stand-alone PV systems, in turn, are used to supply the electricity needed in isolated sites and as well for agricultural pumping (Yahyaoui, n.d.), these systems require a battery bank to provide electricity overnight (Iaquaniello et al., 2017; Muhsen et al., 2018). Both PV systems are employed widely in the literature by using various topologies. In this chapter, these topologies are classified according to the number of power converter stages.

1.2 Single-Phase PV Systems

Single-phase PV systems become an important solution to supply electricity to low energy consumer (until 5 kW) (Hassaine et al., 2014; Zeb et al., 2018). these systems are used in various applications such as in residential and agricultural area. The main advantages of these systems are the implementation simplicity and low maintenance cost which makes it preferable compared to other systems of renewable energy (Wind energy, thermal energy etc.…). Thus,

according to the type of the supplied load, the single-phase PV systems topologies are categorized into two types:

(i) Single-stage PV systems,

(ii) Double-stage PV systems.

1.2.1 Single-Stage: DC to AC converters

Because most of the utilities are alternative, the use of a DC to AC converters (Inverters) becomes substantial to ensure transferring energy from the PV array to the AC utility. Thus, these inverters could be useful to make a direct link between the PV panels and the AC utility in order to supply an AC load or to inject an alternative current into the grid as shown in Figure 1.1.

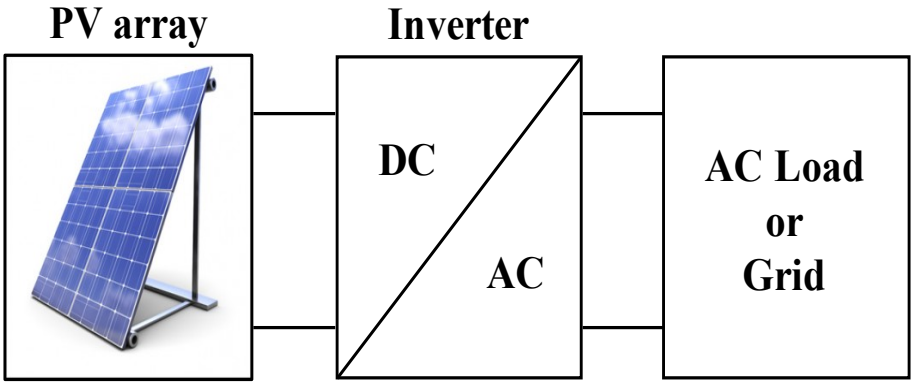

Figure 1. 1 Single-phase PV system with DC-AC inverter.

Due to Statistics in (Hassaine et al., 2014; Zeb et al., 2018), The grid-connected PV systems are the most used solution in PV application. Accordingly, the conversion of the DC component coming from the PV panels to an AC one becomes an obligation. Thus, many authors have used the topology in Figure 1.1. Jain et al. and Caceres et al. have proposed a single stage inverter with a voltage boosting capability (Cáceres and Barbi, 1999; Jain et al., 2007). The proposed solution exhibits good performances in terms of conversion quality and feeding the current into the grid. Moreover, Kim et al. have used the conventional topology of the inverter to inject a current with a low THD into the grid (Kim, 2007). Most of the reported works on the single-phase inverter claim that this topology exhibits simplicity and a good control of the current (Zeb et al., 2018). However, this configuration suffers from a low range DC voltage which reduced the power quality (Zeb et al., 2018). For this reason, the use of a double stage is recommended.

1.2.2 Double Stages

To achieve high level of accuracy in photovoltaic utilizations, conditions of high efficiency and good conversion quality are required. As reported in the previous sections, the single stage

of conversion cannot satisfy both conditions in all ranges of power. Accordingly, the double stage topology in Figure 1.2 is adopted. This latter consists of two stages of conversion, generally a DC-DC converter followed by an inverter. The structure of this topology differs according to the power rating (Ankit et al., 2018; Zeb et al., 2018).

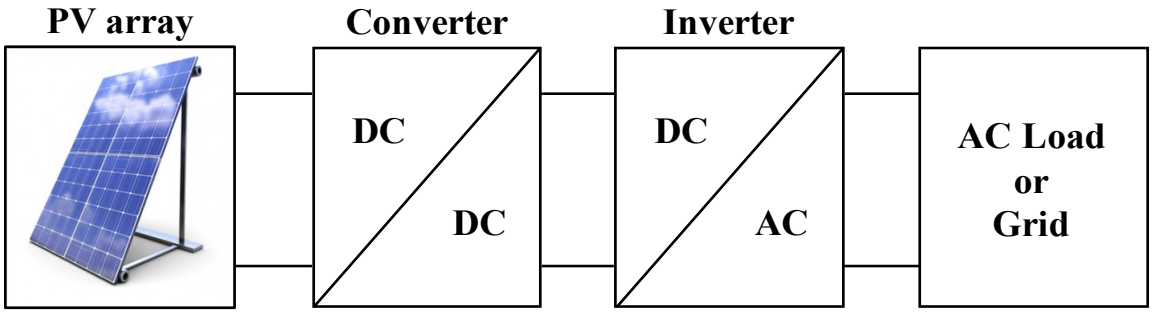

Figure 1. 2 Single-phase double stage PV system.

The reason behind transferring a regulated voltage to the input of the inverter requires the use of DC to DC converters, this topology as presented in Figure 1.2 is used widely in various applications such as pumping systems and energy storage (El-jouni, 2009; Muhsen et al., 2018; Yatimi and Aroudam, 2016). To ensure these functions, diverse type of DC-DC converters are performed between the PV module and the load. The main advantages of these converters are the cost-effectiveness, the energy flow and the ability to maintain the output at a fixed value regarding the input variations (Reshma Gopi and Sreejith, 2018). In the literature, various types of DC-DC converters have been proposed for diverse applications.

1.2.2.1 DC to DC Converters

a) Boost Converter

The boost converter is a type of DC-DC converters which allows providing an output voltage greater than the input one, and due to the conservation law of energy, the input power of the boost converter must be equal to the output, which means that the current at the output of the boost is less the input one. In PV applications, this type of converters is used widely because of its advantages of high efficiency and simplicity of implementation.

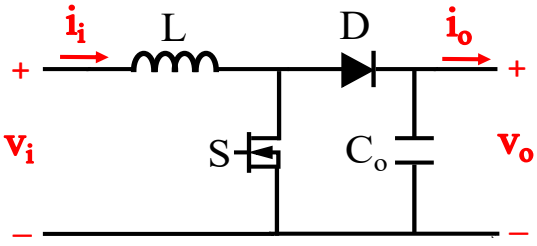

Figure 1. 3 DC-DC boost converter.

The scheme in Figure 1.3 represents the conventional configuration of boost converters. This topology is utilized by various authors in different PV applications. Accordingly, El-Jouni et al. used a boost converter in order to increase the providing voltage from the PV panel (El-jouni, 2009), the increased voltage at the boost output supplied a motor-pump group, the obtained results demonstrate high performance. As another function of the boost converter, is to supply a DC load such as a battery, Yatimi et al. and Guisser et al. used the DC boost converter to upgrade the output voltage to the level of the battery voltage (Par et al., 2014; Yatimi and Aroudam, 2016). Furthermore, other authors performed modifications on the conventional topology in Figure 1.3 in order to improve the boost performances. as reported in (Veerachary et al., 2003), Veerachary et al. proposed an improved version of the conventional boost. This modification is ensured by using a coupled-inductor interleaved to the boost converter, this latter has reduced the switching losses and minimizes the current ripples at the input and the output of the boost converter (Veerachary et al., 2003).

b) Buck Converter

Contrary to the boost converter, the buck provides an output voltage lower than the input one, and according to the conservation law of energy, the buck output current is greater than the input current. The reason behind using the buck converter is the same as all DC to DC converters, but with a lower output voltage compared to the input. For this, various authors have used the buck topology in Figure 1.4 as a solution to regulate this voltage according to the load needs. As reported in (Chew and Siek, 2010), Chew et al. proposed a quad input buck converter to provide a regulated voltage to the battery and the DC load. This developed configuration demonstrates a cost-effective solution by reducing the component count. On the other hand, Mazouz et al. used the buck converter to provide maximum DC power to the group motor-pump, the performance shows that the experimental results were very satisfactory compared to the simulated ones (Mazouz and Midoun, 2011).

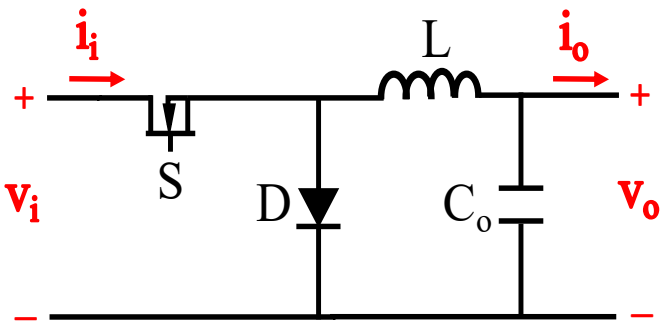

Figure 1. 4 Buck DC-DC converter.

In order to improve the Buck converter performances, diverse modifications have been conducted on the conventional topology (see Figure 1.4). Hence, Zhang et al. proposed to variate the input inductance to adopt the optimal operating of the system according to solar irradiance variations. As a result, this topology reduces the inductance size to 25% and allows the output current continuous regarding the solar irradiance variations (Zhang et al., 2011).

c) Buck-Boost Converter

To ensure both functions of increasing and decreasing the output voltage of DC-DC converters, the buck-boost in Figure 1.5 is adopted. This main idea of this later is to operate with two modes of control by cascading both the boost and the buck converter. In the literature, the evolution of this type of converters has known a remarkable growth in the last decades. Thus, divers improved topologies have been developed in order to increase the performances of the buck-boost converters.

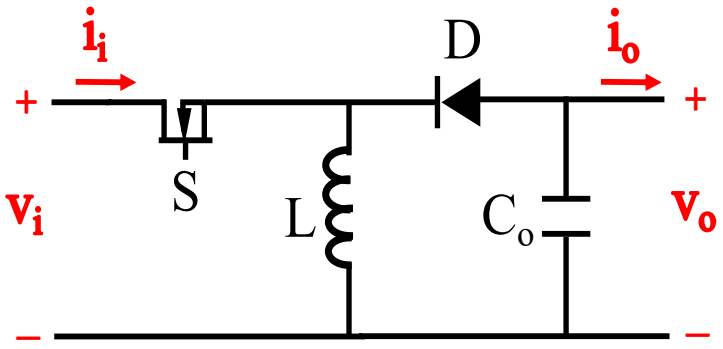

Figure 1. 5 Buck-Boost DC-DC converter.

In (Orellana et al., 2010), Orellana et al. developed a four switch buck-boost converter. This solution is based on the fact of using four switches instead of the usual two switches. The results have been verified experimentally and shown that the proposed topology exhibits high performances and could be suitable for some PV applications (Orellana et al., 2010). Moreover, Sahu et al. proposed a noninverting buck-boost converter dedicated to low voltage uses. The proposed configuration was adopted to supply a battery characterized by its low voltage. The performances of this topology have been verified experimentally and demonstrate the accuracy of this solution.

d) Other DC-DC Converters

In the literature, other DC-DC converters topologies have been adopted in PV systems according to the area of application. As the most used one, we found Cuk, SEPIC and Zeta converters. Cuk converter has the same function as the buck-boost converter but its implementation is more complicated. However, the advantage of this type of converter is to

provide a continuous current at the input and the output (Reshma Gopi and Sreejith, 2018). Also, SEPIC and Zeta converters allow providing an output voltage greater or less than the input voltage. The difference between these converters and the buck-boost is that the output voltage is non-inverted (G and Singh, 2017). In addition, the complexity of these converters is high compared to the boost and the buck converters, which makes these latter widely used in PV applications.

1.3 Three-phase PV Systems

Three-phase PV systems are described by the number of phases at the output of the inverter. As reported in the previous section, the single-phase PV systems are used only in low ranges of power (Fang Lin Luo and Hong Ye, 2013; Hassaine et al., 2014). Thus, for high scale of power and especially in the grid-connected uses, the three-phase inverters are required.

1.4 Objectives and Contributions of this Thesis

1.4.1 Presentation and Objective of the proposed PV system

This thesis deals with the modeling of a simple and robust maximum power point tracking (MPPT) technique for standalone photovoltaic systems in order to supply an alternative load. The standalone PV system in Figure 1.6 could be very useful to cover the need for electricity in different applications such as underground parking and in isolated sites. For this reason, the proposed configuration in Figure 1.6 ensures a transfer of energy from the DC side to the alternative load. This topology consists of a PV panel followed by a boost DC to DC converter in order to increase the PV voltage to the desired value and finally an inverter to convert the DC input to an alternative one.

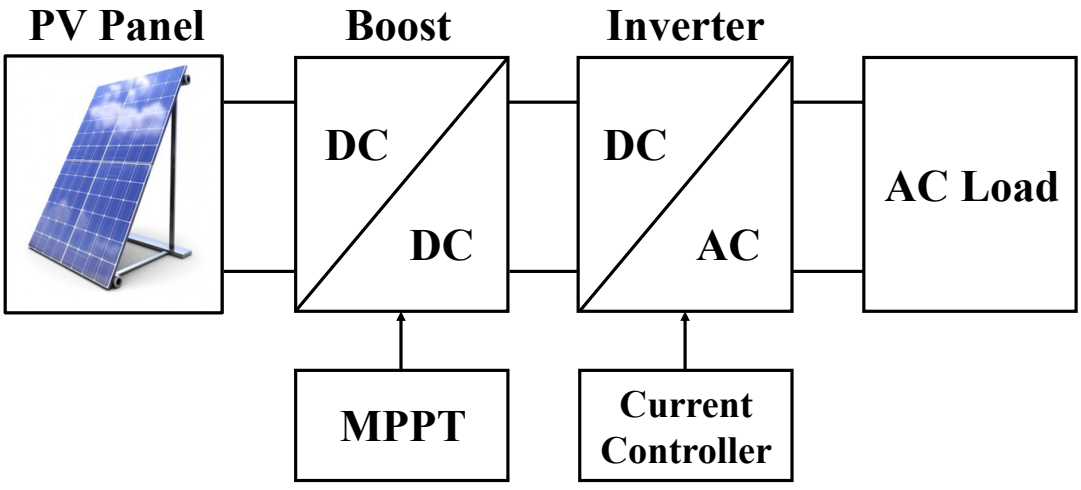

Figure 1. 6 Adopted topology for standalone PV system.

In order to achieve the objectives of this thesis, we have proposed prototype of standalone PV system following the topology in Figure 1.6. Accordingly, A Monocrystalline PV panel (SM55) with the characteristics in the Appendix A is used. This PV module exhibits an output voltage smaller than the required one which necessitates the use of a boost converter to increase this voltage the needed value. Then, the use of a DC to AC inverter to convert DC source energy for the AC load.

As a first thing to do, the modelling and the validation of the PV panel is substantial in order to estimate the generated PV power. For this reason, we have proposed and validated an accurate parameter extraction method to determine the unknown parameters of the PV cell equivalent circuit model. This method is used to build simulated PV array that could provide the output voltage, current and power of the PV panel according to atmospheric variations (solar irradiance and temperature).

The second task is to elaborate a maximum power point tracking technique in order to pursue the maximum power point regardless any sudden change of climatic conditions. This technique must verify the conditions of simplicity and robustness to ensure an MPP tracking of high efficiency.

Finally, both tasks are used to form and control the proposed standalone PV system with properties of good performances, robustness and simplicity of implementation in isolated sites.

1.4.2 Contributions of this Thesis

This thesis presents different contributions about PV panel modelling, maximum power point tracking techniques and the control of standalone PV system, these contributions are presented as follows:

(i) A new method to extract the equivalent circuit parameters is adopted. Then, a hybrid approach that combine different equivalent circuit models according to atmospheric changes is proposed. Both propositions are verified using datasheet manufacturer and real onsite data (This method is presented in Chapter 2).

(ii) An annual evaluation of three MPPT techniques in terms of performances is proposed. This evaluation is performed using a period of one year real climatic data and with a step of one second. The aim of this analysis is to choose the appropriate MPPT technique in terms of the produced energy.

(iii) A modelling and a control approach of a standalone PV system is proposed. For this, an accurate approach of control is used to track the maximum power point in addition of providing

an alternative output current of high quality. These controllers are based on the sliding mode approach.

1.5 Conclusion

The different used topologies in PV applications have been presented. The single and the double stages are discussed to show the performances and utility of these topologies for each PV application. Based on the need of feeding isolated sites with AC energy, we have decided to use the standalone topology with two stages of converters. Thus, to analyze the performances of this topology, the photovoltaic panel and each stage of converters must be discussed, which will be described in the following chapters.

CHAPTER2 : Electrical Performances of the Photovoltaic Module

2.1 Introduction

Following the discussion in previous chapter, the photovoltaic array represents a major component of the PV systems architectures. For this reason, an accurate modeling of the PV panel constitutes an important topic that attracts a lot of researchers. This modeling task is divided into two parts; First, the choice of the equivalent-circuit model and then the parameters extraction of the chosen model. In this chapter, a new method to extract to PV cell equivalent circuit parameters is presented in section 2.2. Afterwards, the influence of climate conditions on the choice of the appropriate equivalent-circuit model is adopted in sections 2.3.

2.2 Parameters Extraction of the PV cell Equivalent-Circuit Model

A PV array consists of several PV modules, each one is composed of many PV cells in series or parallel connections. The photovoltaic cell is a p-n junction fabricated in a thin wafer or layer of semiconductor. In the dark, the current-voltage output curve of the PV module has an exponential behavior similar to the diode's one (Walker, 2001).

When exposed to the light, photon with energy greater than the band gap of the semiconductor can create an electron-hole pair if it knocks an electron in the valence band. These carriers are swept away under the influence of the internal electric fields of the p-n junction and create a current which is proportional to the incident radiation. When the cell is short circuited, this current circulates in the external circuit. When the external circuit is opened, this current is zero because of the intrinsic p-n junction diode. If the shunt resistance is neglected the characteristics of this diode therefore set to the open circuit voltage (Walker, 2001).

In order to use the PV module at its maximum power point (MPP), which increases the ration of the photovoltaic system (Park and Choi, 2015), the parameters of the cell equivalent-circuit model must be determined. In fact, both the single diode models and the two-diode models of the cell equivalent-circuit take into account the series and the shunt resistances (Ishaque et al., 2011b; Laudani et al., 2014; Lo Brano et al., 2010; Ma et al., 2014a; Muhsen et al., 2015; Sandrolini et al., 2010; Yildiran and Tacer, 2016). The number of the parameters depends on the used extraction method.

Because of its good performance the four-parameter model is one of the most used (Celik and Acikgoz, 2007; Khan et al., 2014; Khezzar et al., 2014; Tivanov et al., 2005). This model neglects the shunt resistance R_{sh} and represents the unknown parameters as the series resistance R_s, the ideality factor γ, the saturation current I_{os} and the light generated current I_{sol} (Celik and Acikgoz, 2007)**.** But when photovoltaic cells are exposed to important

temperature variation, it is preferable to use the five-parameter model by adding the shunt resistance R_{sh} in order to have better balance between efficiency and accuracy (Chin et al., 2015; Jordehi, 2016; Mares et al., 2015). The determination of the unknown elements of the five-parameter model remains a challenge for researchers (Khezzar et al., 2014). In literature, various methods have been proposed to determine these parameters using implicit equations (De Soto et al., 2006), iterative and analytics methods (Villalva, 2015; M. G. M. G. G. Villalva et al., 2009; Wang et al., 2017); and intelligent algorithmes (Askarzadeh and Rezazadeh, 2013; Graditi et al., 2016; Jervase et al., 2001; Rajasekar et al., 2013). Some of these methods include the shunt resistance extraction due to its influence on the other parameters (Forniés et al., 2014). Consequently, a precise determination of R_{sh} attracts the attention of many researchers, and the majority of precedent works used numerical fitting and other analytical methods to determine R_{sh} (Chen et al., 2011; Priyanka et al., 2007; Radziemska, 2005).

Ikegami et al. (Ikegami et al., 2001) calculated the parameters using a least-squares fitting of the equivalent model current-voltage characteristic taking into account measured ones. This method requires a fast calculation of the merit function χ^2, which is defined as:

$$\boldsymbol{\chi^2(\delta) = \sum_{i=1}^{N} \left[\frac{I_i(V_i) - I(V_i,\delta)}{\sigma_i}\right]^2} \quad \textbf{(2.1)}$$

where, vector δ stands for the determination of the five-parameter model, N is the number of data points used, I_i and V_i are i-th measured current and voltage values, respectively, σ_i is a standard deviation at that data point, and $I(V_i, \delta)$ denotes the calculated current at V_i (Ikegami et al., 2001). The irradiation and the temperature of the cell are given.

2.2.1 Photovoltaic Array Model

2.2.1.1 Equivalent Circuit Model of the PV cell

The PV cell is a sandwich of two dissimilar materials usually one as elemental metal and the other a solid compound of two elements (a semiconductor) one is doped p-type and the other is doped n-type. It has consequently the same behavior as a diode. Incident light with photons energy, creates electron-hole pairs and induces a voltage at terminals of the cell. This effect can be assimilated to a photo-current source. This later depends on the received irradiation and on the temperature, also it is proportional to exposed area. A shunt resistance represents one part of internal losses while the series one constitutes the second part of internal losses and the metallic contacts losses.

In a PV module, several cells are connected in parallel and series to have important voltage and current levels. Connecting current sources of identical current values in series gives an equivalent current source with the same current value. Connecting diodes in series give an equivalent diode with stretched characteristic on voltage axis. Connecting current sources in parallel gives an equivalent current source taking a current value equals to the sum of components current values. Connecting diodes in parallel give an equivalent diode with stretched characteristic on the current axis.

The equivalent circuit of a PV module is illustrated in Figure 2.1, this model is characterized by the presence of the series and the shunt resistance, which are influenced by environmental conditions (Gow and Manning, 1999; Radziemska, 2005).

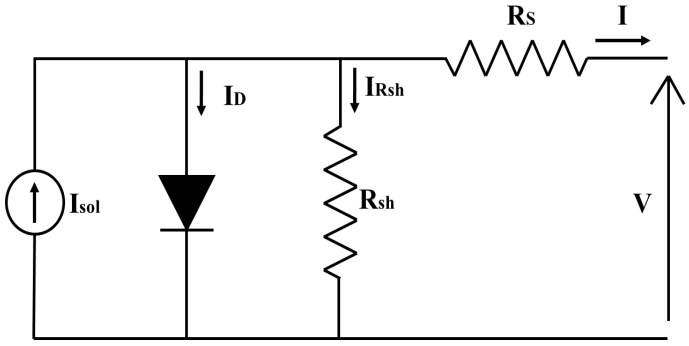

Figure 2. 1 Single-diode PV cell equivalent-circuit model.

While the typical output characteristics are shown in Figure 2.2. The characteristic equation for this PV model was mathematically demonstrated by Shockley (Shockley and Queisser, 1961), its expression is as follows:

$$\boldsymbol{I = I_{sol} - I_{os}\left\{exp\left[\frac{q}{N_{cell}kT\gamma}(V + IR_s) - 1\right]\right\} - \frac{V+R_sI}{R_{sh}}} \quad \textbf{(2.2)}$$

where the reverse cell saturation current I_{os} depends totally on temperature, this current is represented by Equation (2.3) (Lineykin et al., 2014):

$$\boldsymbol{I_{os} = I_{or}\left(\frac{T}{T_r}\right)^3 exp\left(\frac{qE_G}{k\gamma}\left[\frac{1}{T} - \frac{1}{T_r}\right]\right)} \quad \textbf{(2.3)}$$

In order to improve the model sensitivity against temperature variation in the case of high temperature, it is recommended to use the five-parameter model by incorporating the shunt resistance (Chin et al., 2015).

According to Walker et al. (Walker, 2001), the light generated current I_{sol} depends on irradiance and temperature variation and can be written as:

$$\boldsymbol{I_{sol} = [I_{sc} + K_i(T - 298.15)]\frac{\lambda}{1000}} \quad \textbf{(2.4)}$$

where

I_{sc}: short-circuit current [A]

K_i : temperature coefficient of I_{sc} [A/K]

λ : solar irradiance level [W/m^2]

T : cell temperature [K]

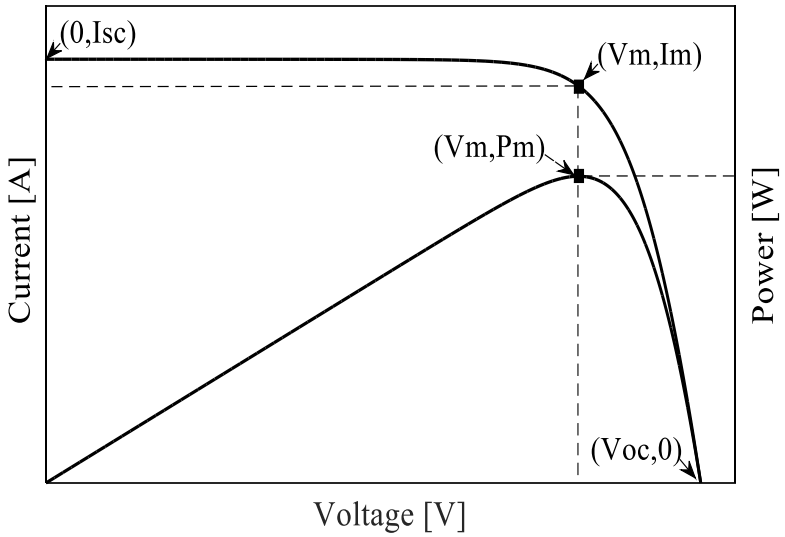

Figure 2. 2 Typical PV cell Current-voltage and Power-Voltage characteristics.

In the interest of extracting the maximum available power from the PV modules, it is necessary to operate the PV modules at their maximum power point (MPP). The output power of the PV panel is $P = IV$. A derivative of the output power P with respect to the output voltage V is equal to zero at MPP [30]. If the equivalent circuit parameters λ and T are given, MPP is obtained by solving Equation (2.5) together with Equations (2.2)-(2.4).

We have:

$$\frac{\partial P}{\partial V} = I + V\frac{\partial I}{\partial V} = 0 \;\Rightarrow\; \frac{\partial I}{\partial V} = -\frac{I}{V} \tag{2.5}$$

Hence: $$I = (V - R_s I)\left\{I_{os} A exp[A(V + R_s I)] + \frac{1}{R_{sh}}\right\} \tag{2.6}$$

where: $A = \frac{q}{\gamma k T N_{cell}}$.

Ideally, a PV array would operate at his MPP, such process is achievable by using a maximum power point tracking (MPPT) controller (De Soto et al., 2006; Gupta et al., 2016). When the model parameters and the irradiance λ are obtained in a real time, a correct MPP can be calculated without knowing the cell temperature or the dependence of the cell parameters with respect to the temperature (Ikegami et al., 2001).

2.2.1.2 New Method to Extract the PV Cell Equivalent Circuit Parameters

a) Proposed Method

The main objective of this research is to determine the unknown parameters I_{os}, R_s, R_{sh} and γ of the single diode model. To find these parameters we need at least four equations (Ma et al., 2014b) . In fact, our method is based on two steps, the first one is the measurement of the shunt resistance in a specific conditions, and the second one consists on the use of the manufacturer characteristic equations under Standard Test Conditions (STC: λ=1 kW/m², A.M=1.5, T=25°C) for the three point $(0, I_{sc})$, $(V_{oc}, 0)$ and (V_m, I_m). The methodology adopted for the proposed method is presented in Figure 2.3.

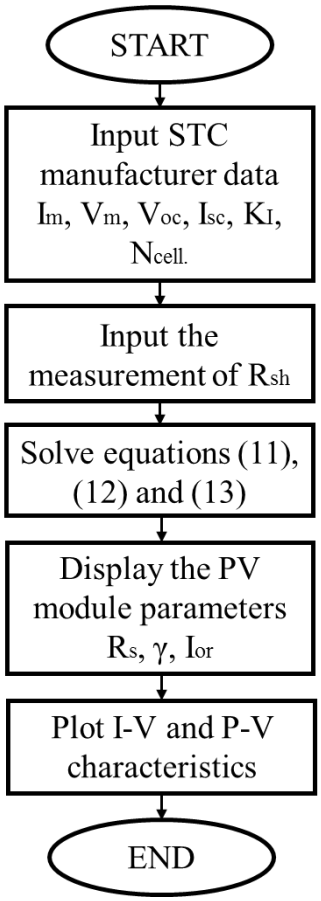

Figure 2. 3 Diagram of the proposed method.

(i) Measurement of Rsh

The shunt resistance R_{sh} of the PV module is measured in laboratory conditions. This measure (Figure 2.4) is obtained on obscurity (I_{sol} = 0) and no wind, using voltmeter and ammeter. We have applied an external negative voltage to the PV panel (diode current I_D = 0).

The measurements of V_{mes} and I_{mes} must be done quickly to avoid the overheating of photocell. The mean value of $V_{mes}/\ I_{mes}$ corresponds to the sum of the R_{sh} and R_s values, it is assumed that the series resistance is negligible because $R_{sh} >> R_s$.

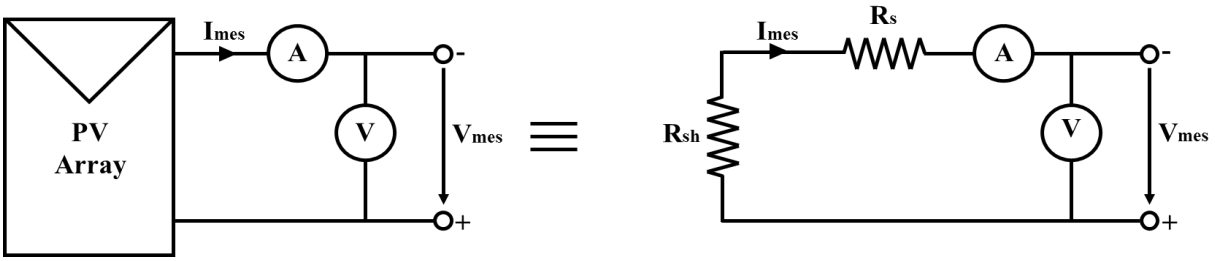

Figure 2. 4 Measurement on obscurity of the shunt resistance of the photovoltaic panel.

(ii) Parameters Extraction of the Single-Diode Model

All constants in the equations above can be determined by examining the electrical specifications cited by the manufacturer of the PV panel in the datasheet (Appendix A). From the datasheet, following equations could be deduced for each condition:

- Open circuit condition: When the PV panel is illuminated and in open circuit, the photo-current flows through the diode and the R_{sh} resistance. So, the relation between *I* and *V* becomes:

$$\mathbf{0} = \boldsymbol{I_{sol}} - \boldsymbol{I_{os}}[\boldsymbol{exp}(\boldsymbol{AV_{oc}}) - \mathbf{1}] - \frac{\boldsymbol{V_{oc}}}{\boldsymbol{R_{sh}}} \quad \textbf{(2.7)}$$

where V_{oc} is the output voltage of the PV panel in open circuit.

- Short circuit condition: When the PV panel is short circuited and illuminated, a negligible current flows through the diode. The current *I* is equal to the rated short circuit current I_{sc}, if we consider that the rated irradiation equals to 1000 W/m². Hence, Equation (2.2) can be written:

$$\boldsymbol{I_{sc}} = \boldsymbol{I_{sol}} - \boldsymbol{I_{os}}[\boldsymbol{exp}(\boldsymbol{AI_{sc}R_s}) - \mathbf{1}] - \frac{\boldsymbol{R_s I_{sc}}}{\boldsymbol{R_{sh}}} \quad \textbf{(2.8)}$$

- Optimum condition: At optimal operating point determined by I_m and V_m values, the following expressions could be found by using Equations (2.2) and (2.6):

$$\boldsymbol{I_m} = \boldsymbol{I_{sol}} - \boldsymbol{I_{os}}\{\boldsymbol{exp}[\boldsymbol{A}(\boldsymbol{V_m} + \boldsymbol{I_m R_s}) - \mathbf{1}]\} - \frac{\boldsymbol{V_m + R_s I_m}}{\boldsymbol{R_{sh}}} \quad \textbf{(2.9)}$$

$$\boldsymbol{I_m} = (\boldsymbol{V_m} + \boldsymbol{I_m R_s})\left\{\boldsymbol{I_{os} A exp}[\boldsymbol{A}(\boldsymbol{V_m} + \boldsymbol{I_m R_s})] + \frac{\mathbf{1}}{\boldsymbol{R_{sh}}}\right\} \quad \textbf{(2.10)}$$

The set of nonlinear equations to solve is illustrated in the following system:

$$\begin{cases} \mathbf{0} = \boldsymbol{I_{sol}} - \boldsymbol{I_{os}}[\boldsymbol{exp}(\boldsymbol{AV_{oc}}) - \mathbf{1}] - \frac{\boldsymbol{V_{oc}}}{\boldsymbol{R_{sh}}} \\ \boldsymbol{I_{sc}} = \boldsymbol{I_{sol}} - \boldsymbol{I_{os}}[\boldsymbol{exp}(\boldsymbol{AI_{sc}R_s}) - \mathbf{1}] - \frac{\boldsymbol{R_sI_{sc}}}{\boldsymbol{R_{sh}}} \\ \boldsymbol{I_m} = \boldsymbol{I_{sol}} - \boldsymbol{I_{os}}\{\boldsymbol{exp}[\boldsymbol{A}(\boldsymbol{V_m} + \boldsymbol{I_mR_s}) - \mathbf{1}]\} - \frac{\boldsymbol{V_m}+\boldsymbol{R_sI_m}}{\boldsymbol{R_{sh}}} \end{cases}$$

The saturation current value I_{os} (=I_{or}) at temperature of 298.15K is calculated using the open circuit voltage $V_{oc}$and short circuit current I_{sc} at this temperature Equation (2.11):

$$\boldsymbol{I_{or}} = \frac{\boldsymbol{I_{sc}} - \frac{\boldsymbol{V_{oc}}-\boldsymbol{R_sI_{sc}}}{\boldsymbol{R_{sh}}}}{\boldsymbol{exp}(\boldsymbol{AV_{oc}})-\boldsymbol{exp}(\boldsymbol{AI_{sc}R_s})} \tag{2.11}$$

The following equations could be obtained by using Equations (2.7)-(2.10):

$$\frac{\boldsymbol{I_{sc}}}{\boldsymbol{exp}(\boldsymbol{AV_{oc}})-\boldsymbol{exp}(\boldsymbol{AI_{sc}R_s})} = \frac{\boldsymbol{I_m}}{\boldsymbol{exp}(\boldsymbol{AV_{oc}})-\boldsymbol{exp}[\boldsymbol{A}(\boldsymbol{V_m}+\boldsymbol{R_sI_m})} \tag{2.12}$$

$$\frac{\boldsymbol{I_m}}{\boldsymbol{exp}(\boldsymbol{AV_{oc}})-\boldsymbol{exp}[\boldsymbol{A}(\boldsymbol{V_m}+\boldsymbol{R_sI_m})} = \frac{\frac{\boldsymbol{I_m}}{\boldsymbol{V_m}-\boldsymbol{R_sI_m}}}{\boldsymbol{Aexp}[\boldsymbol{A}(\boldsymbol{V_m}+\boldsymbol{R_sI_m})]} \tag{2.13}$$

Equations (2.12) and (2.13) are used to determine the R_s resistance and the inverse voltage A. So, the ideality factors γ and the cell saturation reverse current I_{or} at T_r can be obtained.

2.2.2 Results and Discussion

To assess the performance of this method, two types of solar panels are used, the monocrystalline SM55 and the polycrystalline SW255 using manufacturer data at STC which are reported in Table 2.1.

Table 2. 1 Datasheet parameters of the SM55 and the SW255 PV panels at STC.

Parameters	SM 55	SW 255
P_m [W]	55	255
V_m [V]	17.4	30.9
I_m [A]	3.15	8.32
V_{oc} [V]	21.7	38.0
I_{sc} [A]	3.45	8.88
K_i [A/K]	0.04	0.051
K_v [A/K]	-0.34	-0.31
N_{cell}	36	60

The measured values of R_{sh} for the monocrystalline SM55 and for the polycrystalline SW255 are respectively, 6500 Ω and 7000 Ω. From the values provided in the datasheet and the measurement of the shunt resistance R_{sh}, the parameters of the selected PV modules are determined using an implementation of the proposed method at MATLAB m-script. After the extraction process, the obtained results are presented in Table 2.2, these parameters are employed to plot the power-voltage (P-V) and current-voltage (I-V) characteristics.

Table 2. 2Extracted parameters using the proposed method.

Parameters	SM55	SW255
R_s [Ω]	0.1124	0.2035
I_{or} [A]	4.8424 x10^{-6}	0.3098 x10^{-9}
γ	1.7411	1.2659

Before comparing the proposed method with software and literature, the present method is used to plot the I-V curves of the SM55 and the SW255 panels for various values of temperature and irradiance. These curves are compared to datasheet ones (Ag et al., n.d.; Shell SM55, 2002). Unfortunately, the I-V curves of the SW255 for different temperature are not issued at the datasheet.

As seen in Figure 2.5 and Figure 2.6, the SM55 I-V characteristics fit perfectly with the datasheet ones with a very small difference for low irradiance. For the SW255 I-V curves, Figure 2.7 shows good agreement between the proposed method and datasheet, except for irradiance lower than 400 W/m², this disturbance is caused by the error of the extracted data from datasheet.

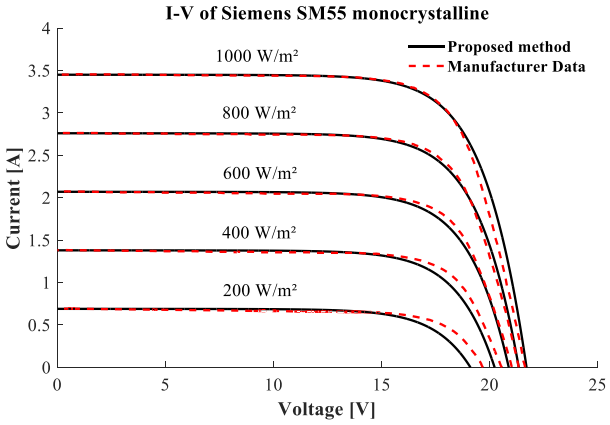

Figure 2. 5 Comparison between the proposed method and the manufacturer Data of the SM55 PV panel for different irradiances, T= 25°C.

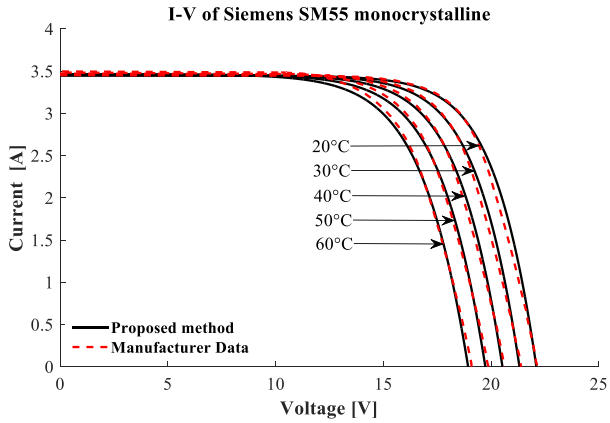

Figure 2. 6 Comparison between the proposed method and the manufacturer Data of the SM55 panel for different temperatures, λ=1000 W/m².

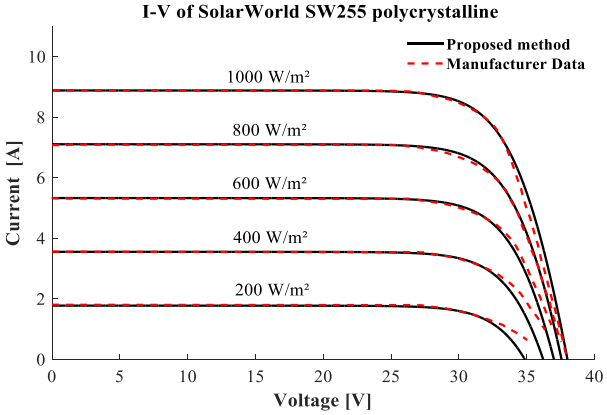

Figure 2. 7 Comparison between the proposed method and the manufacturer Data of the SW255 panel for different irradiances, T= 25°C.

In order to study the accuracy of the proposed method, we have divided the discussion into two parts. In the first part we compare the plotted curves of the SM55 in MATLAB with PVsyst software data (Universidade De Genebra, 2012). And the second part provide a comparison between the plotted curves obtained by the proposed method and Villalva's ones (Villalva, 2015; M. G. M. G. G. Villalva et al., 2009). Note that all these comparisons are done for different values of temperature and irradiance and the average error of each graph is calculated using the following equation:

$$\xi_{avg} = \frac{1}{N}\sum_{i=1}^{N}\left[\frac{X_p(i)-X_c(i)}{X_p(i)}\right] * 100 \qquad (2.14)$$

where $X_p(i)$ are the current and the voltage values at each point of the proposed I-V curve and $X_c(i)$ represent the current and the voltage values at each point of the compared methods, N is the total points of the curve.

2.2.2.1 Comparison with the PVsyst Software (Universidade De Genebra, 2012)

Figure 2.8 shows the current-voltage and power-voltage curves of the monocrystalline panel SM55 for various values of irradiance and at fixed temperature T=25°C, it can be seen that the P-V and the I-V graphs of the proposed method agree well with the one provided by PVsyst ones for high irradiance, while for low radiance levels, only a little discrepancy can be observed, but it is not very important.

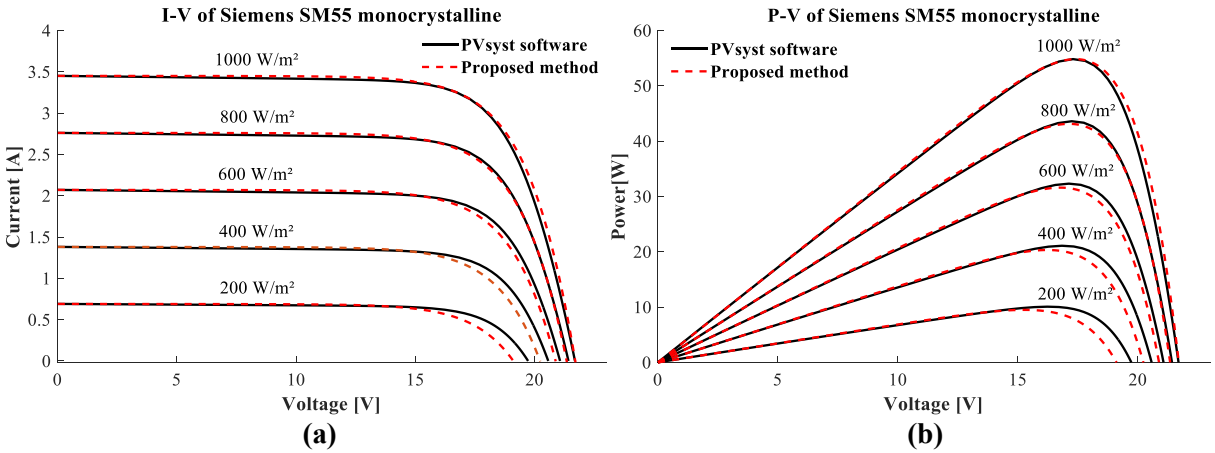

Figure 2. 8 Comparison between the proposed method and PVsyst software I-V (a) and P-V (b) curves of the SM55 for different irradiances, T=25 °C.

Figure 2.9 presents the P-V and the I-V characteristics of the monocrystalline panel SM55 for different values of temperature and at an irradiance of λ=1000W/m². As shown in these figures, the proposed method and the PVsyst have identic curves except for T=55°C. At this temperature, there is a little discordance around the MPP, which is negligible because of the low value of the average error presented in Figure 2.10.

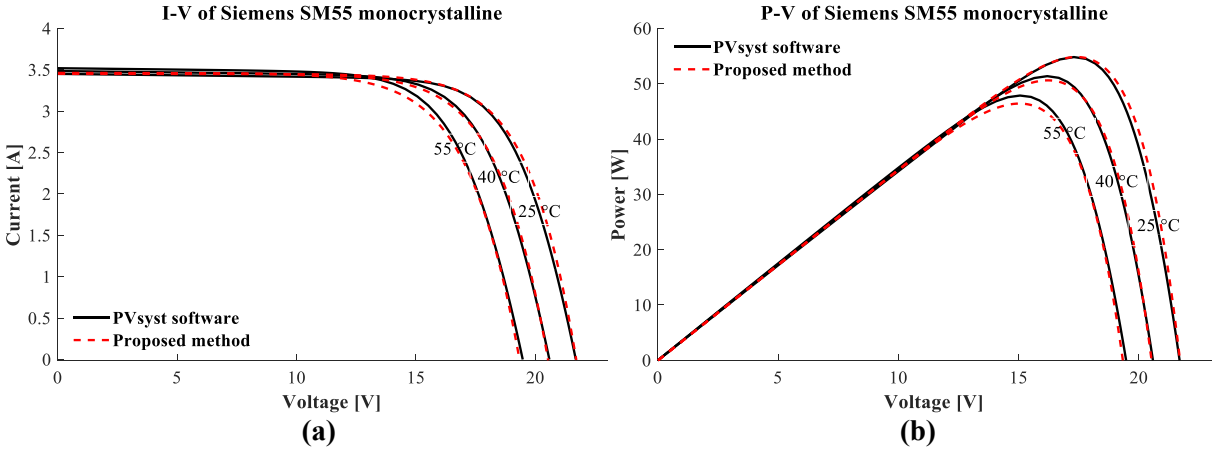

Figure 2. 9 Comparison between the proposed method and PVsyst software I-V (a) and P-V (b) curves of the SM55 for different temperatures, λ=1000 W/m².

From the comparison of the proposed method with the PVsyst, and as observed in Figure 2.10 it is clear that the present method represents a good performance with negligible errors. The database of the PVsyst does not contain the SW255 panel, that's why we didn't compare the polycrystalline technology with the PVsyst software.

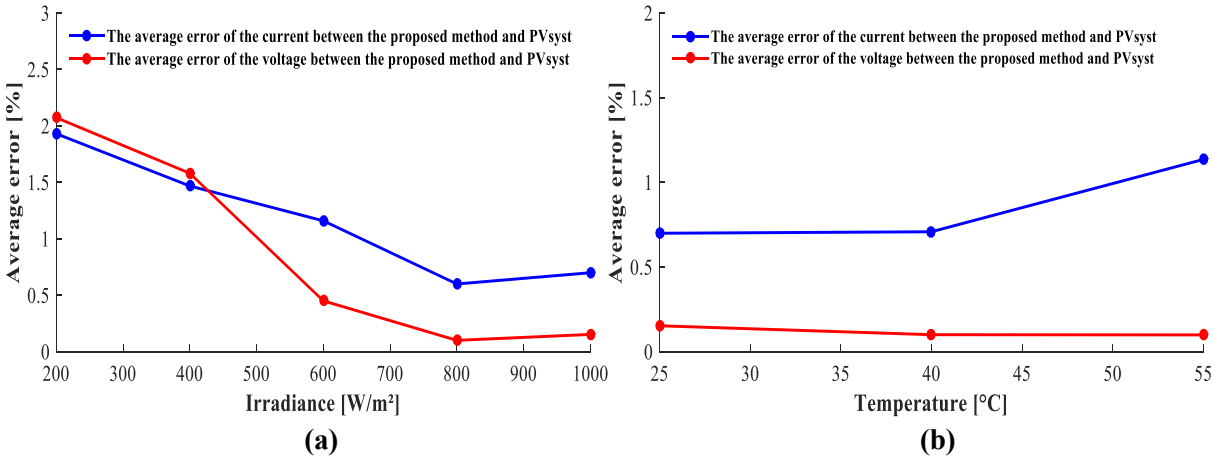

Figure 2. 10 The average errors of the current and the voltage. Different irradiance, T=25 °C (a), and various temperatures, λ=1000W/m² (b).

2.2.2.2 Comparison with the results of Villalva et al. (Villalva, 2015; M. G. M. G. G. Villalva et al., 2009)

Villalva et al. assumed that the ideality factor is constant and they calculated the other parameters using implicit equations (M. G. M. G. G. Villalva et al., 2009). For this reason, we choose to compare our results with their method cited in (Villalva, 2015; M. G. M. G. G. Villalva et al., 2009). While our method is based on the measurement of the shunt resistance and on the extraction of the other parameters using the proposed equations, we compared the I-V and P-V characteristics obtained by using the extracted parameters (Table 2.2) with Villalva's power-voltage and current-voltage curves for the shunt resistance and without it. These tests are done under various weather conditions.

Figure 2.11 describes I-V and P-V characteristics of the monocrystalline panel SM55 for a ranging of radiance from 200 W/m² to 1000 W/m² and at T=25°C. As can be seen in these graphs, the proposed method shows an accurate performance and agrees well with the results reported by Villalva especially at high irradiance. As seen in Figure 2.12 for irradiance lower than 400 W/m² and especially the model without R_{sh} the average error of the current and the voltage exceed 5% which explains the influence of the shunt resistance on the value of V_{oc} because of the term V_{oc}/R_{sh}.

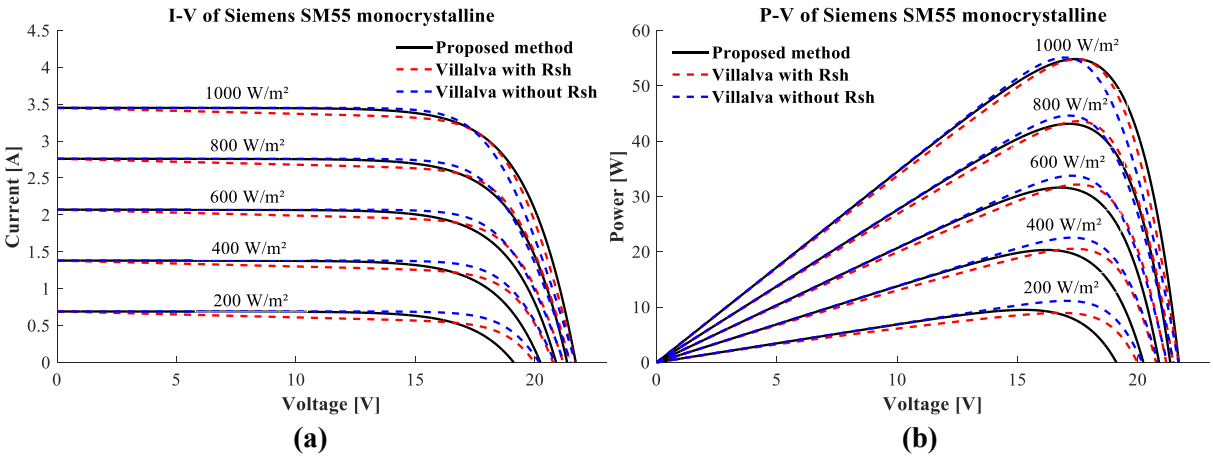

Figure 2. 11 Comparison between the proposed method and Villalva I-V (a) and P-V (b) curves of the SM55 for different irradiances, T=25 °C.

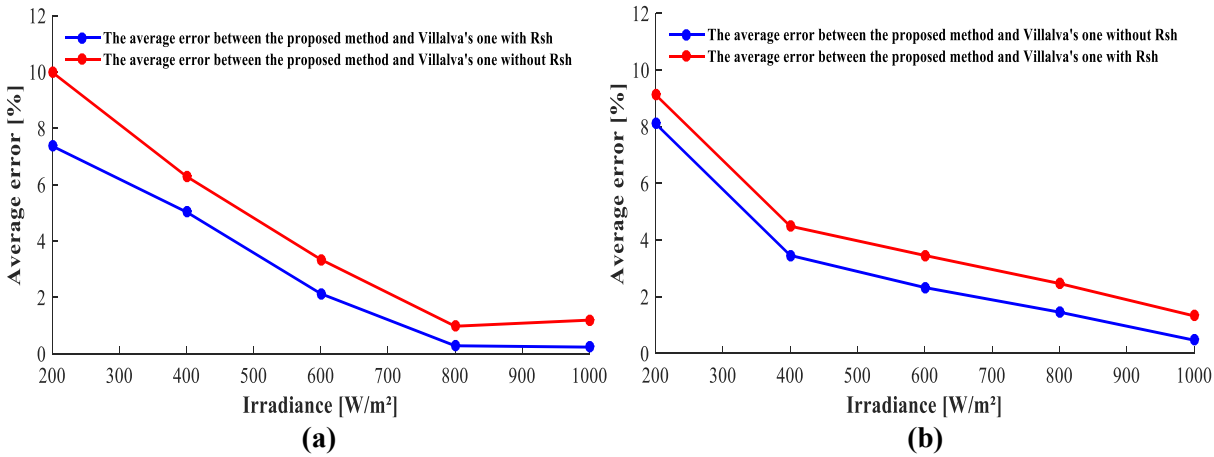

Figure 2. 12 The average errors of the current (a) and the voltage (b) of the SM55 panel at different irradiances, T=25 °C.

Figure 2.13 gives the I-V and P-V curves of the monocrystalline panel SM55 for $T \neq T_r$ and at fixed irradiance λ=1000W/m². As observed, the plotted characteristics obtained through the proposed method significantly match with those from Villalva. Moreover it is noticed in Figure 2.14 that the curves of the model without R_{sh} represents a little degradation in term of voltage and current, this difference is around 2%. The latter shows good performance of the proposed method in the temperature changes.

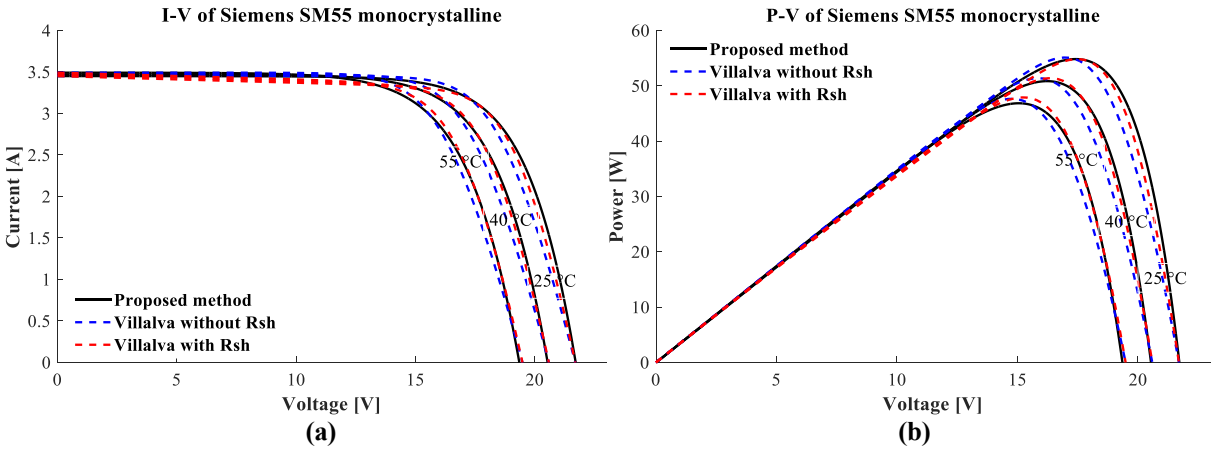

Figure 2. 13 Comparison between the proposed method and Villalva I-V (a) and P-V (b) curves of the SM55 for different temperatures, λ=1000 W/m².

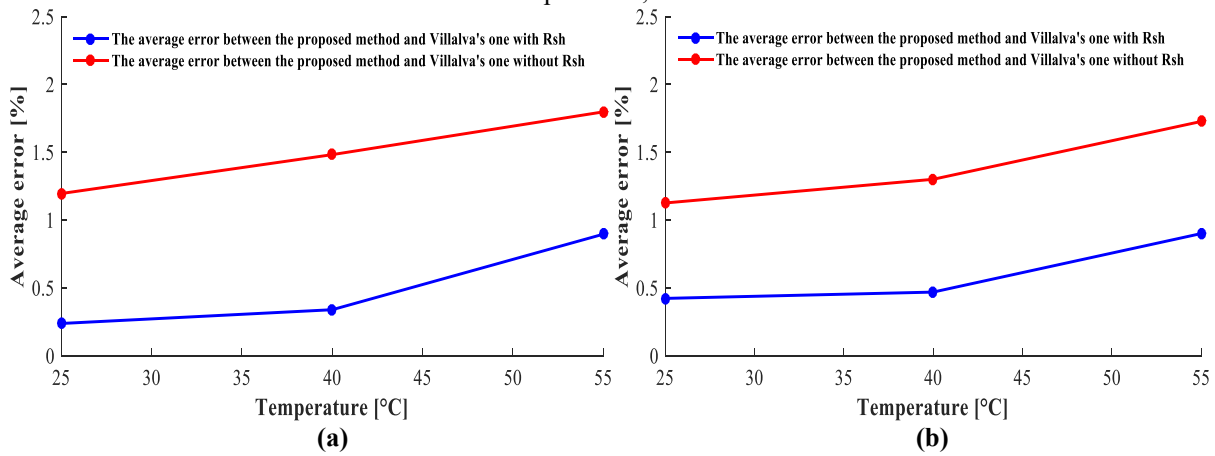

Figure 2. 14 average errors of the current (a) and the voltage (b) of the SW255 panel at different temperatures, λ=1000 W/m².

Figure 2.15 reports the I-V and P-V characteristics of the polycrystalline SW255 for various value of irradiance and at T=25 °C, as shown in this figure, there is a remarkable agreement between the curves obtained by the proposed method and Villalva's ones, with a negligible discrepancy for low irradiance levels. According to Figure 2.16, in the case of Villalva's curves without $R_{sh,}$ this difference can reach up to 5%, but for the model that takes in account R_{sh} the error does not exceed 3%.

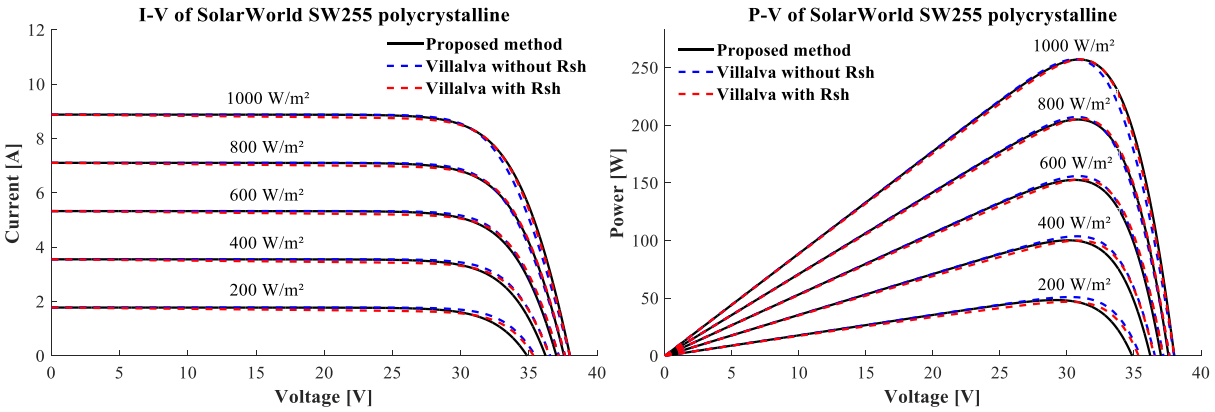

Figure 2. 15 Comparison between the proposed method and Villalva I-V (a) and P-V (b) curves of the SW255 for different irradiances, T=25 °C.

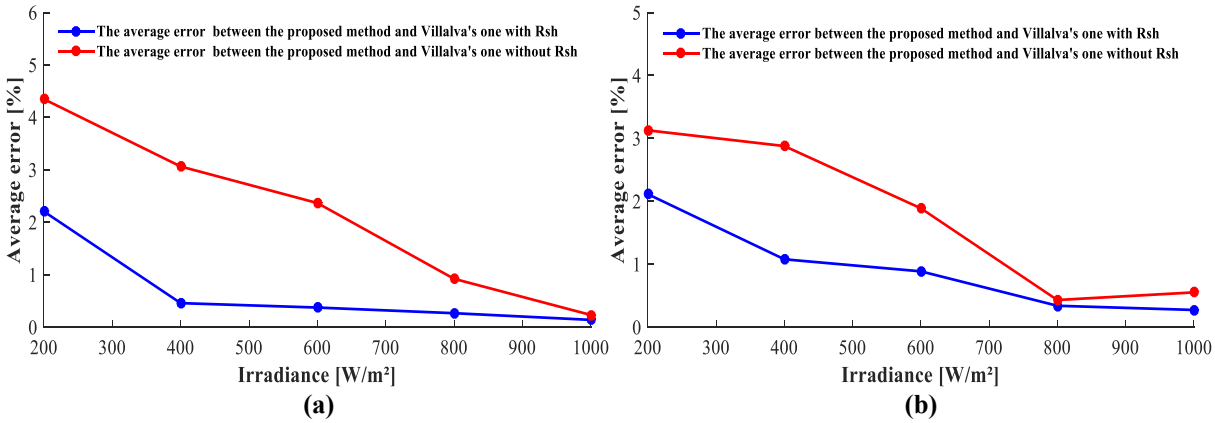

Figure 2. 16 average errors of the current (a) and the voltage (b) of the SW255 panel for different irradiances, T=25 °C.

Figure 2.17 represents the current-voltage and the power-voltage of the polycrystalline SW255 for different values of temperature and λ=1000 W/m², it is clearly observed that the model performs accurately with a very good agreement with results of Villalva, and as reported in Figure 2.18 the error between the two comparisons does not exceed 1%.

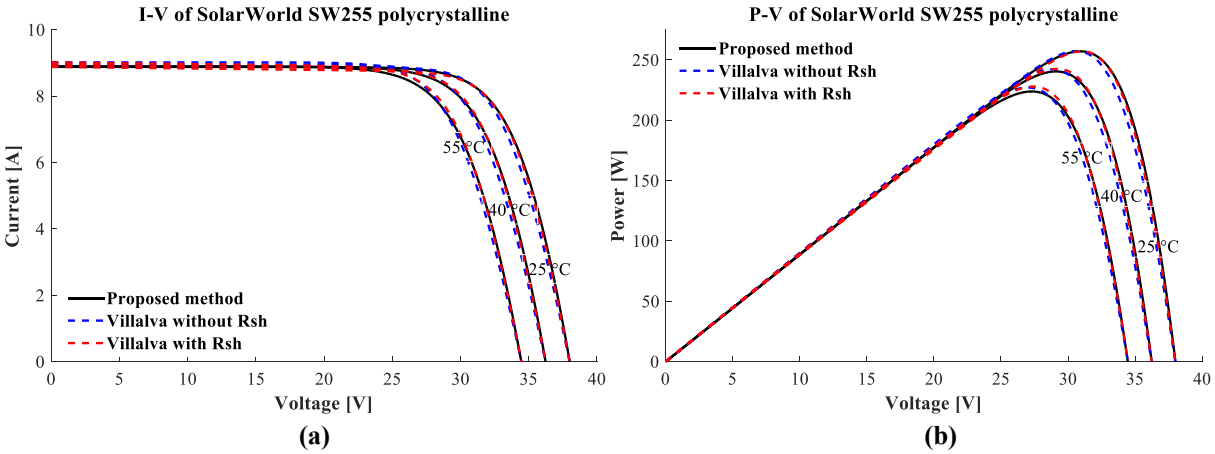

Figure 2. 17 Comparison between the proposed method and Villalva I-V (a) and P-V (b) curves of the SW255 for different temperatures, λ=1000 W/m².

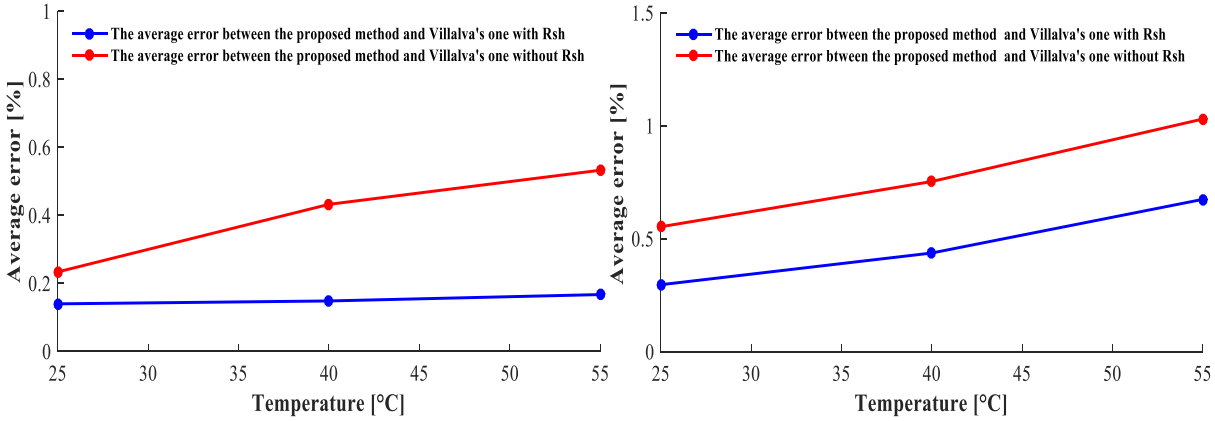

Figure 2. 18 average errors at each instant of the current (a) and the voltage (b) of the SW255 panel for different temperatures, λ=1000 W/m².

From the precedent comparisons, it could be deduced that the proposed method has a very high performance independently of the PV technology, notice that the used panel technologies represent 80% of the PV all market (Sudhakar Babu et al., 2016), which validate the performance of our method.

2.2.2.3 The influence of the measurement errors on the extracted parameters

Even if the measure of the R_{sh} is affected by error, its influence on the calculated parameters is negligible for high values of R_{sh}. Thereby, the expression $1/R_{sh}$ in Equations (2.12) and (2.13) becomes small. In order to highlight this idea, we proposed to vary the value of R_{sh} (we have varied the measurement error between -10% and +10% of the measured values) and to calculated the other parameters. For each value of R_{sh} the calculated parameters are summarized in Table 2.3 for the monocrystalline SM55 and in Table 2.4 for the polycrystalline SW255.

Table 2. 3 Calculated parameters of Mono-Si SM55 PV panel for different values of R_{sh}.

R_{sh} [Ω]	5900	6000	6100	6200	6300	6400	6600	6700	6800	6900	7000	7100
R_s [Ω]	0.1132	0.1131	0.1130	0.1128	0.1127	0.1126	0.1123	0.1122	0.1121	0.1120	0.1119	0.1118
γ	1.7394	1.7397	1.7400	1.7403	1.7406	1.7408	1.7414	1.7416	1.7418	1.7421	1.7423	1.7425
I_{or} [μA]	4.7758	4.7900	4.8011	4.8119	4.8224	4.8326	4.8520	4.8614	4.8702	4.8792	4.8878	4.4962

Table 2. 4 Calculated parameters of the Poly-Si SW255 PV panel for different values of R_{sh}.

R_{sh} [Ω]	6300	6500	6600	6700	6800	6900	7100	7200	7300	7400	7500	7700
R_s [Ω]	0.2039	0.2038	0.2037	0.2036	0.2036	0.2035	0.2034	0.2034	0.2033	0.2033	0.2032	0.2031
γ	1.2647	1.2651	1.2653	1.2655	1.2656	1.2658	1.2661	1.2662	1.2664	1.2665	1.2667	1.2669
I_{or} [nA]	0.3041	0.3058	0.3067	0.3075	0.3083	0.3097	0.3105	0.3112	0.3119	0.3126	0.3132	0.3145

These results illustrate that the parameters R_s, I_{or} and γ variations sill negligible when R_{sh} varies, to prove that the relative percentage error ($\%rerr$) is calculated using the following equation:

$$\%\boldsymbol{rerr} = \left|\frac{\boldsymbol{X_{measured} - X_{varied}}}{\boldsymbol{X_{measured}}}\right| * \mathbf{100} \quad \textbf{(2.15)}$$

Where $\boldsymbol{X_{measured}}$ represents the calculated parameters at the measured values of R_{sh}, and $\boldsymbol{X_{varied}}$ gives the calculated parameters for each varied value of R_{sh}. As observed in Figure 2.19 and Figure 2.20, the obtained *%rerr* of R_s, I_{or} and γ is very low and do not exceed 2%, which demonstrate that the measure employed in our method have a negligible effect on the calculated parameters.

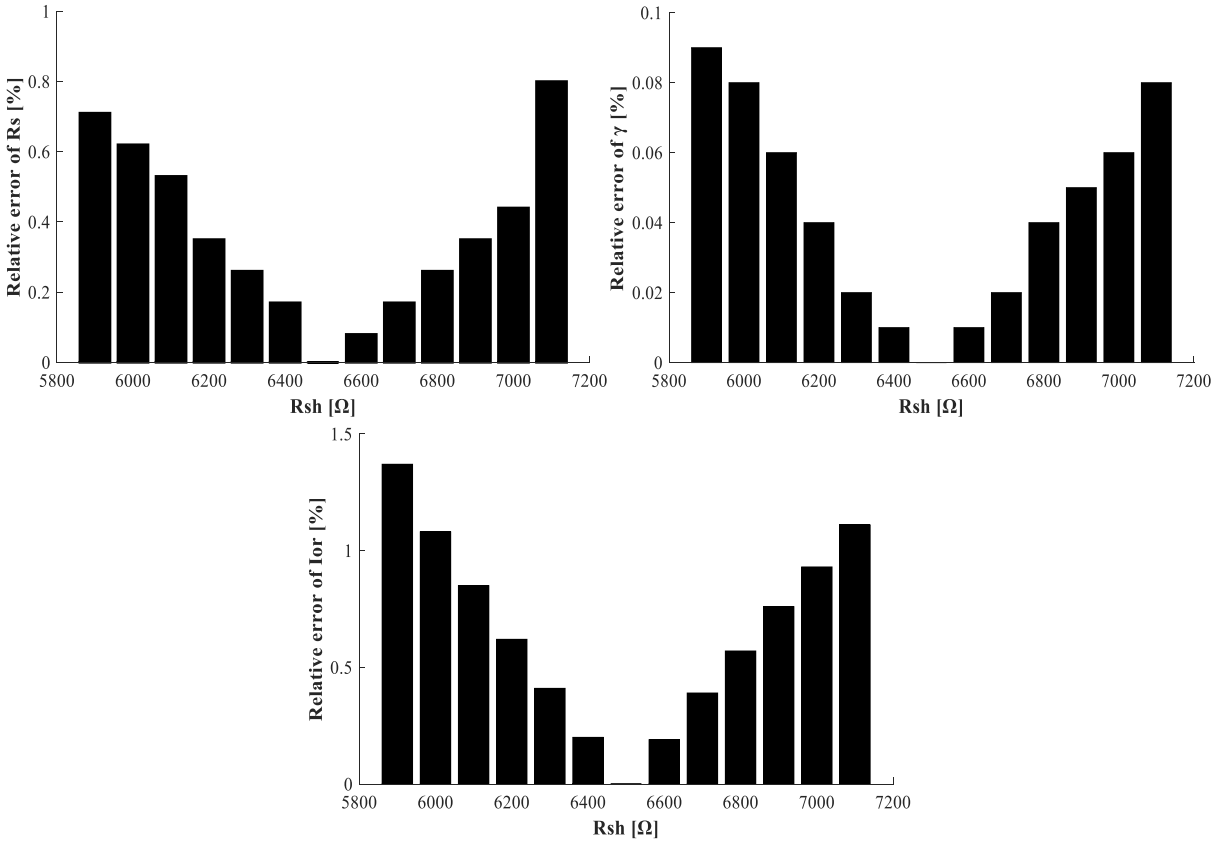

Figure 2. 19 Relative errors of the calculated parameters of the monocrystalline panel SM55 at each varied value of Rsh

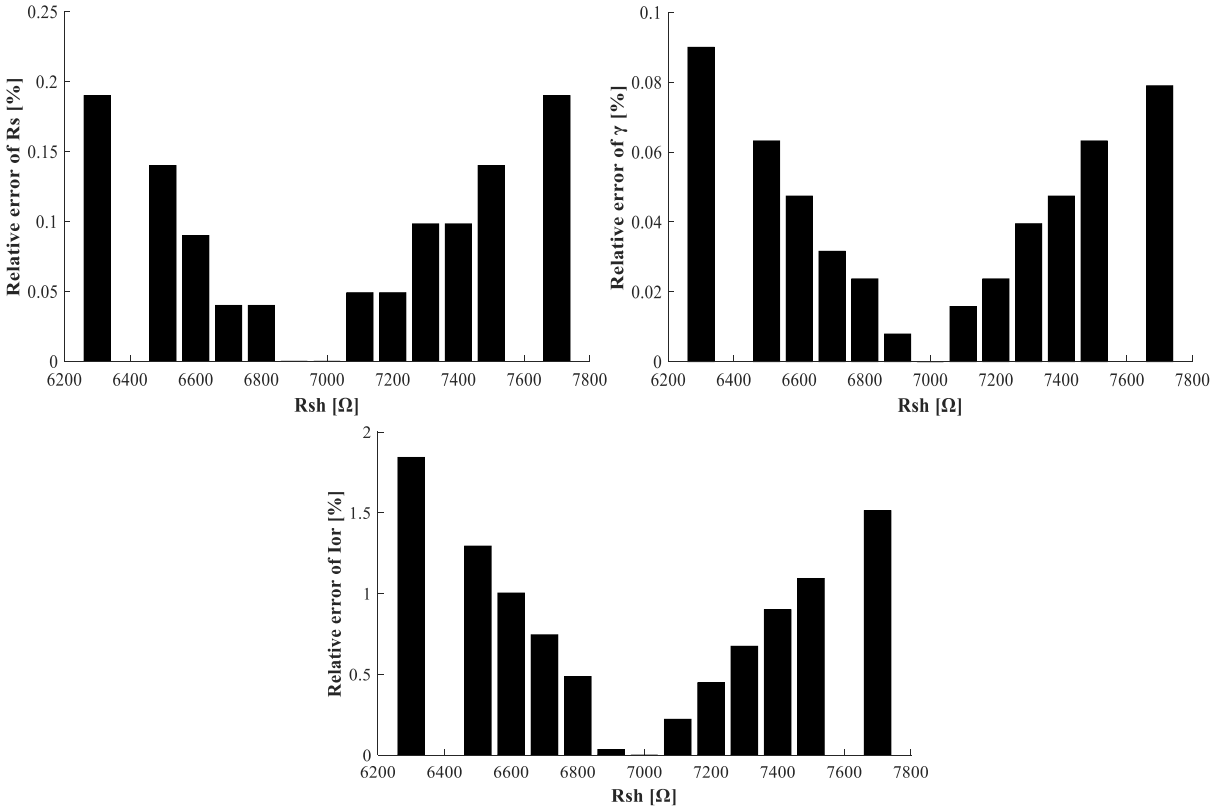

Figure 2. 20 Relative errors of the calculated parameters of the polycrystalline panel SW255 at each varied value of Rsh.

2.3 Influence of Climatic Conditions on the Choice of the PV Cell Equivalent-Circuit Model

As it has been mentioned in the previous section, an accurate modelling of the PV module is required. Hence the choice of an adequate equivalent-circuit model is recommended. In this section, the influence of atmospheric conditions on the choice of the appropriate equivalent-circuit model is discussed. Moreover, a new hybrid approach is proposed and tested under the climate fluctuations of two climatic zones.

2.3.1 A Review on Various PV Cell Equivalent-Circuit Models

The PV cell equivalent-circuit model is an electrical scheme which allows analyzing the electrical performance of the PV module. This model gives the corresponding current-voltage (I-V) and power-voltage (P-V) characteristics for different external changes such as irradiance and temperature (Chaibi et al., 2018). The history of the PV cell equivalent-circuit models knows a rapid progress. The first introduced formulation is the ideal single-diode model which is composed of a diode in parallel with a current source. This model requires the determination of three parameters, namely, the light-generated current I_L, the ideality factor γ and the saturation current of the diode I_{os}. The ideal model is characterized by uncomplicated structure

and simplified parameters extraction. However, the use of this model does not reflect the real behavior of the PV cell (Siddiqui and Abido, 2013; Suthar et al., 2013; M. G. G. Villalva et al., 2009). Thereby, for more realistic PV cell design, the assessment of the losses should be taken into account by adding a block of resistances in series and in parallel with the ideal model (Ishaque and Salam, 2011). To design the contact between the silicon and electrodes surface, a resistance is added in series (Jordehi, 2016); this model is named as the simplified single-diode model (SSDM) and the number of the unknown parameters is increased to four by adding the series resistance R_s. The SSDM model has been used widely to study the performance of the PV cell (Chenni et al., 2007; Ding et al., 2012; Ismail et al., 2013; Ulapane et al., 2011; Walker, 2001). Because of the parameters number, the mathematical solution requires four equations to find the unknown parameters. Therefore, several authors employed the datasheet characteristic equations by considering the point $\{(0, V_{oc}), (I_{sc}, 0), (V_m, I_m)\}$ and another initial equation to extract the SSDM parameters. Weidong et al., Ulapane et al. and Kun et al. used the derivative of power with respect to voltage ($^{\partial P}/_{\partial V} = 0$) as a fourth equation (Ding et al., 2012; Ulapane et al., 2011; Xiao et al., 2004). Furthermore, other researchers such as Kou et al. and Chenni et al. used the relative expressions of the temperature coefficients K_i and/or K_v to solve the set of equation (Chenni et al., 2007; Kou et al., 1998). The way to figure out the unknown parameters differs from a technique to another; whether it is an iterative, analytical or a mathematical method, the extracted parameters show a modest performance, which implied improving this model by adding another parameter which is the shunt resistance. Consequently, the number of parameters increases to five and the extraction process becomes more complicated. This model is named as the detailed single-diode model (SDM) and considered as the most used one due to its good compromise between efficiency and simplicity. Additionally, this model represents the main model of most PV systems modelling software such as PVsyst, SAM and HOMER (Blair et al., 2014; Suite and Co, 2016; Universidade De Genebra, 2012). Moreover, to overcome the complexity of the parameters determination, various techniques have been used in literature (Humada et al., 2016; Jordehi, 2016). Starting with graphic fitting methods, Hadj et al. and De blas et al. used the initial equations given by the manufacturer and confirmed that the initial values of R_{s0} and R_{sh0} are respectively the slope of the open-circuit point $^{\partial V_{oc}}/_{\partial I}$ and the slope of the short circuit point $^{\partial I_{sc}}/_{\partial V}$ (De Blas et al., 2002; Hadj Arab et al., 2004). Therefore, these techniques ensure a set of five equations whose accuracy depends totally on the choice of the initial conditions. Another method has employed experimental measurement to reduce the number of parameters, as reported by Chaibi et al. (Chaibi et al., 2018). The parameters are

extracted by using a measurement under a special condition with initial equations from the manufacturer datasheet. Applying this method to silicon PV cell technologies indicates higher performance for Monocrystalline and low relative errors for Polycrystalline (Chaibi et al., 2018). On the other hand, Villalva et al. estimated an arbitrary value of the ideality factor and used an iteration of the series and the shunt resistances until the datasheet peak power ($P_{max,e}$) coincides with the mathematical peak power ($P_{max,m}$). At this condition ($P_{max,m} = P_{max,e}$), the corresponding resistances are displayed and the other parameters are calculated using explicit equations (M. G. G. Villalva et al., 2009).

Recently, an improved version of the SDM has been proposed. Namely, the double-diode model (DDM); this latter has the same structure as the SDM but using two diodes instead of one diode. Thanks to its high performance, this model has been adopted lately by several authors (Alam et al., 2015; Attivissimo et al., 2013; Et-torabi et al., 2017; Ishaque et al., 2011a; Muhsen et al., 2015; Nassar-Eddine et al., 2016). However, the seven unknown parameters $\{I_L, I_{os1}, I_{os2}, R_s, R_{sh}, \gamma_1, \gamma_2\}$ makes the extraction process more complicated since it needs a set of seven equations to be solved. Therefore, researchers used different approximations to simplify the calculation. As one of the most cited work, Ishaque et al. estimated that the saturation currents are equal and gave an arbitrary value to both ideality factors, hence the number of unknown parameters have been reduced. It was reported that this technique presents a good performance at low irradiance changes (Ishaque et al., 2011a).

In the literature, some works reported the influence of the atmospheric conditions on the performance of the equivalent-circuit models during predicting the PV plant yields. In (Dehghanzadeh et al., 2017), Dehghanzadeh et al. reported that under the high variation of insolation the SDM is more effective compared to the DDM (Dehghanzadeh et al., 2017). While, Sangram et al. and Chin et al. demonstrate that under low insolation or shading conditions the DDM is more suitable (Bana and Saini, 2016; Chin et al., 2015).

2.3.2 PV Cell Equivalent Circuit Models

In order to evaluate the electrical performance of the PV cell, diverse equivalent-circuit models are simulated with the main objective to plot the corresponding I-V and P-V characteristics for different values of irradiance and temperature. The output current of the simplified single-diode model in Figure 2.21 is expressed by the following equation:

$$\boldsymbol{I = I_{sol} - I_{os}\{exp[A(V + IR_s) - 1]\}} \quad \textbf{(2.16)}$$

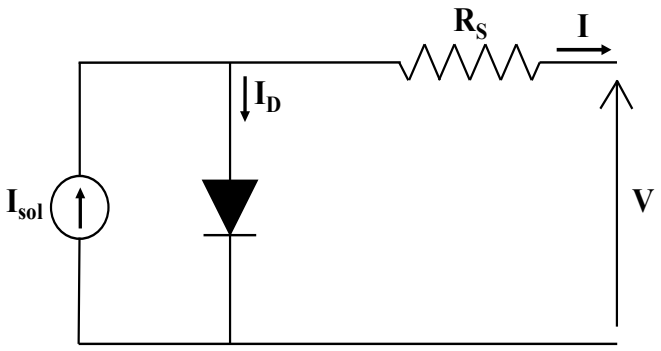

Figure 2. 21 Single-diode equivalent circuit model without the shunt resistance.

While the detailed single-diode model adds the shunt resistance (see Figure 2.1) and the output current of the PV cell is given by Equation (2.2).

For the double-diode model, shown in Figure 2.22, both the circulated currents in the diodes are expressed separately; hence the output current is given by the following equation:

$$\boldsymbol{I = I_{sol} - I_{os1}\{exp[A_1(V + IR_s) - 1]\} - I_{os2}\{exp[A_2(V + IR_s) - 1]\} - \frac{V+R_sI}{R_{sh}}} \qquad \textbf{(2.17)}$$

with $A_i = \frac{q}{\gamma_i k T N_{cell}}$

Where i is associated to the number of each diode, N_{cell} is the number of series cell that constitutes the PV module. For the various levels of irradiance and temperature, the plot the I-V and P-V curves requires the knowledge of the PV cell equivalent-circuit parameters.

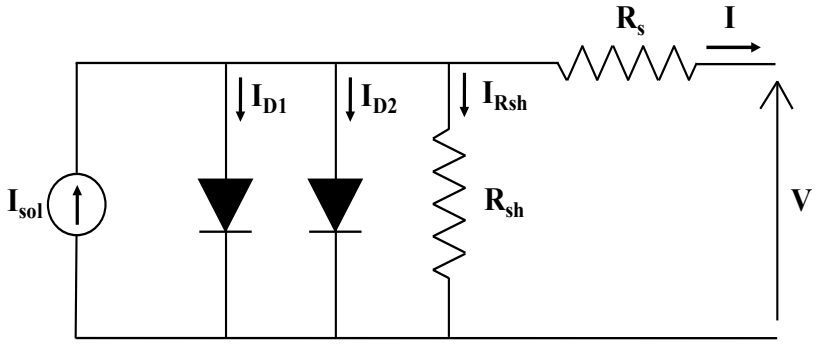

Figure 2. 22 Double-diode equivalent-circuit model

As can be seen in Equations (2.2), (2.16) and (2.17), the output current equations are composed of the electrical parameters and the outputs voltage of the PV module. These parameters are unknown which implies the use of an extraction technique with an accurate performance. For this reason, the method proposed in section 2.1 is used to extract the parameters of the SDM while the method suggested by Ishaque et al. (Ishaque et al., 2011a) technique is employed to determine the DDM parameters. In both methods, the current-generated value depends on the

variation of the irradiance and the temperature. This current is calculated by using equation (2.4) (Motahhir et al., 2018; Walker, 2001).

2.3.2.1 Method of Ishaque et al. (Ishaque et al., 2011a)

The double-diode configuration depicted in Figure 2.22 is another equivalent-circuit model used to evaluate the electrical performance of the PV panel. For this reason, several researchers have adapted some approximations to simplify the calculation process. As reported in (Ishaque et al., 2011a), Ishaque et al. estimated that the saturation currents are equal and used a modification on the equation given by (M. G. M. G. G. Villalva et al., 2009). the modified equation of the saturation current is represented as follows:

$$\boldsymbol{I_{os1} = I_{os2} = \frac{I_{sc}+K_i(T-298.15)}{exp[(V_{oc}+K_v(T-298.15))/\{^{\gamma_1+\gamma_2}/_{p}\}\frac{kTN_{cell}}{q}]}} \quad \textbf{(2.18)}$$

Where the values of the ideality factors γ_1 and γ_2 are taken respectively 1 and 1.2, for p the value is about (≤ 2.2). For R_s and R_{sh} estimation, the resistances are evaluated using an iteration process of the series resistance until achieving the peak power of the datasheet, and this shunt resistance is represented by Equation. (2.19).

$$\boldsymbol{R_{sh} = \frac{V_m+I_mR_S}{I-I_{os}\left[exp\left(\frac{V_m+I_mR_S}{\frac{kTN_{cell}}{q}}\right)+exp\left(\frac{V_m+I_mR_S}{(p-1)\frac{kTN_{cell}}{q}}\right)+2\right]-\frac{P_m}{V_m}}} \quad \textbf{(2.19)}$$

2.3.3 Methodology and data

The present work aims to analyze the performances of the SDM and the DDM under non-standard conditions in order to classify which model is more appropriate to use for different levels of solar irradiance and temperature.

For achieving the aim, it is first essential to analyze each electrical circuit separately. Hence, the selected methods to extract the parameters, Chaibi et al. (Chaibi et al., 2018)**;** and Ishaque et al. (Ishaque et al., 2011a) are implemented in MATLAB environment and applied to two silicon PV modules of different technology. These PV modules are the monocrystalline SM55 and the polycrystalline MSX60, respectively. The technical specifications of both models as given by the manufacturer are presented in Table 2.5 (BP MSX60, 2002; Shell, 2002). It is interesting to note that the choice of the PV panels is based on their widely availability in the market as they account for a share of 80% (Sudhakar Babu et al., 2016). The obtained I-V curves are compared to the data delivered by manufacturers for different levels of irradiance and temperature by using the relative error E_{rel}. It is defined as the difference in percentage

between an exact value from PV module manufacturer datasheet and the estimated one by using the equivalent-circuit models. This error is expressed by the following equation for each sample i-th.

$$\mathbf{E_{rel}}(\%) = \left|\frac{\mathbf{Base\ case(i) - Calculated(i)}}{\mathbf{Calculated(i)}}\right| * \mathbf{100} \quad \textbf{(2.20)}$$

Table 2. 5 Datasheet parameters of SM55 and MSX60 PV panels at STC (Standard Test Conditions).

Parameters	Mono-Si SM55	Poly-Si MSX60
P_m [W]	55	60
V_m [V]	17.4	17.1
I_m [A]	3.15	3.5
V_{oc} [V]	21.7	21.1
I_{sc} [A]	3.45	3.8
K_i [%/K]	0.04	0.06
K_v [%/K]	-0.35	-0.37
N_{cell}	36	36

We introduce a classification in order to identify which model to adopt for a given climate condition to get the best fit between two models SDM and DDM. So, a hybrid approach that combines the single and the double-diode models is suggested. It performs according to the climate variation and selects instantly which model with the lowest error to use between the single and the double diode model. This approach is explained in Figure 2.23.

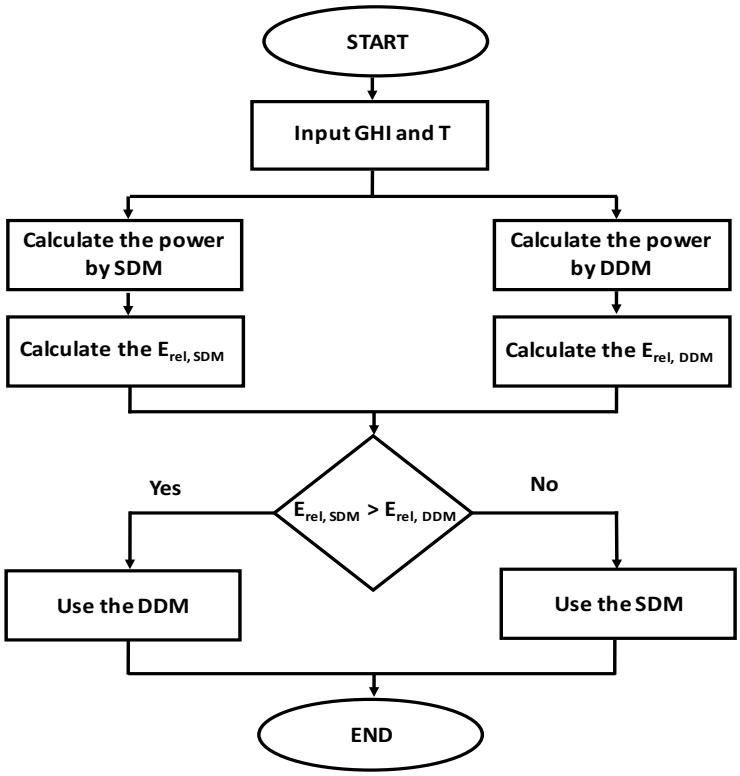

Figure 2. 23 Diagram of the proposed hybrid approach.

Thereafter, an experimental validation is carried out by using real hourly values of titled irradiance λ, cell temperature T and DC output powers (P_{DC}), recorded from 01/12/2017 to 23/12/2017 for a total of 529 samples, of two PV plants located in different climatic zones (Mediterranean (Brindisi, Italy) and Semi-continental (Meknes, Morocco).The installed PV systems are composed of 8 Poly-Si modules and can provide until 2 kW_p for the PV plant located in Meknes and 2.2 kW_p for the plant in Brindisi. The reason behind using these two PV plants is to investigate the performances of the outlined models under various climate fluctuations. Figure 2.24 shows the monthly average values of the horizontal plane irradiance and the ambient temperature over 1 year for each climate zone by using PVGIS website ("PVGIS," n.d.). As observed in this figure, the Semi-continental climate (SCC) has always a superiority in terms of irradiance and temperature values which makes this climate zone cold in winters and hot in summers. Otherwise, the Mediterranean climate is known by its rainy weather in winters and warm, dry in summers.

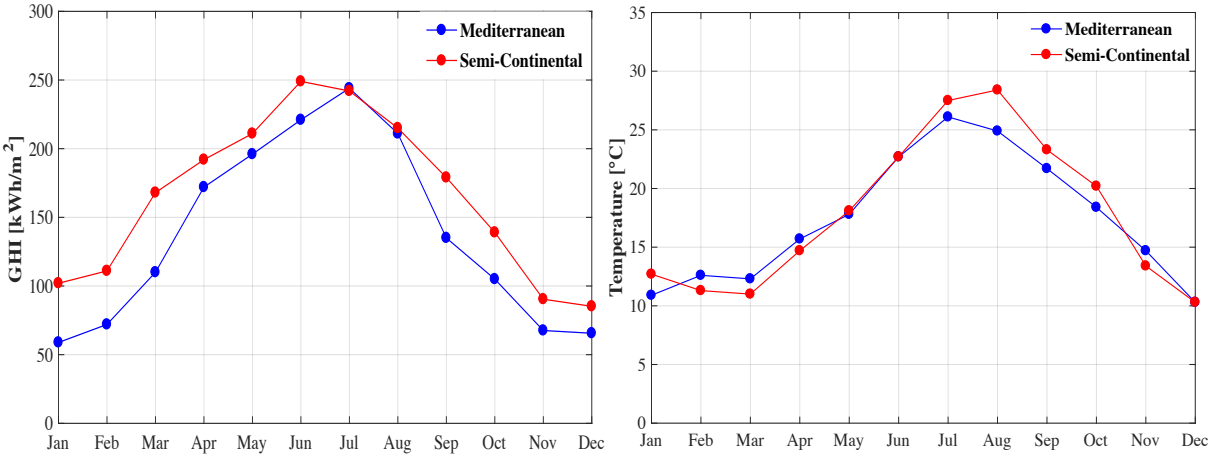

Figure 2. 24 Monthly average values of the horizontal plane irradiance and the ambient temperature for the Mediterranean and the semi-continental climate zone.

The performances of the hybrid approach are assessed by the normalized mean absolute error (NMAE), defined as the average of error between the exact value for the base case and the calculated values. This error can be represented as follows:

$$\mathbf{NMAE}(\%) = \frac{\mathbf{1}}{\mathbf{N}} \sum_{\mathbf{1}}^{\mathbf{N}} \left| \frac{\mathbf{Base\ case(i) - Calculated(i)}}{\mathbf{Max_1^N(Base\ case(i))}} \right| * \mathbf{100} \qquad \mathbf{(2.20)}$$

where N is the total number of samples. It measures the performance improvements achievable by using the hybrid approach with respect to the equivalent-circuit models SDM and DDM.

2.3.4 Results and discussion

The results discussion is divided into two parts:

- Comparison I-V curves, where the I-V characteristics for both Mono-Si and Poly-Si PV panel given by the manufacturer datasheets and by both SDM and DDM are analyzed by a performance evaluation under different conditions of solar irradiance and temperature;
- Implementation of the hybrid approach and its validation against real recorded data from two PV plants experiencing differences in hourly climatic variations, where a best combination of SDM and DDM is used.

2.3.4.1 Comparison of I-V curves

The parameters of the single-diode models are determined using the method proposed by Chaibi et al. (Chaibi et al., 2018) as given in Table 2.6. The double-diode model parameters according to the method suggested by Ishaque et al. (Ishaque et al., 2011a) are displayed in Table 2.7. The photo-generated current is calculated using Equation (2.4). Afterwards, the extracted parameters are inserted in the PV output current equations {Equations (2.2) and (2.17)} so as to plot the corresponding I-V and P-V characteristics of the tested PV models.

Table 2. 6 Extracted parameters using Chaibi et al. method for the single-diode model.

	R_{sh}[Ω]	R_s[Ω]	I_o[μA]	γ
Mono-Si	6500	0.1124	4.8244	1.7409
Poly-Si	7000	0.1880	1.1174	1.5079

Table 2. 7 Extracted parameters using Ishaque et al. method for the double-diode model.

	R_{sh}[Ω]	R_s[Ω]	γ_1	γ_2	$I_{o1} = I_{o2}$ [A]
Mono-Si	144.24	0.34	1	1.2	$4.7039 .10^{-10}$
Poly-Si	166.58	0.47	1	1.2	$2.2324 .10^{-10}$

The I-V curves obtained by the previous methods should agree well with those given by the manufacturer datasheets. Figure 2.25 and Figure 2.26 display the I-V characteristics of the Mono-Si PV panel for various values of irradiance and temperature. It is clear that both curves match perfectly with each other, especially in Figure 2.26 where the temperature varies from 20 °C to 60 °C with a step of 10 °C and the irradiance is fixed at 1000 W/m^2. However, a small difference is observed in Figure 2.25 especially at the irradiance value of 200 W/m^2. Moreover, the application of Chaibi et al. method on the Poly-Si PV panel is given in Figure 2.27, the plotted I-V curves are compared to the datasheet values for a variation of temperature from 0 °C to 75 °C with a step of 25 °C and at fixed irradiance (λ=1000 W/m^2). As can be shown in these figures, the shape of the I-V curves agrees well with manufacturer for temperature levels less than 50 °C, but when the temperature exceeds 50 °C, the I-V form starts to present a significant difference.

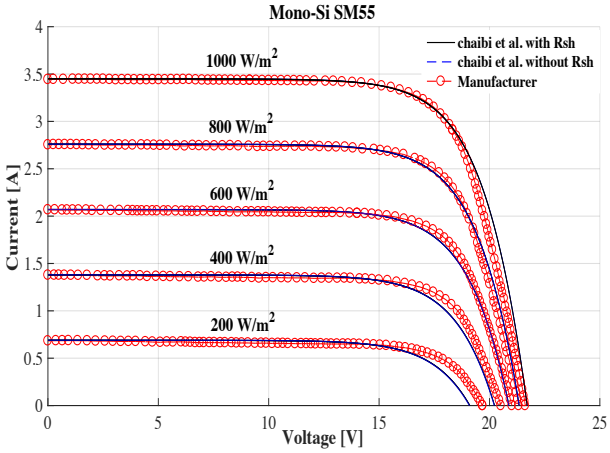

Figure 2. 25 Comparison of the plotted I-V characteristics using Chaibi et al. method and manufacturer data of the Mono-Si SM55 PV panel for different irradiances, T = 25 °C.

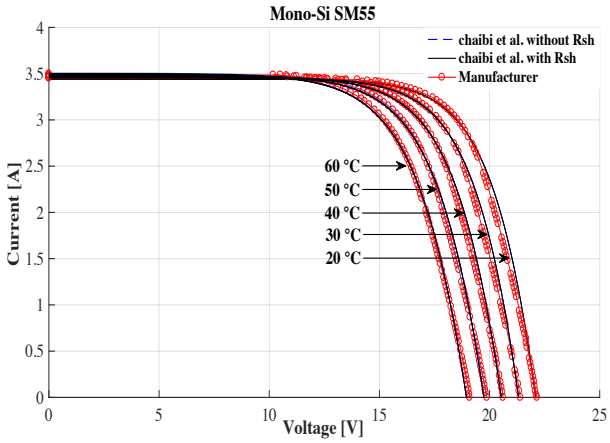

Figure 2. 26 Comparison of the plotted I-V characteristics using Chaibi et al. method and manufacturer data of the Mono-Si SM55 PV panel for different temperatures, λ = 1000 W/m2.

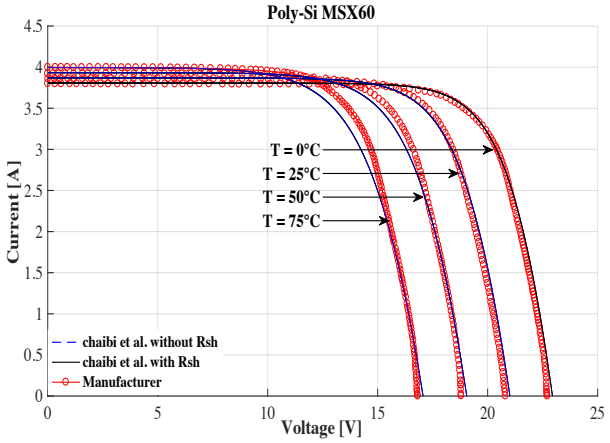

Figure 2. 27 Comparison of the plotted I-V characteristics using Chaibi et al. method and manufacturer data of the Poly-Si MSX60 PV panel for different temperatures, λ = 1000 W/m2.

In the same way, the plotted I-V curves of the double-diode model using Ishaque et al. (Ishaque et al., 2011a) method are evaluated for both PV technologies. As displayed in Figure 2.28 and

Figure 2.29, the use of the double-diode model in the case of Mono-Si technology shows little differences between the obtained I-V curves and the manufacturer graphs, especially in Figure 2.29 for which the temperature is supposed to vary considering a constant value of solar irradiation (λ=1000 W/m^2). However, the application of the double-diode model in the case of Poly-Si PV technology (see Figure 2.30) exhibits a quite similar trend in the I-V curves for all temperatures less than 50 °C. Based on this, it seems that the single-diode model is more preferable to model the Mono-Si PV panels while the double-diode model is more appropriate for Poly-Si PV panels. Note that the I-V curves of the Poly-Si module for different irradiance levels are not provided due to the lack of information on the irradiance variation from manufacturer.

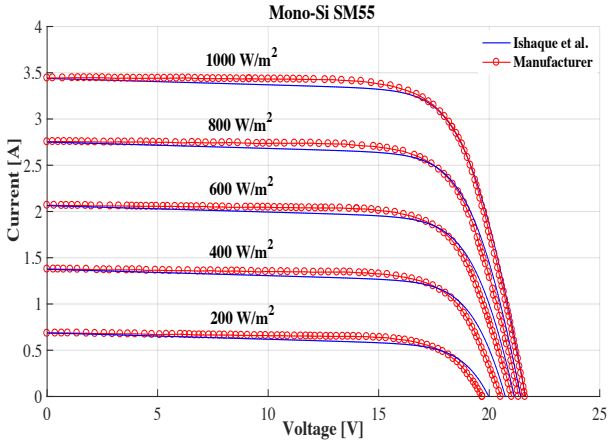

Figure 2. 28 Comparison of the plotted I-V characteristics using Ishaque et al. method and manufacturer data of the Mono-Si SM55 PV panel for different irradiances, T = 25 °C.

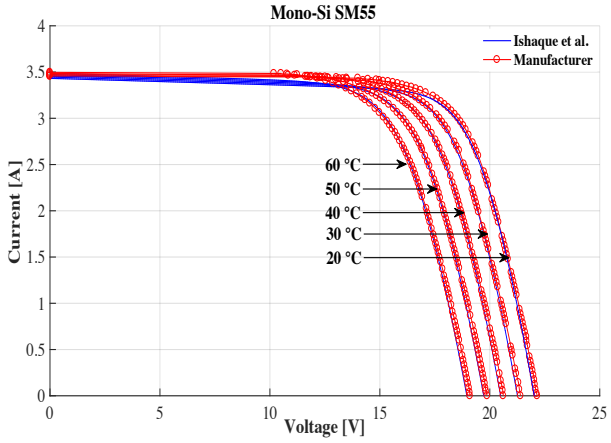

Figure 2. 29 Comparison of the plotted I-V characteristics using Ishaque et al. method and manufacturer data of the Mono-Si SM55 PV panel for different temperatures, λ = 1000 W/m2.

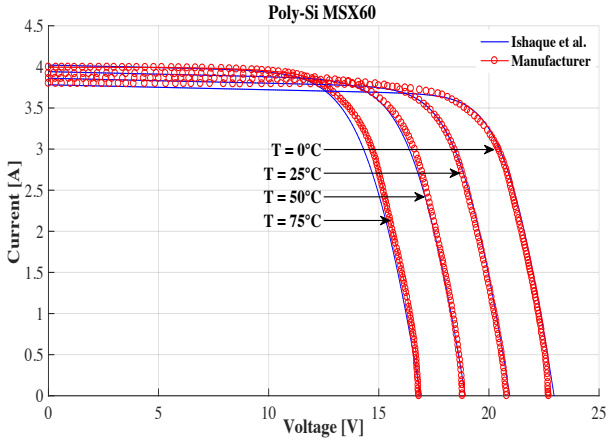

Figure 2. 30 Comparison of the plotted I-V characteristics using Ishaque et al. method and manufacturer data of the Poly-Si MSX60 PV panel for different temperatures, λ = 1000 W/m2.

In order to evaluate the differences between the characteristic points of the PV panel $\{I_{sc}, V_{oc}, P_m\}$ using two equivalent-circuit models (SDM and DDM) and the values extracted from manufacturer datasheet for different weather conditions, we identify three intervals (Low, Medium and High) of irradiance and temperature. For the irradiance, the low values class is below 400 W/m^2, the medium one is between 400 W/m^2 and 800 W/m^2 and the high values class is above 800 W/m^2. For the temperature changes, the low variations are below 25 °C, the medium one are between 25 °C and 40 °C and the last class is for temperatures above 40 °C.

As a first step, the manufacturer I-V curves are used to calculate the corresponding power for each change of climate condition. Based on the climate variations, the relative error is computed using Equation (2.20), where the base case represents the extracted value from manufacturer curves and the calculated one corresponds to the computed values using the SDM and the DDM. These are displayed in Figure 2.31. Based on this categorization, Figure 2.31(a) gives the relative errors of the PV panel output power for the used models at each level of atmospheric conditions. As noticed in Figure 2.31(a), the SDM is more reliable to model the PV panel for low temperature ranges. However, the double-diode model shows good results in medium and high temperature ranges. Furthermore, it can be seen that the double-diode model performs well with low and medium irradiances whereas the single-diode model is more convenient with high irradiance variations.

Besides, in Figure 2.31(b) the relative errors of the open-circuit voltage of the equivalent-circuit models of both PV panel technologies are presented for different levels of temperature and irradiance. As can be seen, the single-diode model seems to be very appropriate to model the Mono-Si modules because of its lower error compared to the double-diode model. On the

opposite side, the double-diode model presents a key solution to model the Poly-Si PV panel especially for medium and high levels of temperature. Moreover, the SDM present good predicted results for low irradiances while the DDM is more pertinent for medium and high ranges of irradiance. For the short-circuit current, the chosen equivalent-circuit models are compared under the same variation of climate conditions and this is for both PV panel technologies. As can be seen in Figure 2.31(c), the relative errors demonstrate that the single-diode model is more appropriate to model the PV panel under the variation of irradiance. Also, this model is more appropriate for temperature variation except for the Poly-Si technology in high temperature changes. Briefly, these curves show that the low irradiance levels engender high errors in the PV output power with a value of 8.40 %. Hence, the lowest value of error is presented at the short circuit currents with a value close to 0 %.

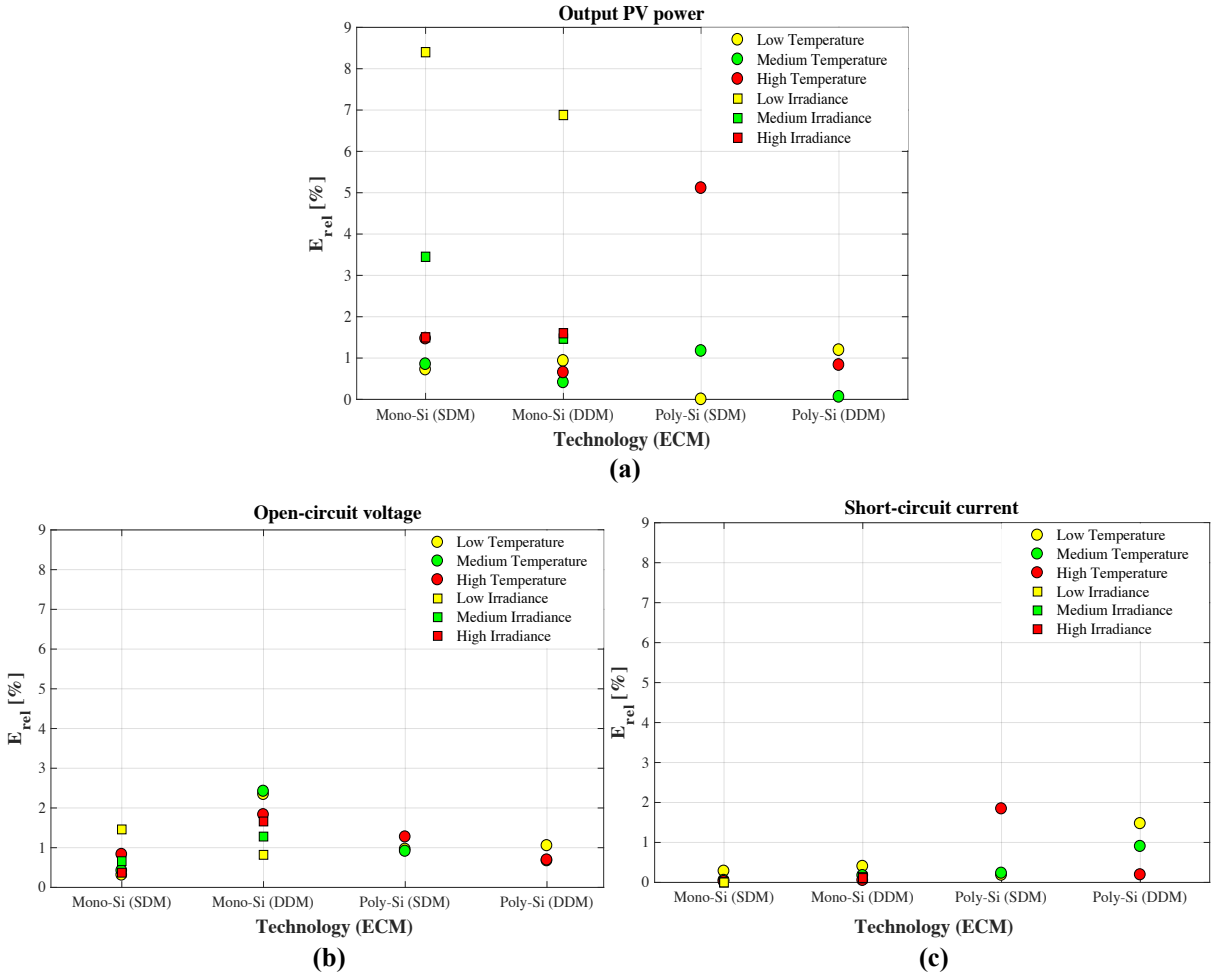

Figure 2. 31 Relative error of (a) the PV output power, (b) the open-circuit voltage, (c) the short circuit current using the SDM and the DDM for different levels of atmospheric conditions. Base case: extracted values from Datasheet.

Such analysis enables the clustering of the performance for both single-diode and double-diode model in different level range of irradiance and temperature according to the flowchart in

Figure 2.23. So, a classification (See Tables 2.8), proposes guidelines in selecting the model to be used in the simulation process with respect to the actual climate condition to achieve the lowest error.

Table 2. 8 Performance classification of equivalent-circuit models for different levels of irradiance and temperature.

	Irradiance			Temperature		
	Low	**Medium**	**High**	**Low**	**Medium**	**High**
Power	DDM	DDM	SDM	SDM	DDM	DDM
Voltage	DDM	SDM	SDM	SDM	SDM	DDM
Current	SDM	SDM	SDM	SDM	SDM	DDM

2.3.4.2 Implementations of the hybrid approach and validation

A comparison of predicted DC outputs and real experimental data, on an hourly basis is carried out. In order to investigate the impact of the climatic condition on the performance of both SDM and DDM, the experimental titled irradiance and modules temperature of both PV plants are utilized to compute the corresponding SDM and DDM powers. Thereafter, the obtained output data series are used to calculate the error between the real generated powers (base case) and the computed ones (SDM and DDM power) using the error formula in Equation (2.20). These errors are presented in Figure 2.32. As can be observed in this figure, the mean error results supports the findings of the previous subsection about the relationship between climate conditions and accuracy of single and double diode model which was summarized in Table 2.8.

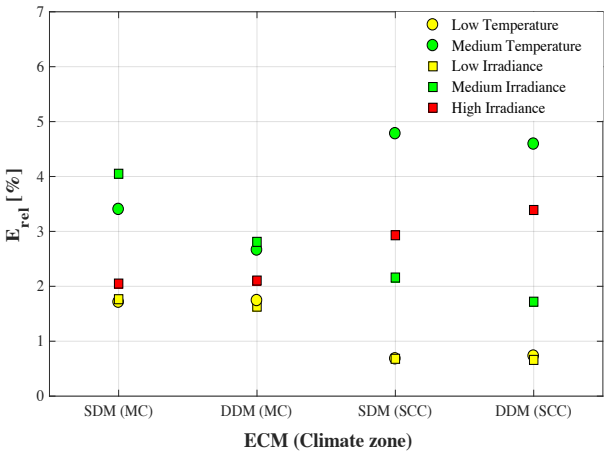

Figure 2. 32 Normalized mean error values of the SDM and the DDM under the variation of the atmospheric condition of The Mediterranean climate (MC) and the Semi-Continental Climate (SCC).

The previously introduced classification in Table 2.8 is used to build a hybrid approach which selects the most suitable model for computing of DC powers based on the actual atmospheric

condition of the two climate zones (Mediterranean and the Semi-continental-climate). These powers are utilized to calculate the normalized absolute mean errors (see Equation(2.20)) between the experimental DC powers and the calculated ones using the hybrid approach for each one of the PV plants. These errors are displayed in Figure 2.33. As can be seen in Figure 2.33(a), the NMAE between hybrid approach and SDM and DDM is significantly high because of the fluctuated cloudy weather of the Mediterranean climate. Furthermore, this approach decreases the error for to up 53.93% for irradiance variations and 49.52% for temperature variations. For the Semi-Continental PV plant in Figure 2.33(b), the NMAE seem to lower compared to Mediterranean PV plant due to the sunny behavior of Meknes city. Moreover, the proposed approach can respectively reduce the error due to irradiance and temperature variations by 21.04% and 14.66%.

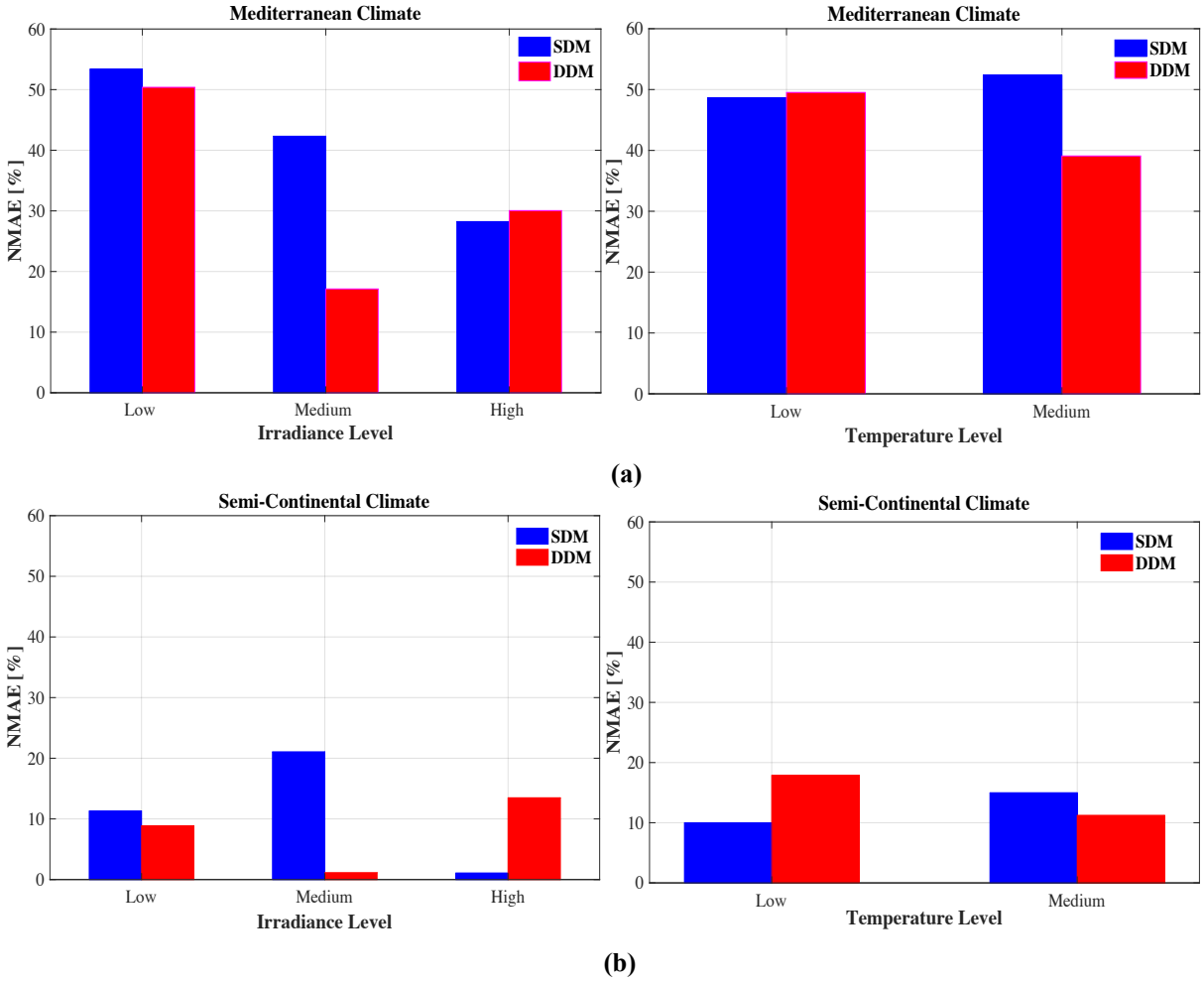

Figure 2. 33 Relative error between the hybrid approach and the SDM and DDM of (a) the Mediterranean and (b) the Semi-continental PV plant for different level of climate conditions. Base case: Hybrid approach.

2.4 Conclusion

This chapter described the modelling of the PV module. For this reason, a new method for the extraction of the equivalent circuit parameters of the PV cell single diode model is presented. The proposed method consists in measuring the shunt resistance R_{sh} and using the manufacturers rated data to calculate the other unknown parameters. The advantage of the proposed method is the use of an experimental measure which does not influence on the other parameters in the case of measurement error. In fact, this measure reduces the number of the unknowns, which simplifies the calculation and the resolution of the equations. The accuracy is proved by comparing the proposed method with manufacturer data, PVsyst software and relevant reference from literature under different weather conditions, these comparisons shown that the proposed method has a fast extraction time and can be applied for different types of solar panels. Thereafter, section 2.2 evaluates the exact electrical performance of the most utilized PV cell equivalent-circuit models. The single-diode and the double-diode models are applied to the commercialized silicon PV module technologies (Monocrystalline SM55, Polycrystalline MSX60). The study outlines the comparison of these models considering the manufacturer's variation of irradiance and temperature. The comparison results demonstrate that the single-diode model seems to be more suitable for high fluctuations of irradiance. In turn, the double-diode model is more reliable for prediction the performance under the medium and low irradiance variations. Furthermore, for the temperature variations, the SDM performs well with low fluctuations and the DDM is more appropriate for medium and high variations.

Therefore, the main research question of this chapter is to assess to which extent an hybrid approach based on both models can enhance the accuracy of PV output prediction.. This approach has the idea to switch to the appropriate model according to the instantaneous variation of solar irradiance and temperature. The performance of the hybrid approach was assessed by computing real atmospheric data of two PV systems implemented in two sites of different climatic zones. An error analysis was performed between the proposed hybrid approach and the conventional SDM and DDM models. The results show that the proposed approach decreases the computing error compared to the SDM and the DDM by up to 53.93% in the case of the cloudy weather conditions and by about 21.04% for sunny climatic conditions.

CHAPTER3 : Principal MPPT Techniques: Study and Choice.

3.1 Motivation

As it has been reported in the previous chapter, the electrical behavior of the PV module depends totally on the variation of the atmospheric conditions (namely the irradiance and the temperature). Moreover, the power-voltage curve of the PV panel is known by its nonlinearity. For these reasons, the need to extract the maximum available power of the panel requires the tracking of the maximum power point instantly.

In this chapter, the effect of MPPT algorithm on the net energy output of solar PV modules is investigated. For this end, three different MPPT algorithms are tested. The innovative aspect met in this chapter is the utilization of real climatic conditions evaluated for duration of one complete year (8760 running hours). A strong calculation effort has been made, as it was essential to fit hourly data to comply well with the time step used in the simulation process. To the best of knowledge of authors, although there are many published papers comparing various MPPT control techniques, a realistic approach to quantify the differences induced in the associated energy yields is missed.

The current chapter establishes an annual comparative simulation of three MPPT techniques in order to study the generated energy of each technique. Section 3.2 reviews some MPPT used in literature. Thereafter, Section 3.3 shows a modelling of the used PV system. Then, the chosen MPPT techniques are presented in Section 3.4. the simulations and results are given in Section 3.5. Finally, we give some concluding remarks.

3.2 Review of Maximum Power Point Tracking Techniques

The weakness of PV systems lies in the low conversion efficiency because of the nonlinearity behavior of the PV cell. This requires the use of maximum power point tracking (MPPT) controllers with the aim of forcing the PV panel to operate at its maximum power point (MPP) despite the changes in outdoor climatic conditions (Allouhi et al., 2016). Mathematically, to ensure the function of maximizing the PV power, a derivative of the PV power P_{pv} with respect to the PV voltage V_{pv} must converge to zero $\frac{\partial P_{pv}}{\partial V_{pv}} = 0$ (Gao et al., 2013; Ikegami et al., 2001). For this reason, several algorithms have been developed and improved (Dileep and Singh, 2017; Gupta et al., 2016; Salas et al., 2006). The most popular one is the classical perturb and observe (P&O) method (Alik and Jusoh, 2018, 2017); this technique is based on perturbing the PV voltage and observing the MPP variation, the history of this method is known by its several improved versions. Starting with the variable step P&O, where the perturbation is adapted to the operating point area. As reported in (Kollimalla et al., 2014),

Kullimalla et al. adjusted the step size to raise the tracking speed and to reduce the oscillating, this adaptive method shown an operating point closer to the MPP and presented a fast response compared to conventional algorithms, furthermore, other researchers such as Hong et al. has developed an adaptive step size according to the error $\frac{\Delta P}{\Delta V}$ (Hong et al., 2015), this solution presented a high tracking performance with low power losses compared to other P&O algorithms. Although, these improved versions of the P&O have arrived to ameliorate the tracking performance but the oscillating around MPP stills the principal cause of energy losses, especially in fast irradiance change. To overcome this issue, other techniques such as the incremental conductance (IC) are required (Motahhir et al., 2017; Tey and Mekhilef, 2014). The IC tracks the MPP by comparing instantly the conductance $\left(-\frac{I}{V}\right)$ with the incremental conductance $\left(\frac{\Delta I}{\Delta V}\right)$ of the PV module (Motahhir et al., 2017). To perform at the MPP, both quantities must be equal. For this reason, the IC method presented the conventional version with a fixed step adapted to the $\frac{\Delta P}{\Delta V}$ operating zone (Loukriz et al., 2016). Unfortunately, the fixed step IC shown a low response under fast irradiance change. Then, Incremental Conductance with variable step corrected partially this problem and becomes widely used. Lui et al. (Liu et al., 2008), Emad et al. (Ahmed and Shoyama, 2011) used the variable step, where the slope of the P-V characteristic is multiplied with the fixed step, which enhanced the tracking speed and shown a superiority compared to the conventional fixed step algorithms. As a result, most of improved version of this technique corrected partially the problem of oscillation and shown a remarkable performance under fast change of atmospheric conditions.

In order to improve the sensitivity of the PV module at the optimal point, artificial intelligence as fuzzy logic (Chen et al., 2016; Radjai et al., 2014); and neuron network algorithms are used (Kulaksiz and Akkaya, 2012). However, the complexity of these methods makes them hard to implement in real life since they need high-performance calculator to ensure the maximum power tracking operation. Accordingly, to have a good compromise between efficiency and cost, numerical theories such as Backstepping and Sliding mode are employed to build an improved MPPT that satisfy the conditions of both good performance and low-cost (Salas et al., 2006).

The sliding mode MPPT (SM-MPPT) is a nonlinear control technique based on the design of a control law that forces the system trajectory to reach the sliding surface. Thanks to its advantages such as a robust behavior in the presence of external variation and the simplicity of implementation. In literature, various controllers have been proposed (Bianconi et al., 2013;

Kim, 2007; Mamarelis et al., 2014). Dahech et al. proposed a robust controller using both the Backstepping and the sliding mode and this hybrid method offered a MPPT controller with high efficiency and low error of tracking (Dahech et al., 2017). Moreover, an adaptive SM-MPPT has been proposed by Koofigar et al. with the aim objective to overcome all the problem caused by external uncertainties, this improved method shown a very high performance of tracking even with fast climate variations (Koofigar, 2016). Hence, most of MPPT based on sliding mode show a very high performance and stability with fast atmospheric changes.

3.3 PV System Modeling

The reason behind testing the MPPT techniques requires the use of a simple PV system. For this, the proposed topology in Figure 3.1 is used. This topology is composed of a photovoltaic array composed of many modules in series and in parallel. The output current of this PV array is given by the following equation:

$$I_{pvg} = N_p I_{sol} - N_p I_{os}\left\{exp\left[\frac{A}{N_s}\left(V_{pv} + I_{pv}R_s\frac{N_s}{N_p}\right) - 1\right]\right\} - \frac{V_{pv}+I_{pv}R_s\frac{N_s}{N_p}}{R_{sh}\frac{N_s}{N_p}} \quad (3.1)$$

where N_p and N_s are respectively the number of module in series and in parallel.

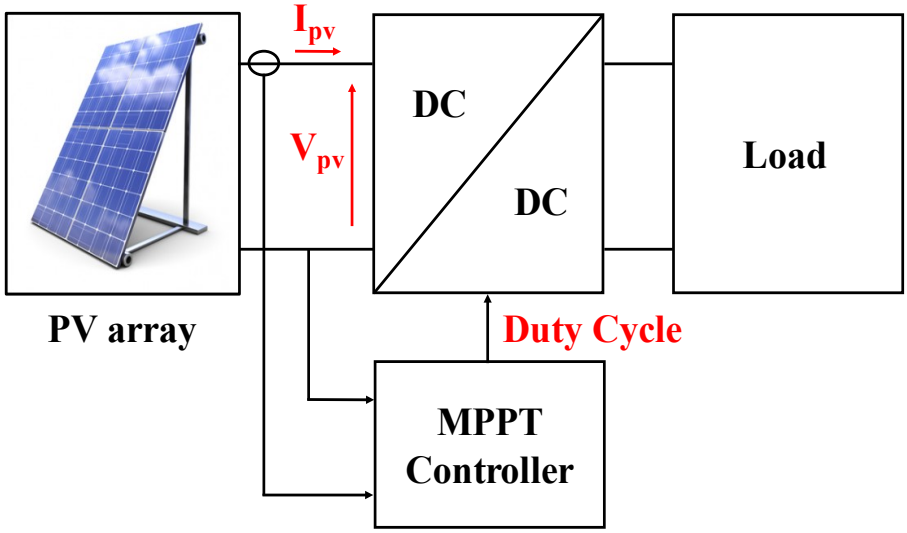

Figure 3. 1 Used configuration of the PV system.

3.3.1 DC-DC Converter

DC-DC boost converter is an adaptation stage mostly used after the PV array in order to adjust the supplied voltage to the load, another function of this converter is allowing the PV system to perform at its MPP by acting on the cyclic duty D, this task is executed by the boost capability of delivering an output voltage V_{DC} larger than the input one V_{pv} (Kchaou et al., 2017). This voltage is defined as:

$$\boldsymbol{V_{DC} = \frac{V_{pv}}{1-D}} \quad \textbf{(3.2)}$$

Figure 3.2 shows the used configuration of the boost converter. The system in state average values can be written as:

$$\begin{cases} \frac{\partial v_{pv}}{\partial t} = \frac{1}{C}\left(i_{pv} - i_L\right) \\ \frac{\partial i_L}{\partial t} = \frac{1}{L}\left[v_{pv} - (1-D)v_{DC}\right] \\ \frac{\partial v_{DC}}{\partial t} = \frac{1}{C_{DC}}\left[i_L(1-D) - i_o\right] \end{cases} \quad \textbf{(3.3)}$$

where v_{pv}, v_{DC}, i_L and i_o are respectively the PV voltage, the boost output voltage, the inductor current and the boost output current, C and L represent the input capacitor and inductor of the converter and C_{DC} is the output capacitor.

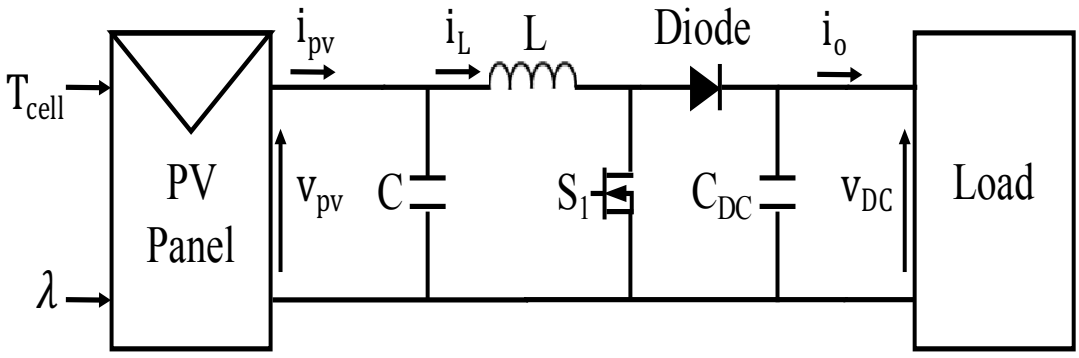

Figure 3. 2 Schematic of the DC-DC boost converter.

3.4 MPPT Techniques

3.4.1 Perturb and Observe (P&O)

The P&O algorithm is an iterative technique performed by perturbing the measured voltage V_{pv} with ΔV until reaching the PV power P_{pv} to its MPP. The P-V characteristic is divided into three operating regions as follows (Alik and Jusoh, 2018):

- If $\frac{\partial P_{pv}}{\partial V_{pv}} > 0$: the operating point is on the left of the MPP

- If $\frac{\partial P_{pv}}{\partial V_{pv}} < 0$: the operating point is on the right of the MPP

- If $\frac{\partial P_{pv}}{\partial V_{pv}} = 0$: the operating point is at the MPP

The flowchart of the P&O algorithm is presented in Figure 3.3. As can be seen, the process of extracting still working even after reaching the MPP which causes oscillation around this point infinitely (Alik and Jusoh, 2017).

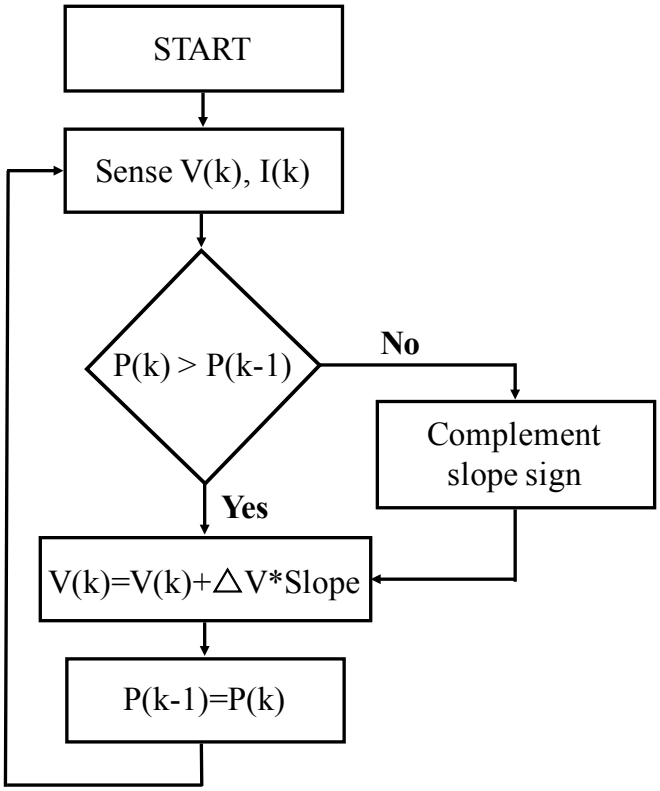

Figure 3. 3 Flowchart of the Perturb and Observe algorithm.

3.4.2 Incremental Inductance (IC)

The incremental conductance technique is developed to correct partially the oscillation problem caused by different iterative techniques. The idea behinds the IC method is to compare the PV conductance $\left(\frac{I_{pv}}{V_{pv}}\right)$ with the derivative conductance $\left(\frac{\Delta I_{pv}}{\Delta V_{pv}}\right)$ instantly (Barth et al., 2016). The operating zones are given as follows (Tey and Mekhilef, 2014):

- If $\frac{\Delta I_{pv}}{\Delta V_{pv}} > -\frac{I_{pv}}{V_{pv}}$: the operating point is on the left of the MPP

- If $\frac{\Delta I_{pv}}{\Delta V_{pv}} < -\frac{I_{pv}}{V_{pv}}$: the operating point is on the right of the MPP

- If $\frac{\Delta I_{pv}}{\Delta V_{pv}} = -\frac{I_{pv}}{V_{pv}}$: the operating point is at the MPP

Figure 3.4 gives the flowchart of the incremental conductance which respects previous conditions. As reported in precedent works (Ahmed and Shoyama, 2011; Liu et al., 2008; Loukriz et al., 2016), the main advantage of this technique is the good performance under fast-changing climate conditions and a lower oscillation around the MPP comparing to the P&O

technique. However, the weakness of this method is the inability to achieve the zero-point condition which causes some power losses (Loukriz et al., 2016).

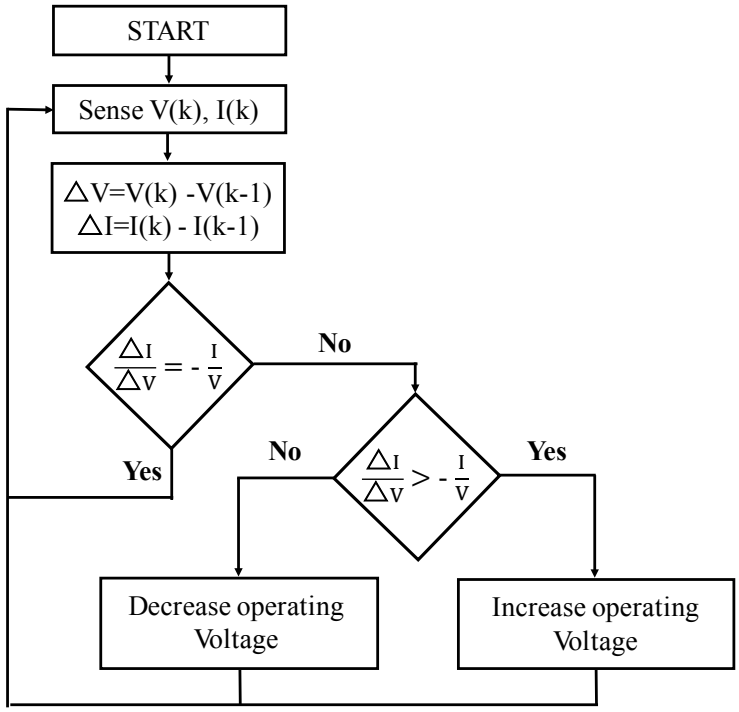

Figure 3. 4 Flowchart of the Incremental Conductance algorithm.

3.4.3 Sliding Mode MPPT

The sliding mode theory allows to design MPPT controller with a robust behavior in presence of external disturbances such as temperature and irradiance variations. This method consists in varying the state trajectory of the system to a predefined sliding surface (Kim, 2007; Tey and Mekhilef, 2014). This function is achieved by developing a control law which forces the output $y = \frac{\partial P_{pv}}{\partial V_{pv}}$ to converge to zero (Kim, 2007). The methodology of the sliding mode is presented as follows:

First, choosing a sliding surface, also called the switching surface which depends on the relative degree r of the system and the output y. For the used PV system in Figure 3.2, this surface can be expressed by Equation. (3.4):

$$\boldsymbol{\sigma = \dot{y} + \beta y} \tag{3.4}$$

and

$$\boldsymbol{\dot{\sigma} = \ddot{y} + \beta \dot{y}} \tag{3.5}$$

where $\dot{y}$ and $\ddot{y}$ are respectively the first and the second time derivative of the output y and β is a positive constant. The time derivative of the sliding surface can be rewritten as under the following form:

$$\dot{\sigma} = f + gu \tag{3.6}$$

with $u = \frac{1}{1-D}$

Then, designing of the control law in order to ensure the stability of the system, the Lyapunov function defined by $V = \frac{1}{2}\sigma^2$ is adopted, only the $\dot{V} < 0$ allows the stability.

By choosing the dynamic function as : $\dot{\sigma} = -m\ sign(\sigma)$.

$$\dot{V} = -m|\sigma| \tag{3.7}$$

From precedent equations, the control law is given by:

$$\begin{cases} u = -\frac{f+m.sign(\sigma)}{g} \\ D = 1 + \frac{g}{f+m.sign(\sigma)} \end{cases} \quad \text{with} \quad m > 0 \tag{3.8}$$

3.5 Simulation Results

The performance of any PV system depends on its behavior under atmospheric variations such as the change of irradiance, temperature and wind velocity. For this reason, a PV array composed of 100 PV modules with the datasheet parameters in Table 3.1 has been simulated under real climatic data of Fez, Morocco.

Table 3. 1 Datasheet parameters of the SM55 and the SW255 PV panels at STC.

Parameters	Mono-Si SM55	Poly-Si MSX60
$\mathbf{P_m}$ **[W]**	55	60
$\mathbf{V_m}$ **[V]**	17.4	17.1
$\mathbf{I_m}$ **[A]**	3.15	3.5
$\mathbf{V_{oc}}$ **[V]**	21.7	21.1
$\mathbf{I_{sc}}$ **[A]**	3.45	3.8
$\mathbf{K_I}$ **[%/K]**	0.04	0.06
$\mathbf{K_v}$ **[%/K]**	-0.35	-0.37
$\mathbf{N_{cell}}$	36	36
$\mathbf{N_s}$	20	20
$\mathbf{N_p}$	5	5
$\mathbf{A_m}$ **[m²]**	0.42	0.55
$\boldsymbol{\eta_{ref}}$ **[%]**	12.89	10.80

Hourly meteorological data were exported from METENORM software. The first set of results pertains power outputs of PV array on a daily basis. Later, an overall comparison in terms of

net energy output generated from PV modules operating with the MPPT techniques presented in Section 3.4.

3.5.1 Daily Analysis

In Figure 3. 5, climatic variations of the first day of each season are presented. Because the PV system is tested under the change of the irradiance and cell temperature, the cell temperature calculations are based on the model given by Duffie et al. (Duffie et al., 2003)**:**

$$\boldsymbol{T_{cell} = T_a + \frac{\lambda}{800}(T_{NOCT} - 20)\left(1 - \frac{\eta_{ref}}{\alpha\tau}\right)\frac{9.5}{5.7+3.8v_w}} \quad \textbf{(3.9)}$$

where, T_a is the ambient temperature, T_{NOCT} is the nominal operating cell temperature defined at ($\lambda = 800\ W/m^2,\ T_a = 20°C, v_w = 1\ m/s$), η_{ref} is the reference module efficiency, $\alpha\tau$ is the transmittance-absorbance product and v_w is the wind velocity (Duffie et al., 2003).

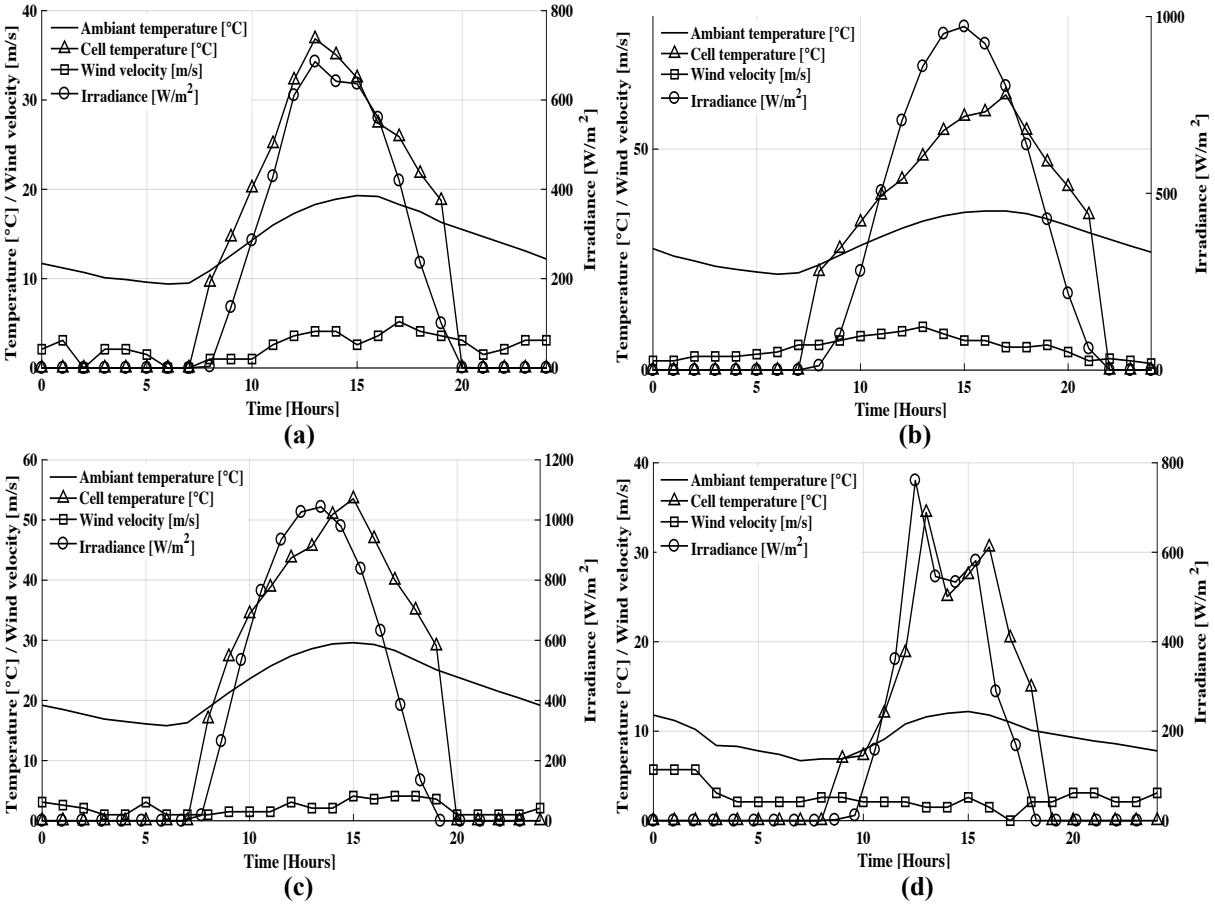

Figure 3. 5 Different daily atmospheric conditions for **(a)** March 21, **(b)** June 21, **(c)** September 21, **(d)** December 21.

Table 3.2 gives the maximum values of the used climate conditions for each day. As shown from this table, for September 21, the maximum incident irradiance is about 1043.4 W/m^2. For the other atmospheric conditions, June 21 recorded the maximum values of the ambient temperature, cell temperature and the wind speed. The corresponding values are respectively,

36°C for ambient temperature, 62.27°C for cell temperature and 9.8 m/s for the wind speed. In addition, the coldest scenario, presented by December 21 shows minimum values of ambient and cell temperatures as well as incident solar radiations.

Table 3. 2 Maximum values of atmospheric condition for the used days.

	March 21	**June 21**	**September 21**	**December 21**
λ_{max} $[W/m^2]$	686.03	971.96	1043.40	760.53
$T_{a_{max}}$ [°C]	19.20	36	29.6	12.2
$T_{cell_{max}}$[°C]	36.85	62.27	53.52	34.45
$v_{w_{max}}$ [m/s]	5.2	9.8	4.1	5.7

In order to evaluate the proposed MPPT controllers, the generated power from the Monocrystalline SM55 PV array is provided in Figure 3.6. This output corresponds to the climatic data previously presented. As can be observed, the SM-MPPT presents a remarkable superiority in terms of level of power tracking and this is true independently of the examined day. However, the P&O MPPT and the IC-MPPT exhibit approximately the same profiles for all the seasons except for the first day of the winter because of the rapid fluctuations of cell temperature and irradiance. As seen in the Figure 3.6(d), the P&O technique shows high tracking performance compared the IC one.

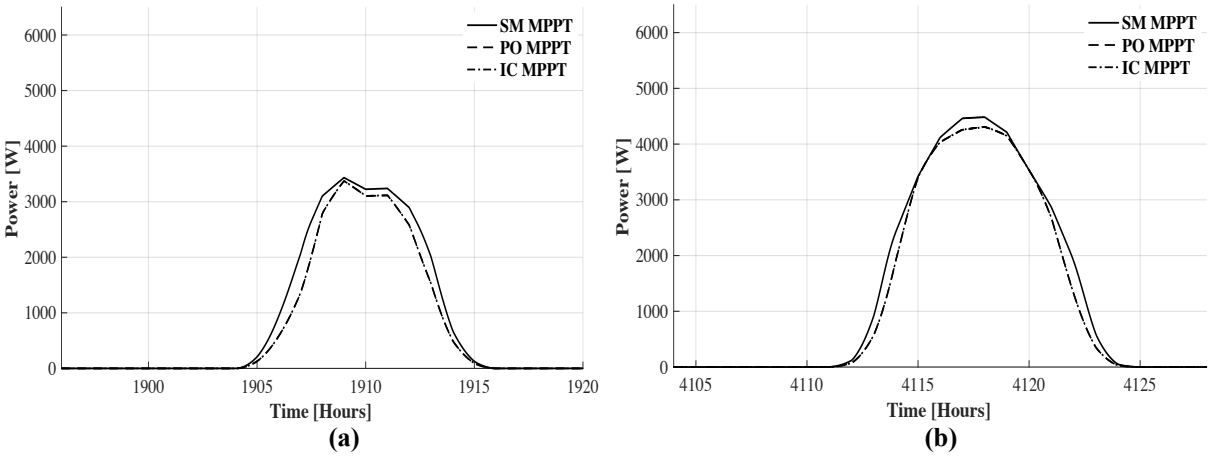

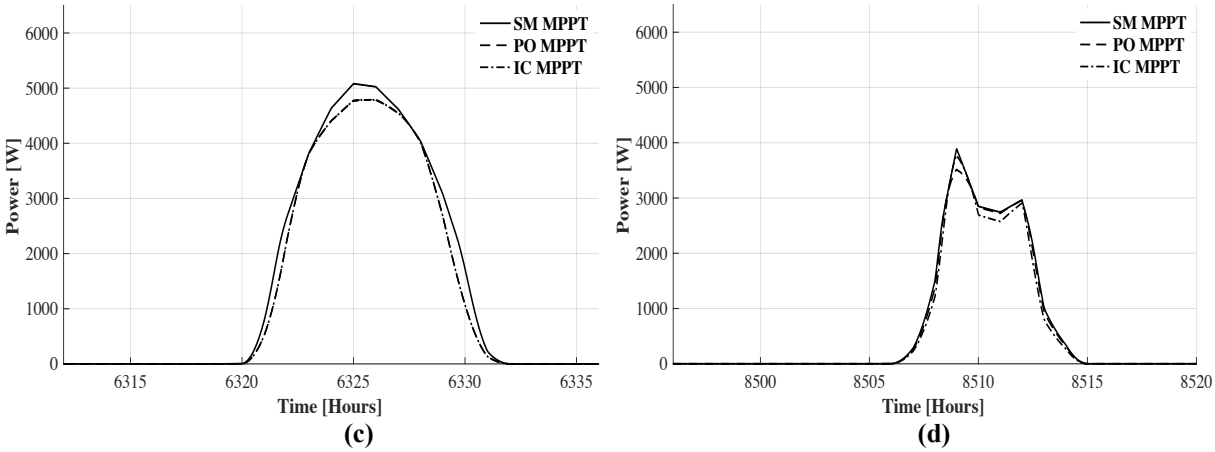

Figure 3. 6 Daily generated power using different MPPT techniques on the Mono-Si PV array SM55 for **(a)** March 21, **(b)** June 21, **(c)** September 21, **(d)** December 21.

Another performance index to be assessed is the real electric efficiency which can be computed using the following Equation:

$$\boldsymbol{\eta = \frac{P_{pv}}{A_m \lambda}} \tag{3.10}$$

where A_m represents the surface of the module. According to SAM software (Gilman, 2015), the nominal efficiency module of the Mono-Si SM55 is about 12.89%. In Figure 3.7, it is noticed that the SM-MPPT reaches rapidly the steady-state of the efficiency and remains around the nominal value. For the P&O and the IC MPPT, the efficiencies are similar except for the winter day because of the fast changes of temperature and irradiance. Also, the P&O shows slightly better efficiency compared to IC method.

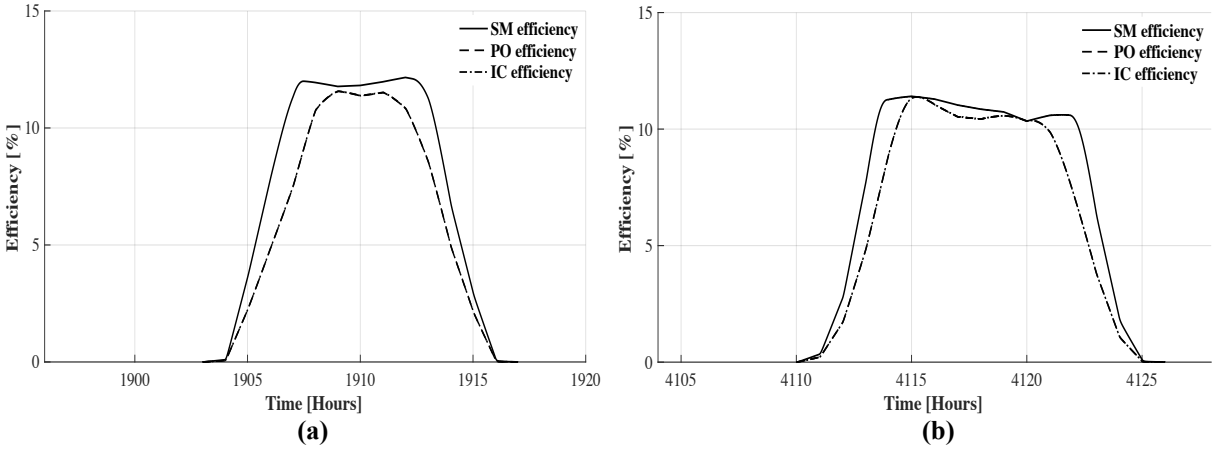

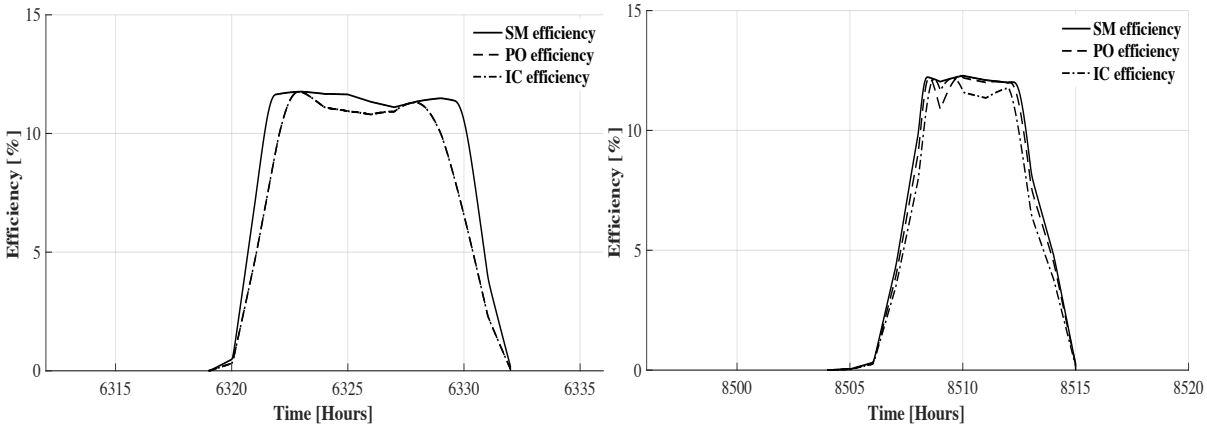

Figure 3. 7 Module Efficiencies using different MPPT techniques on the Mono-Si PV array SM55 for **(a)** March 21, **(b)** June 21, **(c)** September 21, **(d)** December 21.

With the same methodology used in the precedent paragraphs, the Poly-Si MSX60 PV array with the datasheet in Table 3.1 is simulated under the same conditions displayed in Figure 3.5. Figure 3.8 presents the daily generated power using the examined MPPT techniques. As can be seen in this illustration, the generated power using the SM-MPPT confirms the high tracking performance and stability of this technique even with the Poly-Si technology. In fact, the SM-MPPT is known as a robust controller even with an external disturbance. On the other hand, and especially for the Poly-Si technology, the P&O and the IC methods fit perfectly because of its similar approach followed to pursuit the MPP.

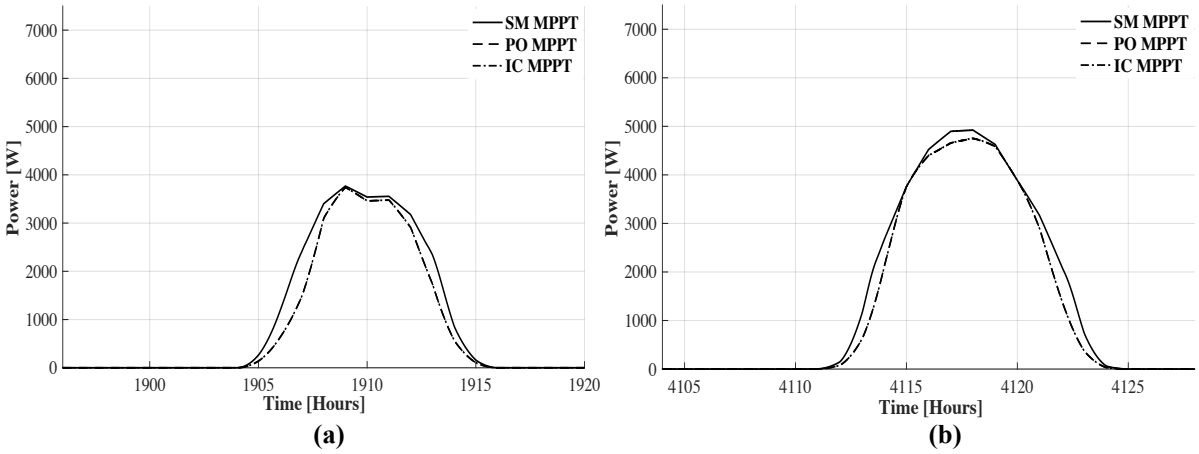

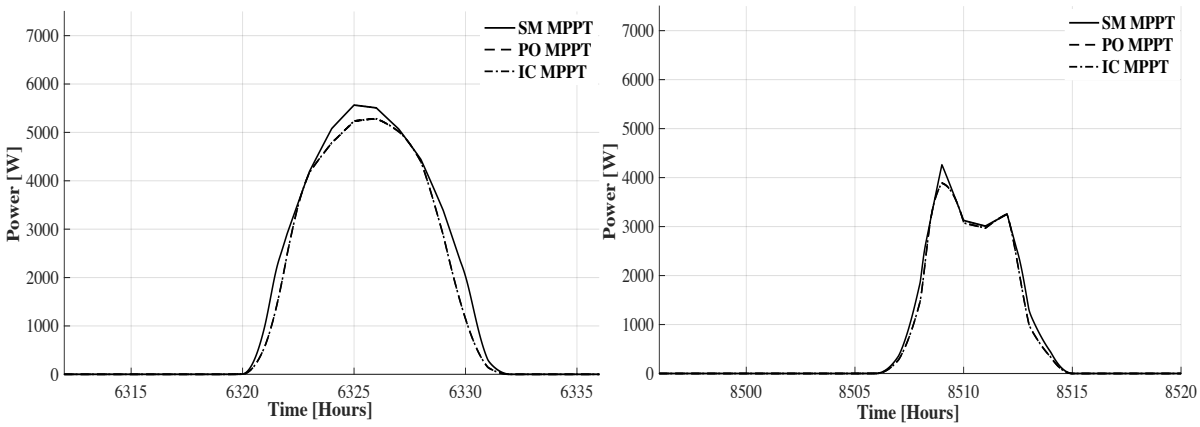

Figure 3. 8 Daily generated power using different MPPT techniques on the Poly-Si PV array MSX60 for **(a)** March 21, **(b)** June 21, **(c)** September 21, **(d)** December 21.

The module efficiency of the MSX 60 is plotted in Figure 3.9. According to SAM software (Gilman, 2015), the nominal module efficiency of the MSX60 is given by a value of 10.80%. As seen in Figure 3.9, both the P&O and the IC method are identical in all cases of atmospheric variations, but the drawbacks of these methods is the low response to attain the steady-state around the nominal efficiency, which causes a lot of losses comparing to the sliding mode technique.

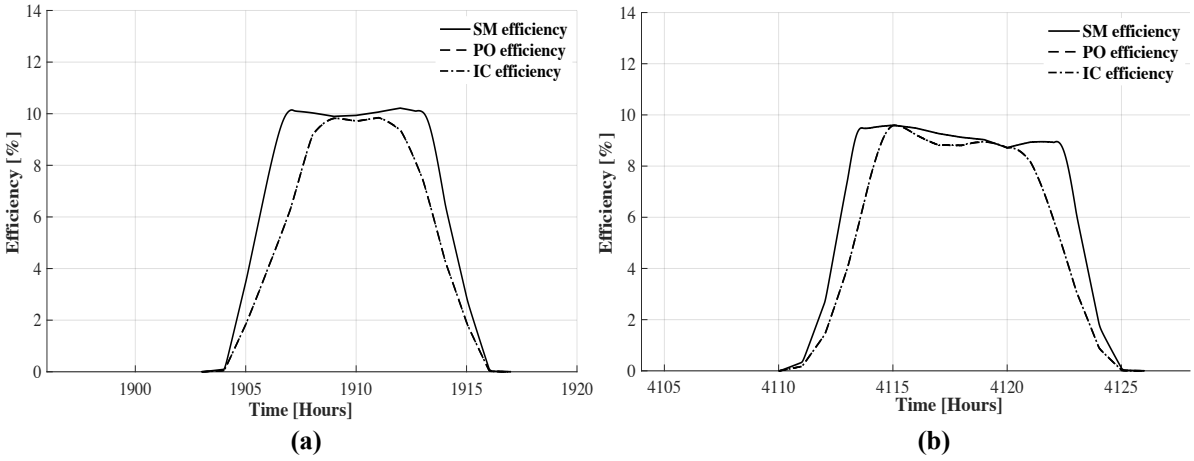

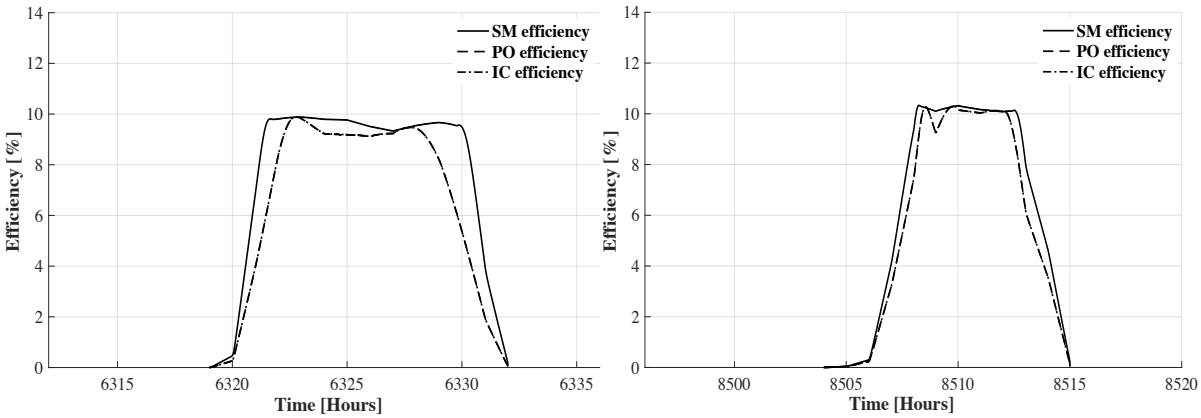

Figure 3. 9 Module Efficiencies using different MPPT techniques on the Poly-Si PV array MSX60 for **(a)** March 21, **(b)** June 21, **(c)** September 21, **(d)** December 21.

From this analysis, it was concluded that the sliding mode MPPT presents a very good solution to track the MPP comparing to the P&O and the IC methods. This superiority is proved from the high efficiency and the good stability achieved by the SM-MPPT. Furthermore, this MPPT technique has a high tracking speed capability which allows transferring the PV energy with minimum losses.

3.5.2 Annual Analysis

Because the daily analysis evaluates the performance of the PV system in a limited period, it is essential to quantify the net energy output of PV arrays generated in single Typical Meteorological Year. Similarly, meteorological data of Fez are used in the calculations. This location is known with high potential of solar energy and a hot weather in the summer and a cold one in the winter. Figures. (3.10) - (3.13) give respectively the annual values of ambient temperature, cell temperature, global incident irradiance and wind velocity. The presented data were generated on an hourly basis and fitted using the MATLAB toolbox to comply with the time step of 1 s used in the simulation processes.

As observed in Figure 3.10, the annual ambient temperature varies between a maximum value of 44.5 °C and a minimal one of -1.5 °C, this database is characterized by the different profiles of daily weathers (sunny, cloudy and mixed days). Figure 3.11 gives the annual cell temperature using the NOCT model (Gilman, 2015); the daily peak of this temperature varies between 17.26 °C and 71.96 °C. Figure 3.12 shows the annual irradiance in the same region. The daily peak irradiance changes between a value of 281.1 W/m^2 and 1156 W/m^2. In Figure 3.13, the annual wind velocity is presented; the wind speed interval varies between 0 m/s and 16.5 m/s.

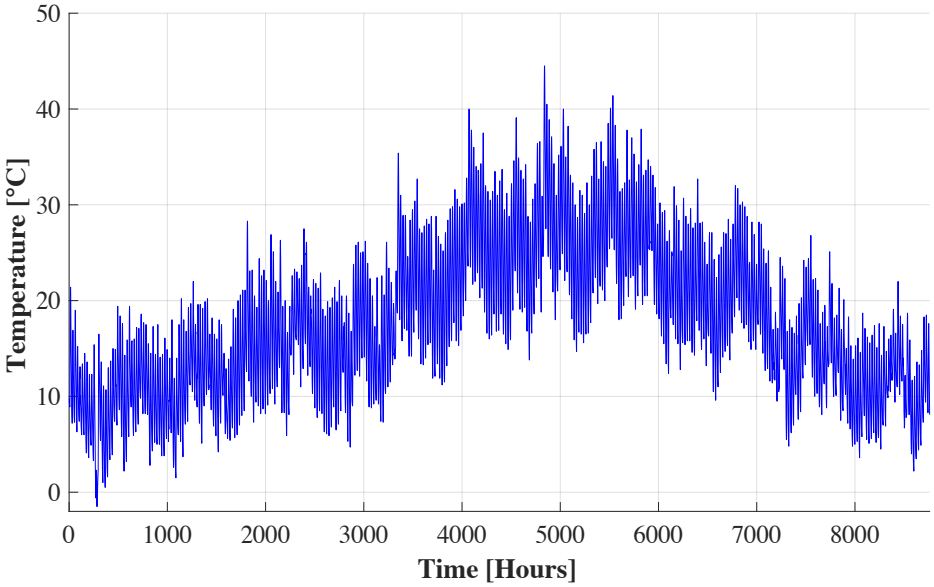

Figure 3. 10 Annual database of the ambient temperature [°C].

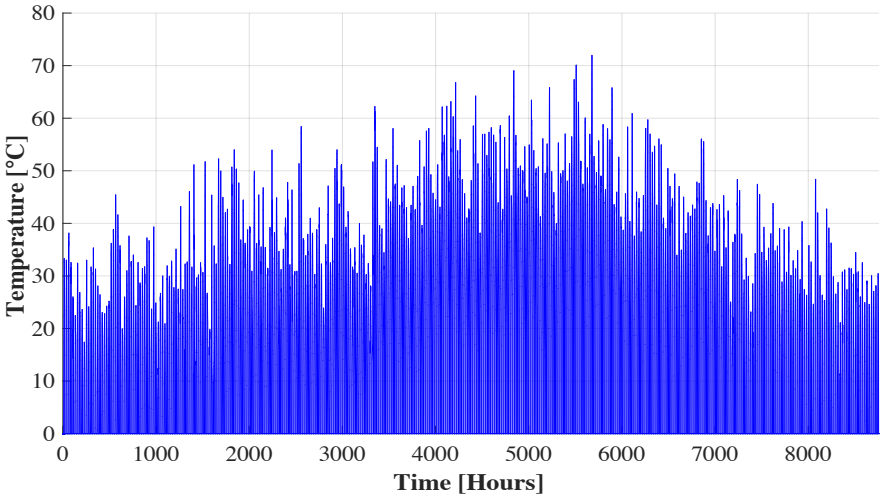

Figure 3. 11 Annual database of the cell temperature [°C].

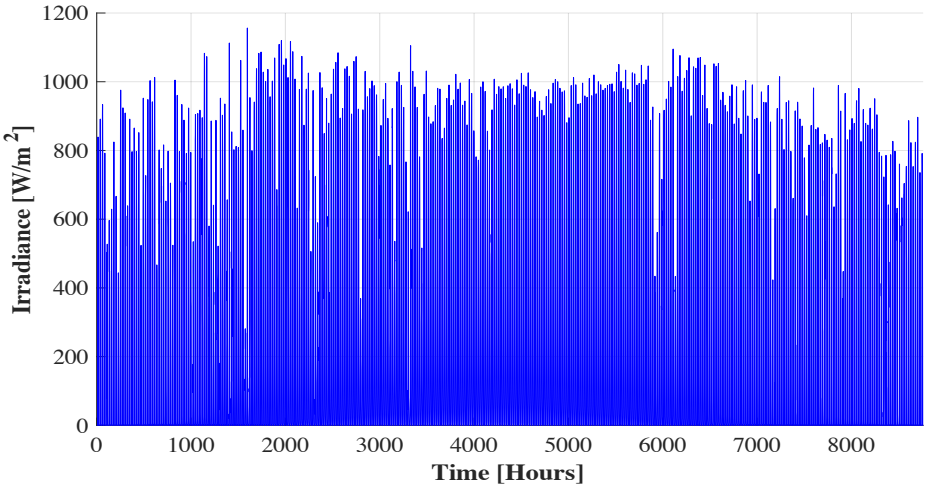

Figure 3. 12 Annual database of the irradiance [W/m2].

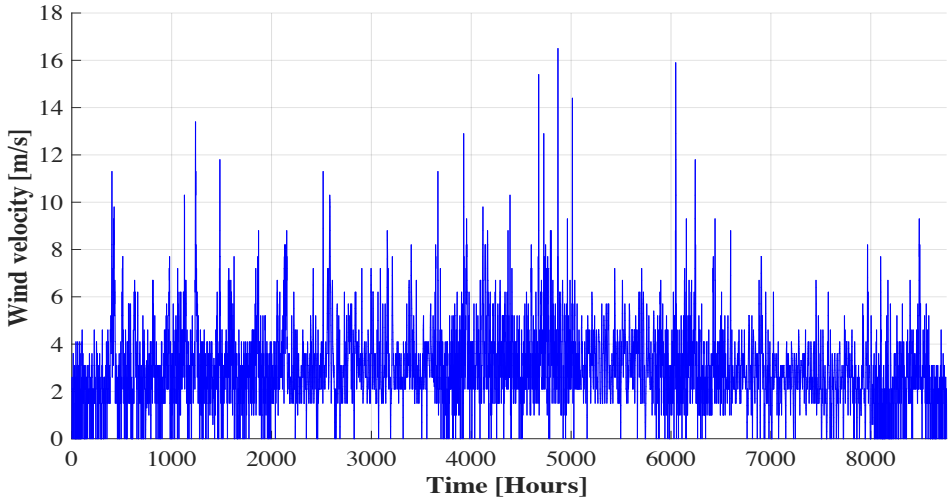

Figure 3. 13 Annual database of the wind velocity [m/s].

The simulation of the selected MPPT controllers (Sliding mode MPPT, P&O and IC) using the previous data. The annual generated power using the different MPPT techniques considering the two module technologies (Mono-Si SM55 and Poly-Si MSX60) are presented respectively in Figure 3.14 and Figure 3.15.

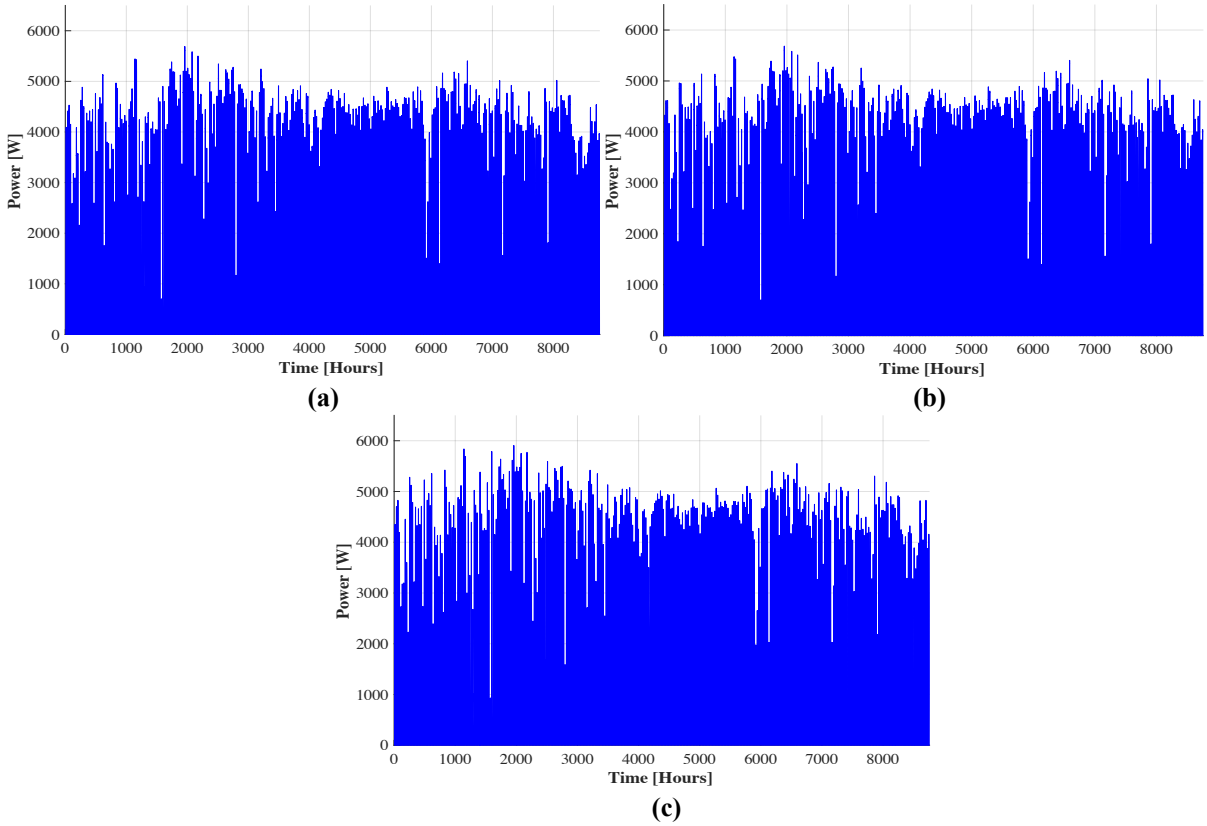

Figure 3. 14 Annual generated power using different MPPT techniques on SM55 PV array (a) P&O MPPT, (b) IC MPPT, (c) SM-MPPT.

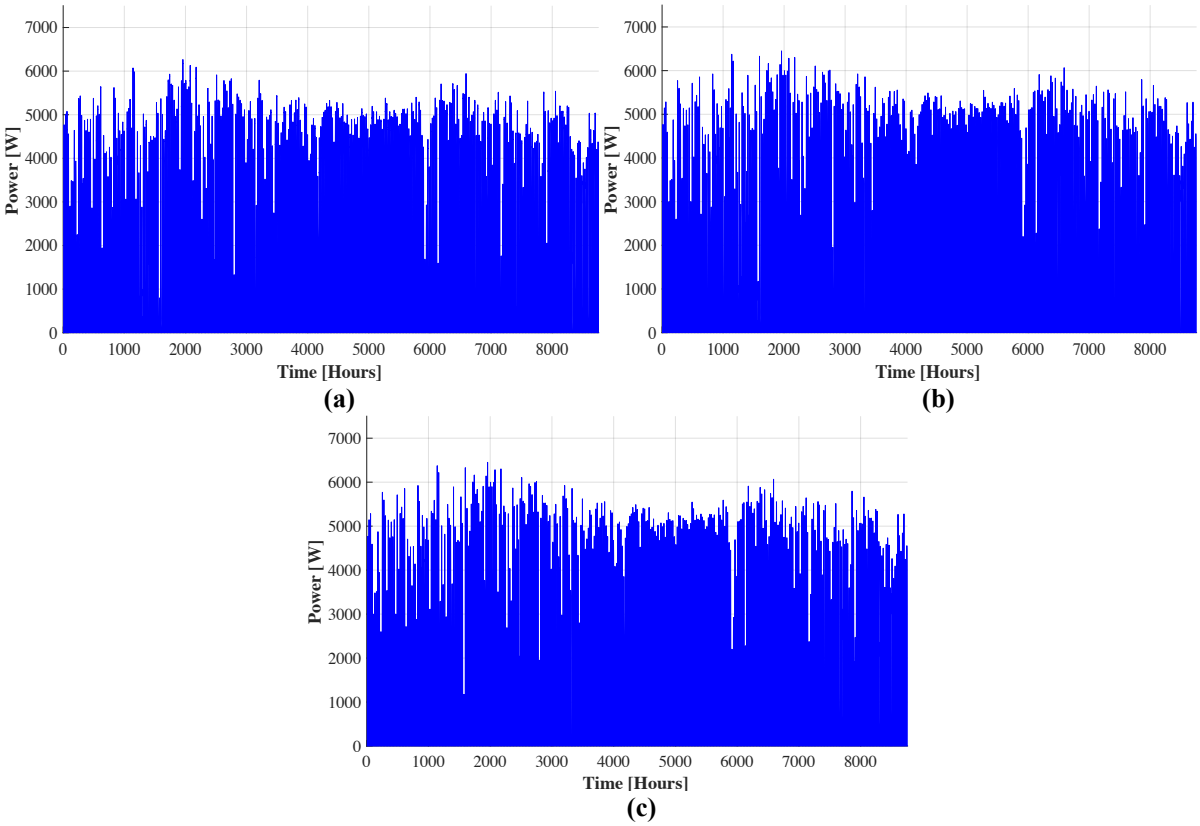

Figure 3. 15 Annual generated power using different MPPT techniques on the Poly-Si MSX60 PV array (a) P&O MPPT, (b) IC MPPT, (c) SM-MPPT.

By using the output results of the annual generated power, the annual produced energy is calculated using the following equation:

$$\boldsymbol{E_{pv} = \frac{1}{3600}\int_0^T P_{pv}dt} \quad \textbf{(3.11)}$$

where T is the final second of the year and the step of integration is chosen as 1 second.

In Figure 3.16, the calculated power is plotted for each technology using the selected MPPT technique; as shown in this figure, the annual produced energy using the SM-MPPT shows a considerable superiority for both technologies comparing to other MPPT techniques, to prove that, the relative gain given by Equation. (3.12) is calculated. These relative gains are presented in Table 3.3.

$$\boldsymbol{ERG\% = \frac{E_R - E_C}{E_C} * 100} \quad \textbf{(3.12)}$$

where E_R is the reference energy chosen as the produced energy using the SM-MPPT, E_C is the compared energy.

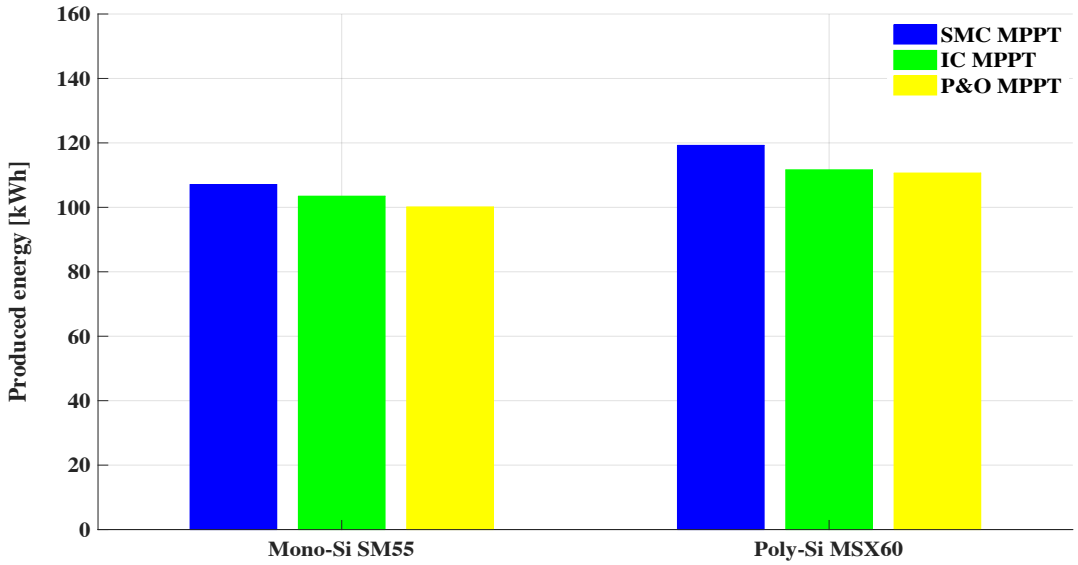

Figure 3. 16 Annual produced PV energy using different MPPT techniques for the Mono-Si SM55 and the Poly-Si MSX60 PV arrays.

As can be observed, the sliding mode MPPT offers more energy outputs than the other techniques. For the Mono-Si technology, the relative gains generated by using the SM-MPPT compared to of the P&O and the IC are respectively 7% and 3.88%. Moreover, the use of sliding mode controller in the Polycrystalline technology gives engenders more energy compared with the PO and the IC methods, this superiority is estimated to be 8.18% and 7.20%, respectively.

Table 3. 3 Relative energy gains in terms of the annual produced energy. Base case: SM-MPPT.

	Mono-Si SM55	**Poly-Si MSX60**
ERG% [P&O]	7	8.18
ERG% [IC]	3.88	7.20

3.6 Conclusion

This chapter examines to what extent the MPPT technique could affect the yearly energy output of a solar photovoltaic field. To draw useful conclusions about this effect, running simulations based on real meteorological and operating conditions is essential. Considering one Typical Meteorological Year for the Moroccan city (Fez), a comparison between three MPPT techniques has been made in terms of daily, annual energy outputs and conversion efficiencies of a solar field comprising 100 PV modules. Poly-crystalline and Mono-crystalline silicon PV technologies have been tested. The total installed capacity is 6 kW_p and 5.5 kW_p, respectively. The main findings of this work is that the SM-MPPT yields the highest energy outputs annually compared to the P&O and IC techniques. More specifically, in terms of yearly energy output, SM-MPPT could achieve up to 8.18% higher energy productions if P&O and the IC methods. Moreover, the technology of PV modules seems to have a significant impact on the net relative

energy gain induced. Higher rates are observed for the Poly-Si modules. At this point, it is interesting to note that further investigations should be undertaken to compare such techniques for other climate conditions and for other PV technologies to gather more information about the choice of a MPPT control technique. In addition, The SM-MPPT seems to be the recommended solution due to its effectiveness and robustness and this technique is chosen and discussed in the next chapter.

CHAPTER4 : Sliding Mode Controllers for Standalone PV Systems: Modeling and Approach of Control.

4.1 Motivation

As it has been concluded in the previous section, the sliding mode control presents good results in terms of tracking the maximum power point compared to P&O and Incremental conductance methods. For this reason, this chapter presents a single-phase standalone photovoltaic (PV) system with two stages of converters. The aim of this study is to track the maximum power point (MPP) so as to transfer the maximum available power to the load and to control the output current in order to feed the AC load by a sinusoidal current. These goals are attained by using the sliding mode to design a control laws in order to command the boost DC-DC and the inverter switches. Thus, a maximum power point tracking (MPPT) and an output current controller based on the sliding mode are proposed. The innovative aspect of this work is to propose a standalone PV system with the controllers based only on the sliding mode control approach.

This chapter is structured as follows: in section 4.3, a description of the PV cell and a modeling of the proposed PV system are given. Section 4.4 and 4.5 are dedicated respectively to the MPPT and the current controller based on sliding mode. The effectiveness of these controllers is simulated and discussed in section 4.6. Finally, some brief concluding remarks are given in section 4.7.

4.2 Problem Formulation

In the literature, nonlinear controllers such as back-stepping and sliding mode (SM) have shown various advantages (Farhat et al., 2017; Levron et al., 2013)**.** The implementation simplicity and the robust behavior against the external disturbances encourage the researchers to use these controllers in various PV system applications.

Thanks to its advantages, the sliding mode has been used widely to control variable structure systems (VSS) (Farhat et al., 2017; Gonzalez Montoya et al., 2016; Sarvi et al., 2013; Yau et al., 2013). Accordingly, the switched mode converters used in PV system applications are the ideal target of this kind of controller (Levron et al., 2013; Martinez-Salamero et al., 2010). Either it is a DC-DC converter or an inverter, the sliding mode control (SMC) has been used widely in the literature.

Kim et al. applied the SM to control the inverter switches in order to force the followed current in the grid to pursue a generated reference current, the simulation and experimental results of this single stage grid-connected PV system shown that the proposed controller can reduce current overshot and contribute to the optimal design of power devices (Kim, 2007; Kim et al., 2006). Furthermore, Chen et al. proposed to control a DC-DC boost converter feeding a

resistive load using sliding mode in finite time, the obtained results showed good performances in terms of stability and fast response. However, the exploitation of this PV system is focalized only for DC loads. For this reason, Laura et al. used an adaptive SM to manage the control of two stages of converters for a grid-connected PV system. Thus, the controlled converters exhibit robustness properties with a fast response to any sudden irradiance change.

Due to the reported benefits of the sliding mode controllers in terms of robustness and fast response, most of researchers used these controllers in grid-connected PV systems (Dhar and Dash, 2015; Kim, 2007). However, the number of works about standalone PV systems still neglected. For this reason, the purpose of this work is to contribute to the modeling and the simulation of the standalone PV system in Figure 4.1 and to control both converters using sliding mode approach. These controllers are described in two parts as follows:

- A sliding mode maximum power point tracking (SM-MPPT) of the PV panel with the objective to command the duty cycle of the boost DC-DC in order to extract the MPP rapidly.
- Design of control law by acting on the PWM of the inverter, this control law has a function to force the output current, which circulates in the load to pursue the calculated reference current.

To design the proposed controllers, climates changes are considered as perturbations, which affect the overall efficiency of the PV system. Therefore, the proposed system is simulated under a fast variation of solar irradiation and temperature to verify the performance and the stability. Then, in order to validate the simulation results, a comparison with one of the most used method in the literature (Incremental Conductance) and an estimation of a daily energy is achieved.

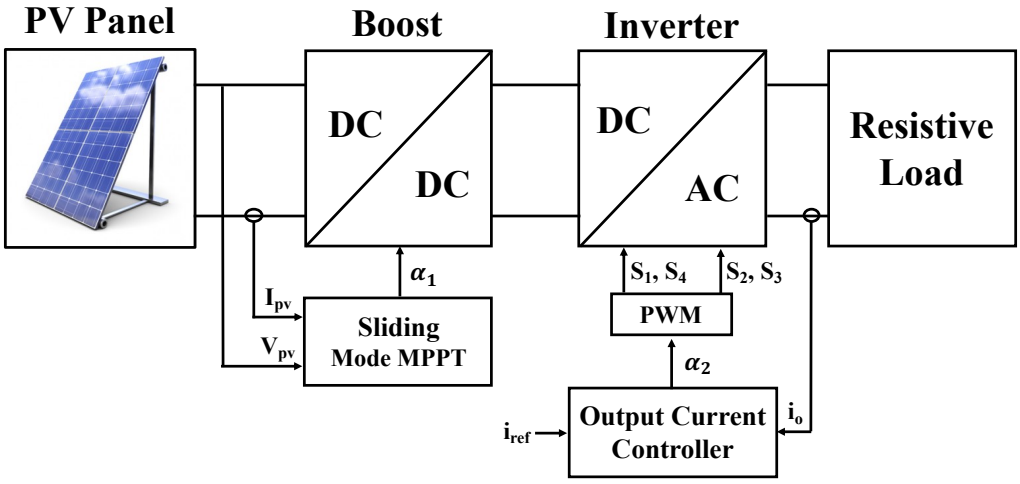

Figure 4. 1 Proposed standalone PV system.

4.3 Mathematical Modeling of the Standalone PV System

4.3.1 Modelling of the PV system

The proposed system in Figure 4.1 presents a single-phase standalone PV system with an alternative output load. The constitution of this system consists of two stages of static converters with the main objective to ensure the conversion of the DC energy coming from the PV panel into an AC utility. To begin this study, we must first perform the mathematical modeling by applying the Kirchhoff laws on the detailed system in Figure 4.2, we found that the system can be written in a set of equations depending on the state of the switches.

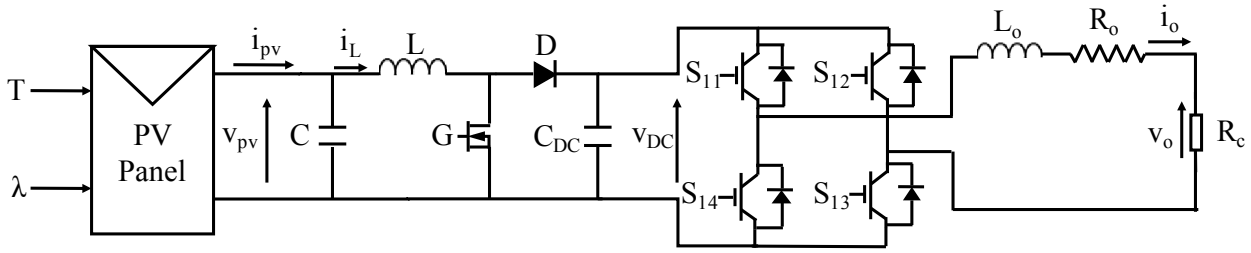

Figure 4. 2 Detailed standalone PV system.

The mathematical modeling of the proposed system in a state space leads us to a set of nonlinear equations expressed by the average model as follows:

$$\boldsymbol{C\frac{\partial v_{pv}}{\partial t} = i_{pv} - i_l} \quad \textbf{(4.1)}$$

$$\boldsymbol{L\frac{\partial i_L}{\partial t} = v_{pv} - v_{DC}(1-\alpha_1)} \quad \textbf{(4.2)}$$

$$\boldsymbol{C_{DC}\frac{\partial v_{DC}}{\partial t} = i_L(1-\alpha_1) + i_o(1-2\alpha_2)} \quad \textbf{(4.3)}$$

$$\boldsymbol{L_o\frac{\partial i_o}{\partial t} = -i_o(R_o + R_c) - v_{DC}(1-2\alpha_2)} \quad \textbf{(4.4)}$$

Where α_1 and α_2 represent respectively the control inputs of the boost converter and the inverter switches.

The precedent equations can be rewritten in the form $\dot{x} = f(x) + \alpha_1 g_1(x) + \alpha_2 g_2(x)$ where the vectors $\dot{x}, f, g_1$ and g_2 are given as follows:

$$\dot{x} = \begin{bmatrix} \dot{v}_{pv} \\ \dot{i}_L \\ \dot{v}_{DC} \\ \dot{i}_o \end{bmatrix}, \qquad f(x) = \begin{bmatrix} \frac{i_{pv}-i_l}{C} \\ \frac{v_{pv}-v_{DC}}{L} \\ \frac{i_L+i_o}{C_{DC}} \\ \frac{-i_o(R_o+R_c)-v_{DC}}{L_o} \end{bmatrix}, \qquad g_1(x) = \begin{bmatrix} 0 \\ \frac{v_{DC}}{L} \\ \frac{-i_L}{C_{DC}} \\ 0 \end{bmatrix}, \qquad g_2(x) = \begin{bmatrix} 0 \\ 0 \\ \frac{-2i_O}{C_{DC}} \\ \frac{2v_{DC}}{L_o} \end{bmatrix}$$

The parametric variations and non-linearity of PV systems caused by external perturbations as the variation of climate conditions push us to use a robust method with a low sensibility to modeling errors. The sliding mode is a new technique which is characterized by its robustness and admits a convergence in a finite time (Taherkhorsandi et al., 2015).

The main objective of the sliding mode approach consists to move the trajectory of the variable state of the system to the sliding surface, and force this variable to stay in the proximity of this surface. To ensure these conditions, we must design a control law which is adaptive to the variable structure (Taherkhorsandi et al., 2015).

The main purpose of this chapter is to use the sliding mode theory to elaborate a control law which allows us to command both the DC-DC and the DC-AC converter.

4.4 Theoretical Background

4.4.1 A Sliding Mode MPPT

The tacking of the maximum power point is the most important operation in photovoltaic systems. In order to perform the P-V characteristic of the PV panel at its MPP, the derivative of the power with respect to the voltage i.e., $\frac{\partial P_{pv}}{\partial V_{pv}}$ must converge to zero (Dahech et al., 2017). For this reason, the sliding mode theory is used to design a control law that acts directly on the duty cycle α_1 of the DC-DC converter as shown in Figure 4.3.

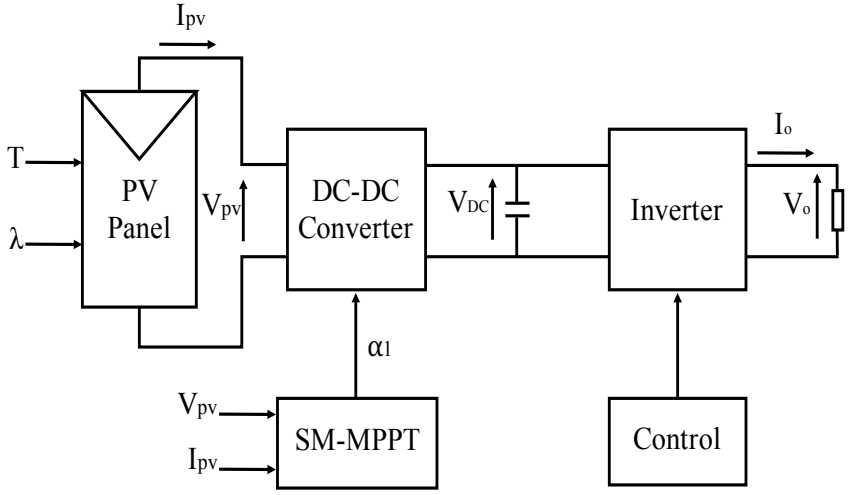

Figure 4. 3 SM-MPPT bloc diagram.

As the first step of this control law design, the choice of the sliding surface. In the case of the PV power maximizing, this surface is selected as follows:

$$\boldsymbol{\sigma_1 = \dot{e}_1 + \gamma_1 e_1} \qquad \textbf{(4.5)}$$

where e_1 is the dynamic error between the regulated output and its reference value which is zero $e_1 = y_1 = \frac{\partial P_{pv}}{\partial V_{pv}}$, γ_1 is a positive parameter calculated from the Hurwitz polynomial.

The time derivative of this surface is given by the following equation:

$$\dot{\sigma}_1 = \ddot{e}_1 + \gamma_1 \dot{e}_1 \tag{4.6}$$

The robust and the stable behavior present the main advantages of this method (Shtessel et al., 2014), this stability is relative to the attractiveness of this surface and proved by the Lyapunov function presented as follow:

$$V_1 = \frac{1}{2}\sigma_1^2 \tag{4.7}$$

In order to provide the asymptotic stability around the equilibrium point. The time derivative of Equation (4.7) must be strictly less than zero ($\dot{V}_1 < 0$), this later can be presented as:

$$\dot{V}_1 = \dot{\sigma}_1 \sigma_1 \tag{4.8}$$

Assuming that the dynamic of the function can be written as $\dot{\sigma}_1 = -\lambda_1 sign(\sigma_1)$, Equation (39) can be rewritten as:

$$\dot{V}_1 = -\lambda_1 |\sigma_1| \tag{4.9}$$

From Equation (4.9) and in order to respect the Lyapunov stability condition, $\lambda_1$must be a positive quantity.

The control law depends totally on the variation of the measured I_{pv} and V_{pv}, and these later varies according to the temperature and the irradiance changes, the strong aspect of the sliding mode MPPT is the stable behavior even with external and parametric variations. In literature, most MPPT based on sliding mode used the reduced equation of I_{pv} in order to simplify the calculations, the strong aspect of this study is the use of the detailed calculation to accurate the results. As seen in the Appendix C, all detailed derivatives are demonstrated to design the exact control law.

By replacing (C.7) and (C.8) in Equation (4.9) and using $\dot{\sigma}_1 = -\lambda_1 sign(\sigma_1)$, the control law is expressed by the following equation:

$$\alpha_1 = \frac{-\lambda_1 sign(\sigma_1) - \gamma_1 e_1 - E}{K} \tag{4.10}$$

where E and K are represented in the appendix C by equations (C.9) and (C.10) respectively.

4.4.2 Output Current Controller

Because most of utilities are alternative, the reason to convert DC energy to AC one becomes an important task. To perform the standalone PV system in AC energy, DC-AC converters are the key solution. Moreover, the reason behind transferring the maximum energy from the DC bus to the load, the sliding mode approach is used.

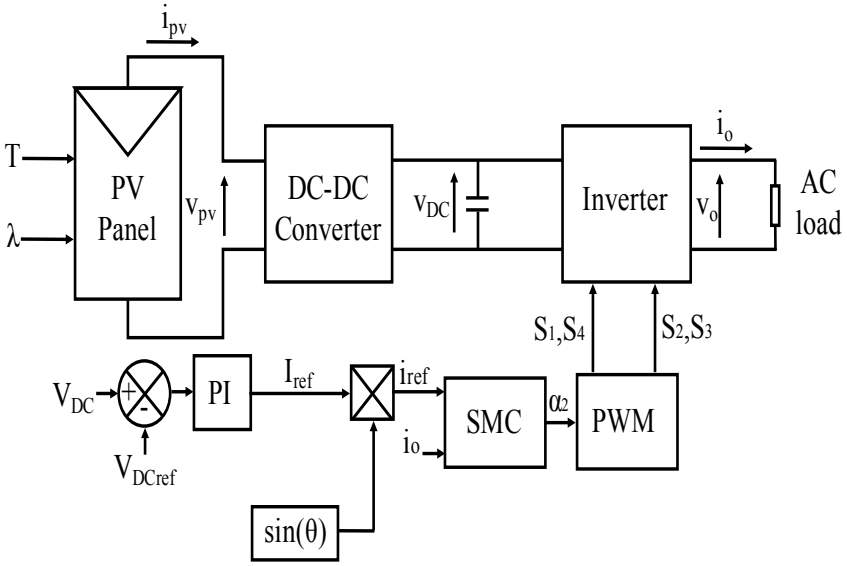

Figure 4. 4 Control strategy followed to elaborate the sliding mode output current controller.

The modeling of the output current controller begins with the design of the sliding surface. Generally, the sliding surface is defined by the differences between the state variable and its reference (Chiu et al., 2012). In addition, the reason to feed the AC load by an alternative sinusoidal current, the proposed strategy in Figure 4.4 allows us to calculate the peak current I_{ref} using a PI loop between the DC bus voltage v_{DC} and its calculated reference value v_{DCref}. Furthermore, to form a sinusoidal reference current i_{ref}, the peak current I_{ref} is multiplied to a generated $sin\,(wt)$, it should be mentioned that AD9833 analog circuit may be used to generate the $sin\,(wt)$ once we start the hardware implementation. The use of this circuit is due to its very low frequency sensibility (Devices, 2003). this current is used to construct the sliding surface given by:

$$\boldsymbol{\sigma_2 = i_o - I_{ref}\sin(wt)} \tag{4.11}$$

To make the switching surface stable and attractive, the Lyapunov function given by ($V_2 = \frac{1}{2}\sigma_2^2$) is used, and the substituting of the dynamic function $\dot{\sigma}_2 = -\lambda_2 sign(\sigma_2)$ in the derivative of Lyapunov function gives the law of control as follows:

$$\boldsymbol{\alpha_2 = \frac{1}{2}\left[1 + \frac{-L_0\lambda_2 sign(\sigma_2) + (R_o + R_c) + L_o\frac{\partial i_{ref}}{\partial t}}{v_{DC}}\right]} \tag{4.12}$$

where: $\frac{\partial i_{ref}}{\partial t} = I_{ref} w cos(wt)$

According to the stability condition of the Lyapunov function which is $\dot{V}_2 = -\lambda_2|\sigma_2|$, the coefficient λ_2 must be strictly superior to zero.

4.5 Theoretical Results

Before starting the simulation, a theoretical value of current, voltage and power at the MPP are computed using the fsolve function of MATLAB to find the unknow values of current and voltage using the PV current equation (Equation 2.1) and the derivative of the power with respect to the voltage (Appendix C.4). Thereafter, the calculated values of the current, the voltage and power are summarized in Table 4.1 for different levels of solar irradiance and temperature.

Table 4. 1 PV system parameters used in the simulation.

	$\mathbf{I_{PV}}$ **[A]**	$\mathbf{V_{PV}}$ **[V]**	$\mathbf{P_{PV}}$ **[W]**
$\boldsymbol{\lambda}$ **= 250 W/m^2, T = 25 °C**	15.56	0.77	12.13
$\boldsymbol{\lambda}$ **= 500 W/m^2, T = 25 °C**	16.52	1.56	25.90
$\boldsymbol{\lambda}$ **= 1000 W/m^2, T = 25 °C**	17.40	3.14	54.80
$\boldsymbol{\lambda}$ **= 1000 W/m^2, T = 50 °C**	15.43	3.12	48.21
$\boldsymbol{\lambda}$ **= 750 W/m^2, T = 25 °C**	15.04	2.33	35.18

4.6 Simulation Results

This section is divided into two parts, the first concerns the performances evaluation of the proposed controllers. For this reason, both the SM-MPPT and the output current controller have been implemented in MATLAB Sumlink and tested under severe variations of the atmospheric conditions. Thereafter, the second subsection presents a daily analysis of the net produced energy using the SM-MPPT and the modified incremental conductance proposed by Motahhir et al. (Motahhir et al., 2017); under the fluctuation of two whether profiles (Sunny and Cloudy).

4.6.1 Performance Validation

Before beginning the test performance, the used PV panel must be modeled. For this reason, the Monocrystalline SM55 PV module with the datasheet parameters displayed in Table 2.1 (Chapter 2) has been modeled using an accurate method from the literature (Chaibi et al., 2018). Thereafter, the extracted parameters using Chaibi et al. method and the simulation parameters are presented in Table 4.2.

Table 4. 2 PV system parameters used in the simulation.

Parameters	**Values**
DC-DC boost parameters (M. Salhi, 2009)**:**	
L [mH]	3.5
C [uF]	4700
C_{DC} [uF]	670
L_o [mH]	2.2
R_o [Ω]	0.7
Sliding mode parameters:	
λ_1	*5000*
λ_2	500
γ_1	150
PI controller coefficients:	
K_p	0.85
K_i	0.001
f (Hz)	50
ω (rad/s)	314.1593

In order to evaluate the proposed sliding model controllers, the system must be tested under a severe variation of the atmospheric conditions. Hence, Figure 4.5 displays the used fluctuations of irradiance and temperature. Consequently, Figure 4.6 gives the response of the SM-MPPT. As noticed in these curves, the duty cycle in Figure 4.6(a) changes instantly to its optimal value with each climate variation. Furthermore, in Figure 4.6(b) the sliding surface converges immediately its reference state regardless of the sudden variation of irradiance. Otherwise, when the temperature varies suddenly from 25 °C to 50 °C, the sliding surface spikes and comebacks rapidly to the equilibrium state. To show the effect of these spikes on the output PV power, Figure 4.7 presents the response of the PV power for each change of irradiance and temperature.

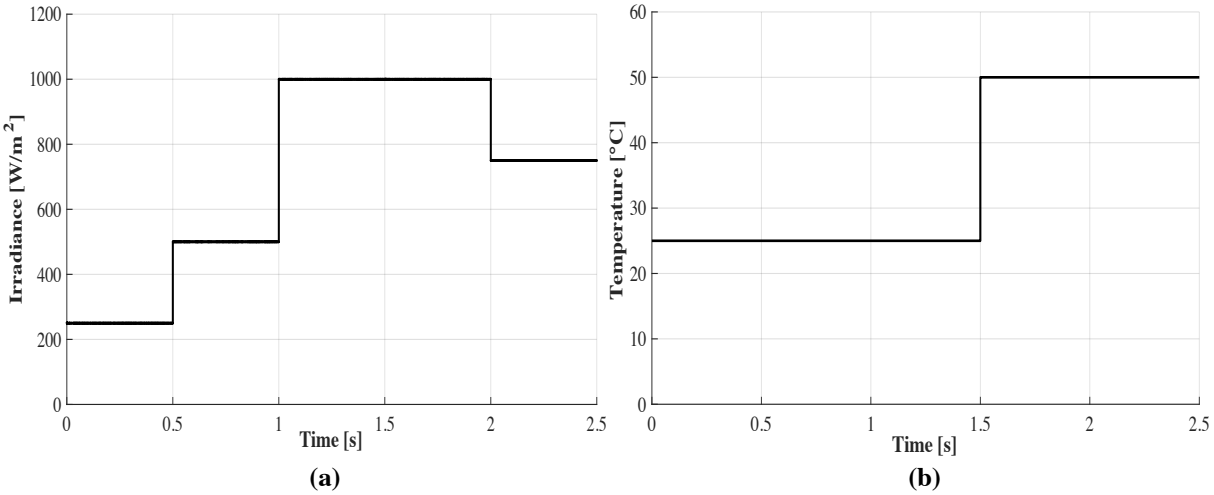

(a) **(b)**

Figure 4. 5 Irradiance (a) and temperature (b) fluctuations used in the simulation.

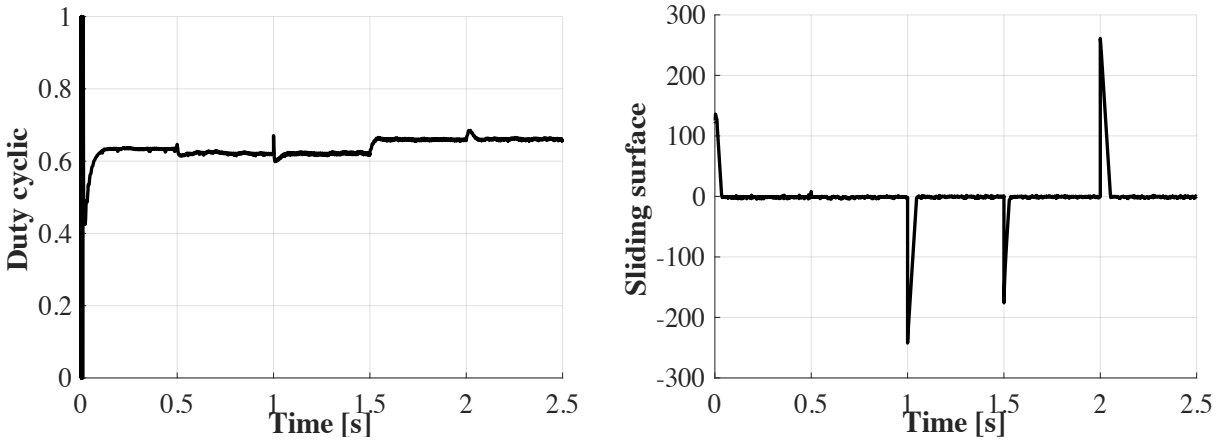

Figure 4. 6 Duty cycle and the sliding surface used to design the control law of the boost converter.

As observed, the power reaches instantly the reference despite any rapid change of irradiance. For the temperature, the high increase of temperature from 25 °C to 50 °C causes a negligible time of response to achieve the optimal value. In addition, Figure 4.7 compares the controlled power with the corresponding one to the incremental conductance method and to the theoretical power. As noticed in this comparison (Figure 4.7(a)-7(b)), the SM-MPPT reaches rapidly the theoretical values calculated in Table 4.1, but the IC method takes time to attain the theoretical value. Moreover, the IC-MPPT oscillates around the optimal value and loses the tracking because of the rapid increase of the temperature (see Figure 4.7(b)). Therefore, it can be deduced that the SM-MPPT presents high performances in terms of stability and fast response even with severe atmospheric changes.

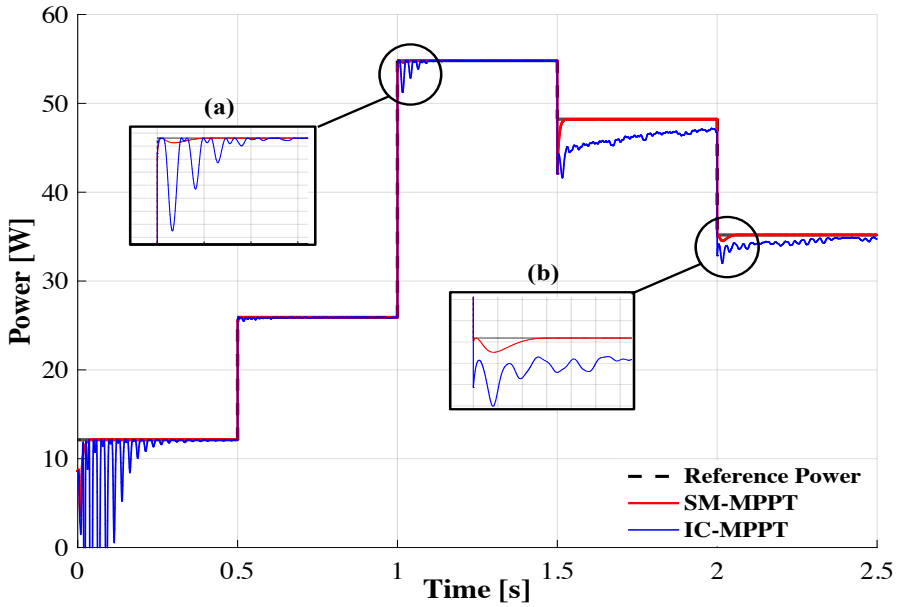

Figure 4. 7 Output power of the SM55 PV panel using the SM-MPPT and IC-MPPT.

Besides, to accurate the power results, the MPPT efficiency is computed using Equation (4.13):

$$\zeta_{MPPT} = \frac{P_{Measured}}{P_{Thoeritical}} * 100 \quad (4.13)$$

where the $P_{measured}$ is the calculated power using the SM-MPPT or the IC-MPPT. Accordingly, these calculated efficiencies are plotted in Figure 4.8 for each change of irradiance and temperature. As seen in this figure, the SM-MPPT efficiency values are close to 99% for all the variations of irradiance and temperature. However, the IC efficiency changes dramatically with atmospheric variation, especially for the temperature's one.

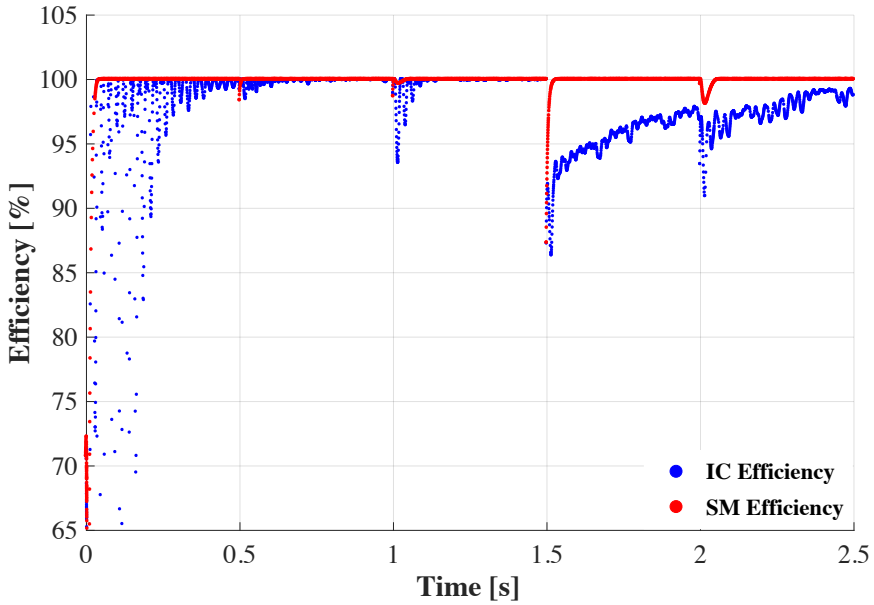

Figure 4. 8 Tracking efficiencies of the SM-MPPT and the incremental conductance technique.

These performances are summarized Table 4.3 to show the comparison between the SM-MPPT and the IC-MPPT in terms of the mean tracking efficiency, the oscillation level and the time of response. As shown, the SM-MPPT presents high performances and exceeds the IC-MPPT for any sudden change of irradiance and temperature.

Table 4. 3 Performance comparison between the SM-MPPT and the IC-MPPT.

	Efficiency	**Oscillations**		**Response time**	
		Sudden change of λ	**Sudden change of T**	**Sudden change of λ**	**Sudden change of T**
SM-MPPT	99.10 %	Neglected	Neglected	Very fast	Fast
IC-MPPT	92.16 %	High	High	Slow	Very slow

The second part of this subsection consists in evaluating the performance of the sliding mode output current controller. The objective of this later is to force the output current i_o to pursue the reference value of current generated from the PI regulator. To verify this purpose, the

developed input control and the sliding surface are plotted in Figure 4.9. As shown, the control input performs as a sinusoidal waveform with a significant fluctuation of the amplitude due to the reference current variation. Furthermore, the sliding surface oscillates around zero which means that the state variable converges to its reference value.

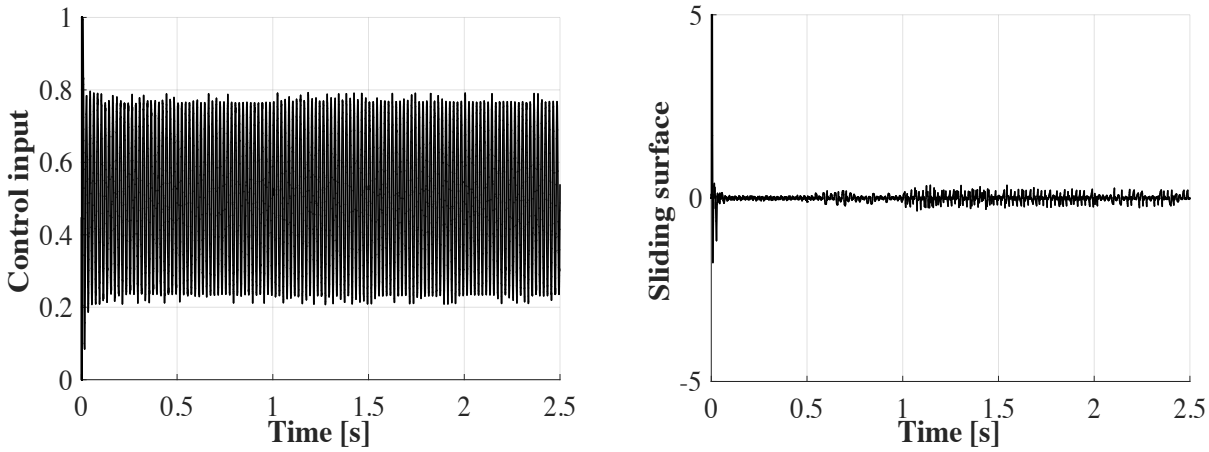

Figure 4. 9 Control input and the sliding surface used to design the control law of the inverter.

Therefore, the controlled output current is plotted with its reference value in Figure 4.10. As can be seen in this curve, the output current fits perfectly with the reference current and changes its value according to the change of this reference current. The quality of this controlled current is examined using the FTT analysis.

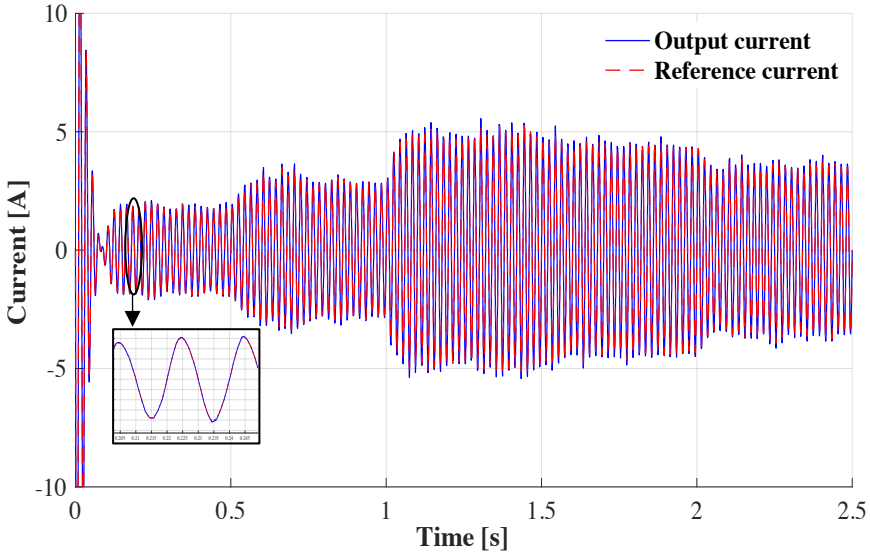

Figure 4. 10 Reference and the controlled output current.

The obtained results in Figure 4.11 indicates that the harmonics distortion has a value of 3.47% which is less than the international standard (5%).

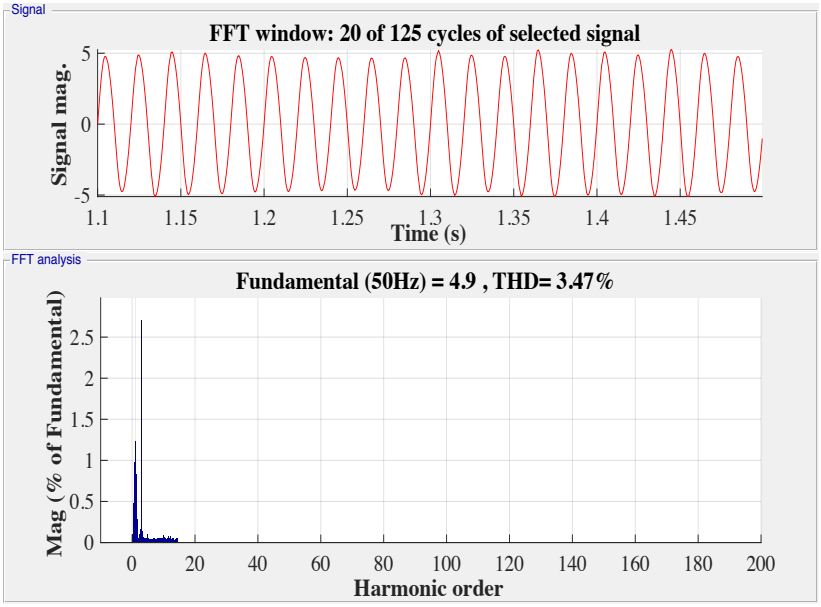

Figure 4. 11 Harmonics distortion analysis of the controlled output current.

The previous results demonstrate the robustness and the high performance of the sliding mode controllers. In order to accurate these results, the proposed PV system and controllers must be evaluated under real climatic fluctuations.

The output current and voltage are displayed in figure 4.12 demonstrate the robustness and the high quality of the proposed controllers.

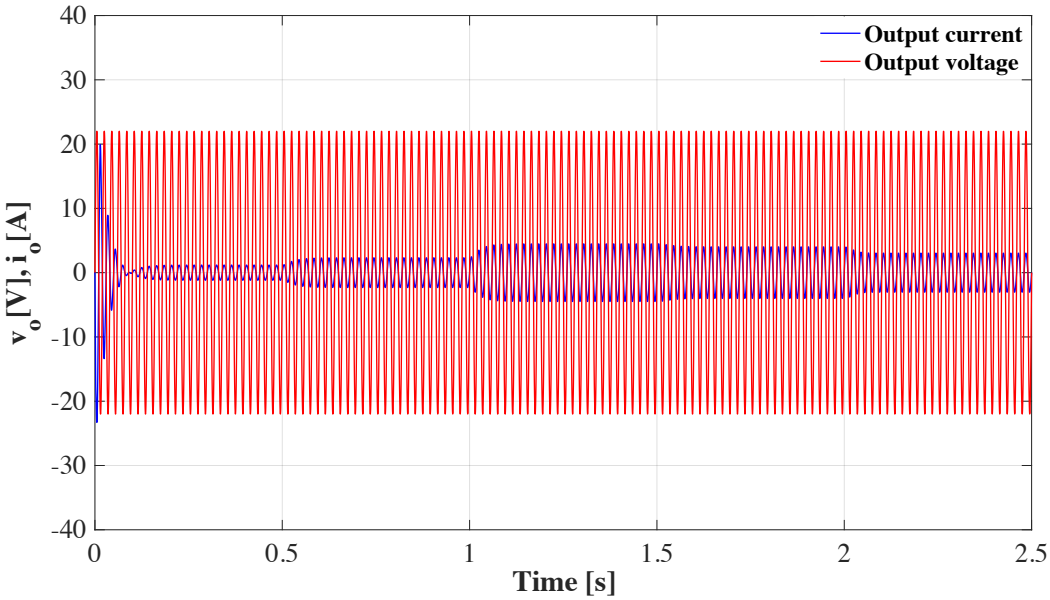

Figure 4. 12 Output current and voltage at the level of the resistive load.

4.6.2 Daily Performance

In order to estimate the performance of the Sliding Mode MPPT controller. This later and the incremental conductance technique are evaluated under a daily change of irradiance and

temperature. The daily atmospheric conditions of a sunny and a cloudy day are illustrated in Figure 4.13. As can be seen in Figure 4.13(a), the irradiance variation of both the sunny and the cloudy days is characterized respectively by its gradual increase until a maximum values of 1035.42 W/m^2 and 863.59 W/m^2, then a decrease till approximately the initial values can be noticed. In the case of the temperature variation (see Figure 4.13(b)), the sunny day presents high fluctuations between a maximum value of 46.10 °C and a minimum value of 27.80 °C. However, the cloudy day is characterized by its low-temperature changes compared to the sunny profile with a variation between a maximum and a minimum values of 37.57 °C and 14.35 °C, respectively.

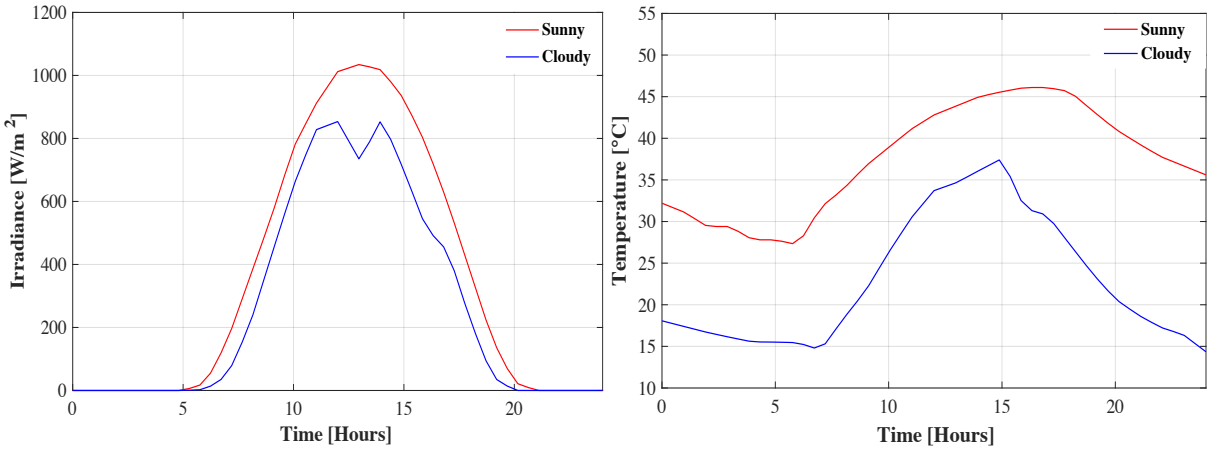

Figure 4. 13 Daily climate condition of a sunny (a) and a cloudy (b) day.

Considering the profiles illustrated in Figure 4.13, the daily generated power using both whether profiles (Sunny and Cloudy) is displayed in Figure 4.14. As observed in Figure 4.14(a), the generated power using the climate series data of the sunny profile are presented for the SM-MPPT and the IC-MPPT. As observed in this figure, it is clear that, as expected that the SM-MPPT shows a superiority for low atmospheric variations. However, at the high climate levels, the corresponding powers to the IC-MPPT are close to SM-MPPT ones. Thus, The IC technique presents good performances for high atmospheric variations, but the SM-MPPT stills more accurate. Consequently, the SM-MPPT and the IC-MPPT controllers generate respectively 423.49 Wh and 374.69 Wh of energy which explains the superiority of the SM-MPPT. Furthermore, the SM-MPPT controller generates a surplus estimated to 13.02% of energy more than the IC-MPPT. In the cloudy climate conditions, Figure 4.14(b) shows accurate higher performance of the SM-MPPT compared to the incremental conductance technique; this superiority is demonstrated by the fact that the SM based MPPT generates 332.48 Wh which significantly exceeds energy generation by the IC-MPPT (estimated at

260.63 Wh). Accordingly, the proposed SM-MPPT induces up to 27.57% of energy more than the IC-MPPT.

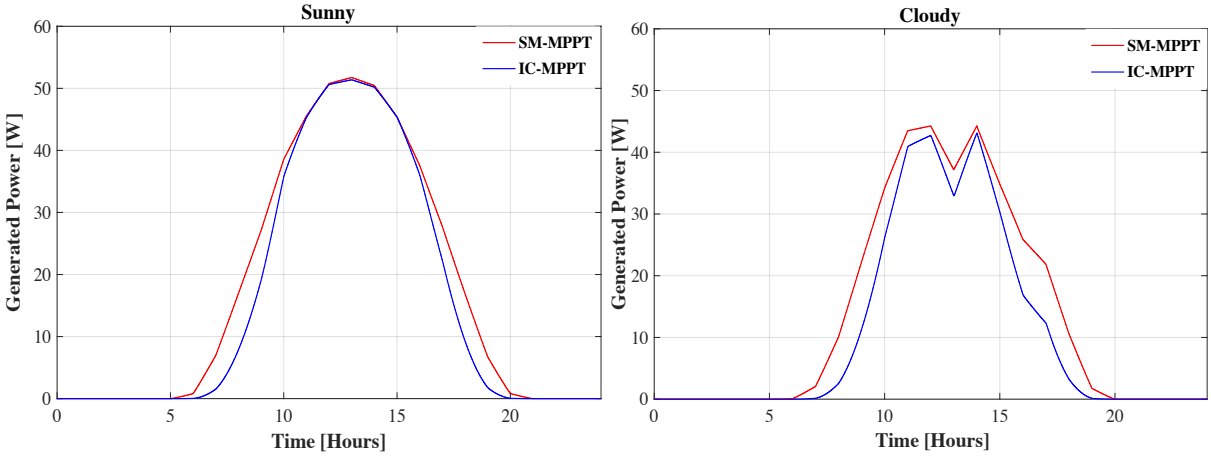

Figure 4. 14 Daily generated power using the SM-MPPT and the IC method for a sunny and a cloudy whether profiles.

4.7 Conclusion

In this chapter, robust controllers based on sliding mode theory are applied on two converters for single phase standalone PV system. The suggested controllers consist of SM-MPPT and an output current controller. Besides, the generation of the reference current is performed directly from the PI controller. In presence of any sudden change of irradiance and temperature, the controllers react rapidly in order to reach the reference values without oscillation around the MPP, this proves that our method, the sliding mode with a constant reference is better than classical one which is based on variable steps. In addition, the system stays stable because of Lyapunov function.

The performance of the controllers is verified through numerical simulations, the PV system results show very good tracking performances and high stability compared to the IC-MPPT. In addition, the output current has a sinusoidal form with a THD of 3.47%. Moreover, the daily performance shows that the SM-MPPT yields the highest energy compared to the IC techniques. More specifically, the suggested SM-MPPT could achieve until to 13.02% for the sunny whether profile and up 27.57% for the cloudy one. Due to its high performances, the suggested controllers could be a key solution for different use of the standalone PV system such as in isolated sites and pumping PV systems.

General conclusion and perspectives

The main objectives of this thesis were to contribute to the design and the optimization of a standalone photovoltaic system to feed an alternative load through an inverter. Thus, two controllers have been developed in order to enhance the efficiency of the proposed standalone photovoltaic system.

To achieve the assigned objectives, we have first developed an efficient method to extract the unknown parameters of the PV cell equivalent circuit model. This method allows the modelling PV module in addition to simulate the output of the PV panel for different levels of solar irradiance and temperature. The proposed method has been validated using manufacturer data and one of the most cited works in the literature, and the results have proved high levels of accuracy and simplicity. Then, a comparative study of the most used equivalent-circuit models is investigated in order to demonstrate the influence of the atmospheric conditions on the choice of the appropriate equivalent-circuit model. Accordingly, a hybrid approach that combines two of the most accurate models is proposed. The main idea of this approach is to switch to the appropriate equivalent-circuit model according to the climatic variation. This approach is validated experimentally using atmospheric data of two different climatic zones and shown good results in predicting power compared to the classical used models.

After developing a validated PV module, the tracking of its MPP is substantial to improve the overall efficiency. For this reason, three MPPT techniques have been evaluated in order to choose the most appropriate technique. In fact, the examined MPPT have been assessed under a one year of real climatic conditions with a step of one second. The reason behind using this kind of evaluation is to demonstrate the most accurate MPPT techniques in terms of yearly energy output. The simulation results indicate that the sliding mode MPPT yields the highest energy outputs annually compared to the other techniques. Afterwards, based on the annual evaluation, the sliding mode approach is used to control the DC to DC converter and the inverter. The main objectives of these controllers id to track the MPPT and to feed the alternative load with a current of high quality. Both controllers have been developed and simulated under MATLAB environment and have shown effectiveness in terms of tracking the MPP with an MPPT efficiency of 99%, in addition of feeding the AC load with a very low THD current.

Due to its several advantages of the good tracking and high efficiency, the proposed controllers could be a key solution to control the standalone PV systems and this solution could be

applicable for different use in PV applications such as underground car parks, the cellar of a hospital.

As perspectives, the proposed PV system operates only with the presence of solar irradiance. For this, the solution to add batteries could be very useful to make this standalone PV system working even at night. In addition, the tested loads were resistive which gives the possibility to use other types of loads such as AC motors due to its pertinence in agricultural applications. Finally, the implementation of the proposed controllers to accurate the results and make them more realistic.

References

Ag, S., Plus, S., Plus, S., Sunmodule, n.d. Protect SW 250 – 255 poly.

Ahmed, E.M., Shoyama, M., 2011. Stability study of variable step size incremental conductance/impedance MPPT for PV systems. 8th Int. Conf. Power Electron. - ECCE Asia "Green World with Power Electron. ICPE 2011-ECCE Asia 386–392. https://doi.org/10.1109/ICPE.2011.5944555

Alam, D.F., Yousri, D.A., Eteiba, M.B., 2015. Flower Pollination Algorithm based solar PV parameter estimation. Energy Convers. Manag. 101, 410–422. https://doi.org/https://doi.org/10.1016/j.enconman.2015.05.074

Alik, R., Jusoh, A., 2018. An enhanced P&O checking algorithm MPPT for high tracking efficiency of partially shaded PV module. Sol. Energy 163, 570–580. https://doi.org/10.1016/j.solener.2017.12.050

Alik, R., Jusoh, A., 2017. Modified Perturb and Observe (P&O) with checking algorithm under various solar irradiation. Sol. Energy 148, 128–139. https://doi.org/10.1016/j.solener.2017.03.064

Allouhi, A., Saadani, R., Kousksou, T., Saidur, R., Jamil, A., Rahmoune, M., 2016. Grid-connected PV systems installed on institutional buildings: Technology comparison, energy analysis and economic performance. Energy Build. 130, 188–201. https://doi.org/10.1016/j.enbuild.2016.08.054

Ankit, Sahoo, S.K., Sukchai, S., Yanine, F.F., 2018. Review and comparative study of single-stage inverters for a PV system. Renew. Sustain. Energy Rev. 91, 962–986. https://doi.org/10.1016/j.rser.2018.04.063

Askarzadeh, A., Rezazadeh, A., 2013. Artificial bee swarm optimization algorithm for parameters identification of solar cell models. Appl. Energy 102, 943–949. https://doi.org/10.1016/j.apenergy.2012.09.052

Attivissimo, F., Adamo, F., Carullo, A., Lanzolla, A.M.L., Spertino, F., Vallan, A., 2013. On the performance of the double-diode model in estimating the maximum power point for different photovoltaic technologies. Meas. J. Int. Meas. Confed. 46, 3549–3559. https://doi.org/10.1016/j.measurement.2013.06.032

Bana, S., Saini, R.P., 2016. A mathematical modeling framework to evaluate the performance of single diode and double diode based SPV systems. Energy Reports 2, 171–187. https://doi.org/10.1016/j.egyr.2016.06.004

Barth, N., Jovanovic, R., Ahzi, S., Khaleel, M.A., 2016. PV panel single and double diode

models: Optimization of the parameters and temperature dependence. Sol. Energy Mater. Sol. Cells 148, 87–98. https://doi.org/10.1016/j.solmat.2015.09.003

Bianconi, E., Calvente, J., Giral, R., Mamarelis, E., Petrone, G., Ramos-Paja, C.A., Spagnuolo, G., Vitelli, M., 2013. A fast current-based MPPT technique employing sliding mode control. IEEE Trans. Ind. Electron. 60, 1168–1178. https://doi.org/10.1109/TIE.2012.2190253

Blair, N., Dobos, A.P., Freeman, J., Neises, T., Wagner, M., Ferguson, T., Gilman, P., Janzou, S., 2014. System advisor model, sam 2014.1. 14: General description. NREL Rep. No. TP-6A20-61019, Natl. Renew. Energy Lab. Golden, CO 13. https://doi.org/10.2172/1126294

BP, 2017. BP Statistical Review of World Energy 2017. Br. Pet. 1–52. https://doi.org/http://www.bp.com/content/dam/bp/en/corporate/pdf/energy-economics/statistical-review-2017/bp-statistical-review-of-world-energy-2017-full-report.pdf

BP MSX60, 2002. bp solar msx60 Solar PV module datasheet [WWW Document]. URL http://www.troquedeenergia.com/Produtos/LogosModulosSolares/BP-MSX-60-64.pdf

Cáceres, R.O., Barbi, I., 1999. A boost DC-AC converter: Analysis, design, and experimentation. IEEE Trans. Power Electron. 14, 134–141. https://doi.org/10.1109/63.737601

Celik, A.N., Acikgoz, N., 2007. Modelling and experimental verification of the operating current of mono-crystalline photovoltaic modules using four- and five-parameter models. Appl. Energy 84, 1–15. https://doi.org/10.1016/j.apenergy.2006.04.007

Chaibi, Y., Salhi, M., El-jouni, A., Essadki, A., 2018. A new method to extract the equivalent circuit parameters of a photovoltaic panel. Sol. Energy 163. https://doi.org/10.1016/j.solener.2018.02.017

Chen, Y., Wang, X., Li, D., Hong, R., Shen, H., 2011. Parameters extraction from commercial solar cells I-V characteristics and shunt analysis. Appl. Energy 88, 2239–2244. https://doi.org/10.1016/j.apenergy.2010.12.048

Chen, Y.T., Jhang, Y.C., Liang, R.H., 2016. A fuzzy-logic based auto-scaling variable step-size MPPT method for PV systems. Sol. Energy 126, 53–63. https://doi.org/10.1016/j.solener.2016.01.007

Chenni, R., Makhlouf, M., Kerbache, T., Bouzid, A., 2007. A detailed modeling method for photovoltaic cells. Energy 32, 1724–1730. https://doi.org/10.1016/j.energy.2006.12.006

Chew, K.W.R., Siek, L., 2010. Single inductor quad-input-dual-output buck converter for photovoltaic systems, in: IECON Proceedings (Industrial Electronics Conference). pp.

704–709. https://doi.org/10.1109/IECON.2010.5675033

Chin, V.J., Salam, Z., Ishaque, K., 2015. Cell modelling and model parameters estimation techniques for photovoltaic simulator application: A review. Appl. Energy 154, 500–519. https://doi.org/10.1016/j.apenergy.2015.05.035

Chiu, C.-S., Ouyang, Y.-L., Ku, C.-Y., 2012. Terminal sliding mode control for maximum power point tracking of photovoltaic power generation systems. Sol. Energy 86, 2986–2995. https://doi.org/10.1016/j.solener.2012.07.008

Dahech, K., Allouche, M., Damak, T., Tadeo, F., 2017. Backstepping sliding mode control for maximum power point tracking of a photovoltaic system. Electr. Power Syst. Res. 143, 182–188. https://doi.org/10.1016/j.epsr.2016.10.043

De Blas, M.A., Torres, J.L., Prieto, E., García, A., 2002. Selecting a suitable model for characterizing photovoltaic devices. Renew. Energy 25, 371–380. https://doi.org/10.1016/S0960-1481(01)00056-8

De Soto, W., Klein, S. a., Beckman, W. a., 2006. Improvement and validation of a model for photovoltaic array performance. Sol. Energy 80, 78–88. https://doi.org/10.1016/j.solener.2005.06.010

Dehghanzadeh, A., Farahani, G., Maboodi, M., 2017. A novel approximate explicit double-diode model of solar cells for use in simulation studies. Renew. Energy 103, 468–477. https://doi.org/10.1016/j.renene.2016.11.051

Del Fabbro, B., Valentinčič, A., Gubina, A.F., 2016. An adequate required rate of return for grid-connected PV systems. Sol. Energy 132, 73–83. https://doi.org/10.1016/j.solener.2016.03.006

Devices, A., 2003. Ad9833.

Dhar, S., Dash, P.K., 2015. A Finite Time Fast Terminal Sliding Mode I–V Control of Grid-Connected PV Array. J. Control. Autom. Electr. Syst. 26, 314–335. https://doi.org/10.1007/s40313-014-0166-y

Dileep, G., Singh, S.N., 2017. Application of soft computing techniques for maximum power point tracking of SPV system. Sol. Energy 141, 182–202. https://doi.org/10.1016/j.solener.2016.11.034

Ding, K., Bian, X., Liu, H., Peng, T., 2012. A MATLAB-simulink-based PV module model and its application under conditions of nonuniform irradiance. IEEE Trans. Energy Convers. 27, 864–872. https://doi.org/10.1109/TEC.2012.2216529

Duffie, J. a., Beckman, W. a., Worek, W.M., 2003. Solar Engineering of Thermal Processes, 4nd ed., Journal of Solar Energy Engineering. https://doi.org/10.1115/1.2930068

El-jouni, A., 2009. Commande d ' un Système de Pompage Photovoltaïque pour un Fonctionnement Optimal.

Ellabban, O., Abu-Rub, H., Blaabjerg, F., 2014. Renewable energy resources: Current status, future prospects and their enabling technology. Renew. Sustain. Energy Rev. 39, 748–764. https://doi.org/10.1016/j.rser.2014.07.113

Et-torabi, K., Nassar-eddine, I., Obbadi, A., Errami, Y., Rmaily, R., Sahnoun, S., El fajri, A., Agunaou, M., 2017. Parameters estimation of the single and double diode photovoltaic models using a Gauss–Seidel algorithm and analytical method: A comparative study. Energy Convers. Manag. 148, 1041–1054. https://doi.org/10.1016/j.enconman.2017.06.064

Fang Lin Luo and Hong Ye, 2013. Advanced DC / AC Inverters, Advanced Dc / Ac Inverters. Taylor & Francis Group.

Farhat, M., Barambones, O., Sbita, L., 2017. A new maximum power point method based on a sliding mode approach for solar energy harvesting. Appl. Energy 185, 1185–1198. https://doi.org/10.1016/j.apenergy.2016.03.055

Forniés, E., Balenzategui, J.L., Alonso-García, M. del C., Silva, J.P., 2014. Method for module Rsh determination and its comparison with standard methods. Sol. Energy 109, 189–199. https://doi.org/10.1016/j.solener.2014.08.031

G, D., Singh, S.N., 2017. Selection of non-isolated DC-DC converters for solar photovoltaic system. Renew. Sustain. Energy Rev. 76, 1230–1247. https://doi.org/10.1016/j.rser.2017.03.130

Gao, X., Li, S., Gong, R., 2013. Maximum power point tracking control strategies with variable weather parameters for photovoltaic generation systems. Sol. Energy 93, 357–367. https://doi.org/10.1016/j.solener.2013.04.023

Gilman, P., 2015. SAM Photovoltaic Model Technical Reference SAM Photovoltaic Model Technical Reference. Sol. Energy 63, 323–333. https://doi.org/NREL/TP -6A20- 64102

Gonzalez Montoya, D., Ramos Paja, C.A., Giral, R., 2016. Maximum power point tracking of photovoltaic systems based on the sliding mode control of the module admittance. Electr. Power Syst. Res. 136, 125–134. https://doi.org/10.1016/j.epsr.2016.02.001

Gow, J.A., Manning, C.D., 1999. Development of a photovoltaic array model for use in power-electronics simulation studies. IEE Proc. - Electr. Power Appl. 146, 193. https://doi.org/10.1049/ip-epa:19990116

Graditi, G., Ferlito, S., Adinolfi, G., Tina, G.M., Ventura, C., 2016. Energy yield estimation of thin-film photovoltaic plants by using physical approach and artificial neural networks.

Sol. Energy 130, 232–243. https://doi.org/10.1016/j.solener.2016.02.022

Gupta, A., Chauhan, Y.K., Pachauri, R.K., 2016. A comparative investigation of maximum power point tracking methods for solar PV system. Sol. Energy 136, 236–253. https://doi.org/10.1016/j.solener.2016.07.001

Hadj Arab, A., Chenlo, F., Benghanem, M., 2004. Loss-of-load probability of photovoltaic water pumping systems. Sol. Energy 76, 713–723. https://doi.org/10.1016/j.solener.2004.01.006

Hassaine, L., Olias, E., Quintero, J., Salas, V., 2014. Overview of power inverter topologies and control structures for grid connected photovoltaic systems. Renew. Sustain. Energy Rev. 30, 796–807. https://doi.org/10.1016/j.rser.2013.11.005

Hong, Y., Pham, S.N., Yoo, T., Chae, K., Baek, K.H., Kim, Y.S., 2015. Efficient Maximum Power Point Tracking for a Distributed PV System under Rapidly Changing Environmental Conditions. IEEE Trans. Power Electron. 30, 4209–4218. https://doi.org/10.1109/TPEL.2014.2352314

Humada, A.M., Hojabri, M., Mekhilef, S., Hamada, H.M., 2016. Solar cell parameters extraction based on single and double-diode models: A review. Renew. Sustain. Energy Rev. 56, 494–509. https://doi.org/10.1016/j.rser.2015.11.051

Iaquaniello, G., Montanari, W., Salladini, A., 2017. Standalone CSP-DG system for electrification of remote areas and desalinated water supply. Sol. Energy 157, 1056–1063. https://doi.org/10.1016/j.solener.2017.09.026

Ikegami, T., Maezono, T., Nakanishi, F., Yamagata, Y., Ebihara, K., 2001. Estimation of equivalent circuit parameters of PV module and its application to optimal operation of PV system. Sol. Energy Mater. Sol. Cells 67, 389–395. https://doi.org/10.1016/S0927-0248(00)00307-X

Ishaque, K., Salam, Z., 2011. An improved modeling method to determine the model parameters of photovoltaic (PV) modules using differential evolution (DE). Sol. Energy 85, 2349–2359. https://doi.org/10.1016/j.solener.2011.06.025

Ishaque, K., Salam, Z., Taheri, H., 2011a. Simple, fast and accurate two-diode model for photovoltaic modules. Sol. Energy Mater. Sol. Cells 95, 586–594. https://doi.org/10.1016/j.solmat.2010.09.023

Ishaque, K., Salam, Z., Taheri, H., Shamsudin, A., 2011b. A critical evaluation of EA computational methods for Photovoltaic cell parameter extraction based on two diode model. Sol. Energy 85, 1768–1779. https://doi.org/10.1016/j.solener.2011.04.015

Ismail, M.S., Moghavvemi, M., Mahlia, T.M.I., 2013. Characterization of PV panel and global

optimization of its model parameters using genetic algorithm. Energy Convers. Manag. 73, 10–25. https://doi.org/10.1016/j.enconman.2013.03.033

Jain, S., Agarwal, V., Member, S., 2007. A Single-Stage Grid Connected Inverter Topology for Solar PV Systems With Maximum Power Point Tracking. IEEE Trans. Power Electron. 22, 1928–1940. https://doi.org/10.1109/TPEL.2007.904202

Jervase, J.A., Bourdoucen, H., Al-Lawati, A., 2001. Solar cell parameter extraction using genetic algorithms. Meas. Sci. Technol. 12, 1922–1925. https://doi.org/10.1088/0957-0233/12/11/322

Jordehi, A.R., 2016. Parameter estimation of solar photovoltaic (PV) cells: A review. Renew. Sustain. Energy Rev. 61, 354–371. https://doi.org/10.1016/j.rser.2016.03.049

Kaundinya, D.P., Balachandra, P., Ravindranath, N.H., 2009. Grid-connected versus stand-alone energy systems for decentralized power-A review of literature. Renew. Sustain. Energy Rev. 13, 2041–2050. https://doi.org/10.1016/j.rser.2009.02.002

Kchaou, A., Naamane, A., Koubaa, Y., M, N., 2017. Second order sliding mode-based MPPT control for photovoltaic applications. Sol. Energy 155, 758–769. https://doi.org/10.1016/j.solener.2017.07.007

Khan, F., Baek, S.H., Kim, J.H., 2014. Intensity dependency of photovoltaic cell parameters under high illumination conditions: An analysis. Appl. Energy 133, 356–362. https://doi.org/10.1016/j.apenergy.2014.07.107

Khezzar, R., Zereg, M., Khezzar, a., 2014. Modeling improvement of the four parameter model for photovoltaic modules. Sol. Energy 110, 452–462. https://doi.org/10.1016/j.solener.2014.09.039

Kim, I.-S., 2007. Sliding mode controller for the single-phase grid-connected photovoltaic system Il-Song. Sol. Energy 81, 405–414. https://doi.org/10.1016/j.solener.2006.04.005

Kim, I.S., Kim, M.B., Youn, M.J., 2006. New maximum power point tracker using sliding-mode observer for estimation of solar array current in the grid-connected photovoltaic system. IEEE Trans. Ind. Electron. 53, 1027–1035. https://doi.org/10.1109/TIE.2006.878331

Kollimalla, S.K., Member, Student, Mishra, M.K., Member, Senior, 2014. Variable Perturbation Size Adaptive P & O MPPT Algorithm for Sudden Changes in Irradiance. IEEE Trans. Sustain. Energy 5, 718–728. https://doi.org/10.1109/TEC.2014.2320930

Koofigar, H.R., 2016. Adaptive robust maximum power point tracking control for perturbed photovoltaic systems with output voltage estimation. ISA Trans. 60, 285–293. https://doi.org/10.1016/j.isatra.2015.11.003

Kou, Q., Klein, S.A., Beckman, W.A., 1998. A method for estimating the long-term performance of direct-coupled PV pumping systems. Sol. Energy 64, 33–40. https://doi.org/10.1016/S0038-092X(98)00049-8

Kousksou, T., Allouhi, A., Belattar, M., Jamil, A., El Rhafiki, T., Arid, A., Zeraouli, Y., 2015. Renewable energy potential and national policy directions for sustainable development in Morocco. Renew. Sustain. Energy Rev. 47, 46–57. https://doi.org/10.1016/j.rser.2015.02.056

Kulaksiz, A.A., Akkaya, R., 2012. A genetic algorithm optimized ANN-based MPPT algorithm for a stand-alone PV system with induction motor drive. Sol. Energy 86, 2366–2375. https://doi.org/10.1016/j.solener.2012.05.006

Kumar, A., Kandpal, T.C., 2005. Solar drying and CO2 emissions mitigation: Potential for selected cash crops in India. Sol. Energy 78, 321–329. https://doi.org/10.1016/j.solener.2004.10.001

Laudani, A., Riganti Fulginei, F., Salvini, A., 2014. Identification of the one-diode model for photovoltaic modules from datasheet values. Sol. Energy 108, 432–446. https://doi.org/10.1016/j.solener.2014.07.024

Levron, Y., Shmilovitz, D., Yoash Levron, D.S., 2013. Maximum Power Point Tracking Employing Sliding Mode Control. IEEE Trans. Circuits Syst. I Regul. Pap. 60, 724–732. https://doi.org/10.1109/TCSI.2012.2215760

Lineykin, S., Averbukh, M., Kuperman, A., 2014. An improved approach to extract the single-diode equivalent circuit parameters of a photovoltaic cell/panel. Renew. Sustain. Energy Rev. 30, 282–289. https://doi.org/10.1016/j.rser.2013.10.015

Liu, Fangrui, Duan, S., Liu, Fei, Liu, B., Kang, Y., 2008. [11]A variable step size INC MPPT method for PV systems. IEEE Trans. Ind. Electron. 55, 2622–2628. https://doi.org/10.1109/TIE.2008.920550

Lo Brano, V., Orioli, A., Ciulla, G., Di Gangi, A., 2010. An improved five-parameter model for photovoltaic modules. Sol. Energy Mater. Sol. Cells 94, 1358–1370. https://doi.org/10.1016/j.solmat.2010.04.003

Loukriz, A., Haddadi, M., Messalti, S., 2016. Simulation and experimental design of a new advanced variable step size Incremental Conductance MPPT algorithm for PV systems. ISA Trans. 62, 30–38. https://doi.org/10.1016/j.isatra.2015.08.006

M. Salhi, R.E.-B., 2009. Maximum Power Point Tracking Controller for PV Systems using a PI Regulator with Boost DC/DC Converter. Autom. Control Syst. Eng. J. Volume 8.

Ma, T., Yang, H., Lu, L., 2014a. Solar photovoltaic system modeling and performance

prediction. Renew. Sustain. Energy Rev. 36, 304–315. https://doi.org/10.1016/j.rser.2014.04.057

Ma, T., Yang, H., Lu, L., 2014b. Development of a model to simulate the performance characteristics of crystalline silicon photovoltaic modules/strings/arrays. Sol. Energy 100, 31–41. https://doi.org/10.1016/j.solener.2013.12.003

Mamarelis, E., Petrone, G., Spagnuolo, G., 2014. Design of a sliding-mode-controlled SEPIC for PV MPPT applications. IEEE Trans. Ind. Electron. 61, 3387–3398. https://doi.org/10.1109/TIE.2013.2279361

Mares, O., Paulescu, M., Badescu, V., 2015. A simple but accurate procedure for solving the five-parameter model. Energy Convers. Manag. 105, 139–148. https://doi.org/10.1016/j.enconman.2015.07.046

Martinez-Salamero, L., Cid-Pastor, A., Giral, R., Calvente, J., Utkin, V., 2010. Why is sliding mode control methodology needed for power converters? Proc. EPE-PEMC 2010 - 14th Int. Power Electron. Motion Control Conf. 25–31. https://doi.org/10.1109/EPEPEMC.2010.5606524

Mazouz, N., Midoun, A., 2011. Control of a DC/DC converter by fuzzy controller for a solar pumping system. Int. J. Electr. Power Energy Syst. 33, 1623–1630. https://doi.org/10.1016/j.ijepes.2011.06.016

Motahhir, S., El Ghzizal, A., Sebti, S., Derouich, A., 2017. MIL and SIL and PIL tests for MPPT algorithm. Cogent Eng. 4, 1–18. https://doi.org/10.1080/23311916.2017.1378475

Motahhir, S., Ghzizal, A. El, Sebti, S., Derouich, A., 2018. Modeling of Photovoltaic System with modified Incremental Conductance Algorithm for fast changes of irradiance. Int. J. Photoenergy 2018, 13. https://doi.org/10.1155/2018/3286479

Muhsen, D.H., Ghazali, A.B., Khatib, T., Abed, I.A., 2015. Parameters extraction of double diode photovoltaic module's model based on hybrid evolutionary algorithm. Energy Convers. Manag. 105, 552–561. https://doi.org/10.1016/j.enconman.2015.08.023

Muhsen, D.H., Khatib, T., Abdulabbas, T.E., 2018. Sizing of a standalone photovoltaic water pumping system using hybrid multi-criteria decision making methods. Sol. Energy 159, 1003–1015. https://doi.org/10.1016/j.solener.2017.11.044

Nassar-Eddine, I., Obbadi, A., Errami, Y., El Fajri, A., Agunaou, M., 2016. Parameter estimation of photovoltaic modules using iterative method and the Lambert W function: A comparative study. Energy Convers. Manag. 119, 37–48. https://doi.org/10.1016/j.enconman.2016.04.030

Orellana, M., Petibon, S., Estibals, B., Alonso, C., 2010. Four Switch Buck-Boost converter for

Photovoltaic DC-DC power applications, in: IECON Proceedings (Industrial Electronics Conference). pp. 469–474. https://doi.org/10.1109/IECON.2010.5674983

Par, I.I., Productique-informatique, A., Sup, E.N., Pr, E., 2014. L ' HABILITATION UNIVERSITAIRE M ' hammed GUISSER Stratégies de Commande pour l ' Optimisation des Systèmes Photovoltaïques Autonomes et Connectés au Réseau.

Park, J.Y., Choi, S.J., 2015. A novel datasheet-based parameter extraction method for a single-diode photovoltaic array model. Sol. Energy 122, 1235–1244. https://doi.org/10.1016/j.solener.2015.11.001

Priyanka, Lal, M., Singh, S.N., 2007. A new method of determination of series and shunt resistances of silicon solar cells. Sol. Energy Mater. Sol. Cells 91, 137–142. https://doi.org/10.1016/j.solmat.2006.07.008

PVGIS [WWW Document], n.d. URL https://ec.europa.eu/jrc/en/scientific-tool/pvgis

Radjai, T., Rahmani, L., Mekhilef, S., Gaubert, J.P., 2014. Implementation of a modified incremental conductance MPPT algorithm with direct control based on a fuzzy duty cycle change estimator using dSPACE. Sol. Energy 110, 325–337. https://doi.org/10.1016/j.solener.2014.09.014

Radziemska, E., 2005. Dark I-U-T measurements of single crystalline silicon solar cells. Energy Convers. Manag. 46, 1485–1494. https://doi.org/10.1016/j.enconman.2004.08.004

Rajasekar, N., Krishna Kumar, N., Venugopalan, R., 2013. Bacterial Foraging Algorithm based solar PV parameter estimation. Sol. Energy 97, 255–265. https://doi.org/10.1016/j.solener.2013.08.019

Reshma Gopi, R., Sreejith, S., 2018. Converter topologies in photovoltaic applications – A review. Renew. Sustain. Energy Rev. 94, 1–14. https://doi.org/10.1016/j.rser.2018.05.047

Sadorsky, P., 2009. Renewable energy consumption, CO2 emissions and oil prices in the G7 countries. Energy Econ. 31, 456–462. https://doi.org/10.1016/j.eneco.2008.12.010

Salas, V., Olías, E., Barrado, A., Lázaro, A., 2006. Review of the maximum power point tracking algorithms for stand-alone photovoltaic systems. Sol. Energy Mater. Sol. Cells 90, 1555–1578. https://doi.org/10.1016/j.solmat.2005.10.023

Sandrolini, L., Artioli, M., Reggiani, U., 2010. Numerical method for the extraction of photovoltaic module double-diode model parameters through cluster analysis. Appl. Energy 87, 442–451. https://doi.org/10.1016/j.apenergy.2009.07.022

Sarvi, M., Soltani, I., NamazyPour, N., Rabbani, N., 2013. A New Sliding Mode Controller for DC/DC Converters in Photovoltaic Systems. J. Energy 2013, 1–7. https://doi.org/10.1155/2013/871025

Shell, 2002. Shell SM55.

Shell SM55, 2002. Shell SM55 Solar PV module datasheet [WWW Document]. URL http://www.atlantasolar.com/pdf/Shell/ShellSM55_USv1.pdf

Shockley, W., Queisser, H.J., 1961. Detailed balance limit of efficiency of p-n junction solar cells. J. Appl. Phys. 32, 510–519. https://doi.org/10.1063/1.1736034

Shtessel, Y., Edwards, C., Fridman, L., Levant, A., 2014. Sliding mode control and observation, Sliding Mode Control and Observation. https://doi.org/10.1007/978-0-8176-4893-0

Siddiqui, M.U., Abido, M., 2013. Parameter estimation for five- and seven-parameter photovoltaic electrical models using evolutionary algorithms. Appl. Soft Comput. J. 13, 4608–4621. https://doi.org/10.1016/j.asoc.2013.07.005

Sudhakar Babu, T., Prasanth Ram, J., Sangeetha, K., Laudani, A., Rajasekar, N., 2016. Parameter extraction of two diode solar PV model using Fireworks algorithm. Sol. Energy 140, 265–276. https://doi.org/10.1016/j.solener.2016.10.044

Suite, S., Co, B., 2016. Homer User Manual.

Suthar, M., Singh, G.K., Saini, R.P., 2013. Comparison of mathematical models of photo-voltaic (PV) module and effect of various parameters on its performance. 2013 Int. Conf. Energy Effic. Technol. Sustain. 1354–1359. https://doi.org/10.1109/ICEETS.2013.6533584

Taherkhorsandi, M., Castillo-Villar, K.K., Mahmoodabadi, M.J., Janaghaei, F., Yazdi, S.M.M., 2015. Optimal Sliding and Decoupled Sliding Mode Tracking Control by Multi-objective Particle Swarm Optimization and Genetic Algorithms, Advances and Applications in Sliding Mode Control systems. https://doi.org/10.1007/978-3-319-11173-5_2

Tey, K.S., Mekhilef, S., 2014. Modified incremental conductance MPPT algorithm to mitigate inaccurate responses under fast-changing solar irradiation level. Sol. Energy 101, 333–342. https://doi.org/10.1016/j.solener.2014.01.003

Tivanov, M., Patryn, A., Drozdov, N., Fedotov, A., Mazanik, A., 2005. Determination of solar cell parameters from its current-voltage and spectral characteristics. Sol. Energy Mater. Sol. Cells 87, 457–465. https://doi.org/10.1016/j.solmat.2004.07.033

Ulapane, N.N.B., Dhanapala, C.H., Wickramasinghe, S.M., Abeyratne, S.G., Rathnayake, N., Binduhewa, P.J., 2011. Extraction of parameters for simulating photovoltaic panels. 2011 6th Int. Conf. Ind. Inf. Syst. ICIIS 2011 - Conf. Proc. 539–544. https://doi.org/10.1109/ICIINFS.2011.6038128

Universidade De Genebra, 2012. User's Guide, PVsyst Contextual Help.

Veerachary, M., Senjyu, T., Uezato, K., 2003. Neural-Network-Based Maximum-Power-Point

Tracking of Coupled-Inductor 50, 749–758.

Villalva, M.G., 2015. Modeling and simulation of photovoltaic arrays MODELING AND SIMULATION OF PHOTOVOLTAIC ARRAYS 2012, 1244–1254.

Villalva, M.G.G., Gazoli, J.R.R., Filho, E.R.R., 2009. Comprehensive Approach to Modeling and Simulation of Photovoltaic Arrays. IEEE Trans. Power Electron. 24, 1198–1208. https://doi.org/10.1109/TPEL.2009.2013862

Villalva, M.G.M.G.G., Gazoli, J.R.R.J.R., Filho, E.R.E.R.R., 2009. Comprehensive Approach to Modeling and Simulation of Photovoltaic Arrays. IEEE Trans. Power Electron. 24, 1198–1208. https://doi.org/10.1109/TPEL.2009.2013862

Walker, G., 2001. Evaluating Mppt Converter Topologies Using a Matlab Pv Model. J. Electr. Electron. Eng. 21, 49–56. https://doi.org/10.7237/

Wang, G., Zhao, K., Shi, J., Chen, W., Zhang, H., Yang, X., Zhao, Y., 2017. An iterative approach for modeling photovoltaic modules without implicit equations. Appl. Energy 202, 189–198. https://doi.org/10.1016/j.apenergy.2017.05.149

Xiao, W., Dunford, W.G., Capel, A., 2004. A novel modeling method for photovoltaic cells. PESC Rec. - IEEE Annu. Power Electron. Spec. Conf. 3, 1950–1956. https://doi.org/10.1109/PESC.2004.1355416

Yahyaoui, I., n.d. Tesis Doctoral : Sizing and Energy Management for. Universidad de Velladolid.

Yatimi, H., Aroudam, E., 2016. Assessment and control of a photovoltaic energy storage system based on the robust sliding mode MPPT controller. Sol. Energy 139, 557–568. https://doi.org/10.1016/j.solener.2016.10.038

Yau, H.T., Lin, C.J., Wu, C.H., 2013. Sliding mode extremum seeking control scheme based on PSO for maximum power point tracking in photovoltaic systems. Int. J. Photoenergy 2013. https://doi.org/10.1155/2013/527948

Yildiran, N., Tacer, E., 2016. Identification of photovoltaic cell single diode discrete model parameters based on datasheet valuesYildiran, N., & Tacer, E. (2016). Identification of photovoltaic cell single diode discrete model parameters based on datasheet values. Solar Energy, 127, . Sol. Energy 127, 175–183. https://doi.org/10.1016/j.solener.2016.01.024

Zeb, K., Uddin, W., Khan, M.A., Ali, Z., Ali, M.U., Christofides, N., Kim, H.J., 2018. A comprehensive review on inverter topologies and control strategies for grid connected photovoltaic system. Renew. Sustain. Energy Rev. 94, 1120–1141. https://doi.org/10.1016/j.rser.2018.06.053

Zhang, L., Hurley, W.G., Wölfle, W.H., 2011. A new approach to achieve maximum power

point tracking for PV system with a variable inductor. IEEE Trans. Power Electron. 26, 1031–1037. https://doi.org/10.1109/TPEL.2010.2089644

Appendix A: Photovoltaic Panels Characteristics

A.1 Shell Solar SM55

Shell Solar

Product Information Sheet

Shell SM55 Photovoltaic Solar Module

General

The Shell SM55 module contains 36 series connected 103 x103 mm PowerMax® mono-crystalline silicon solar cells.

The Shell SM55 can generate a peak power of 55 watts at 17.4 volts.

The Shell SM55 solar module has been designed for rural and industrial applications.

Qualifications and Certificates

The Shell SM55 solar module meets the following requirements:

- **IEC 61215**
- **UL - Listing 1703**
- **TÜV Isolation Class II**

All Shell Solar modules are produced in EN-ISO 9001 certified factories.

Limited Warranties

- **Peak Power for 25 years**

Shell SM55 Module

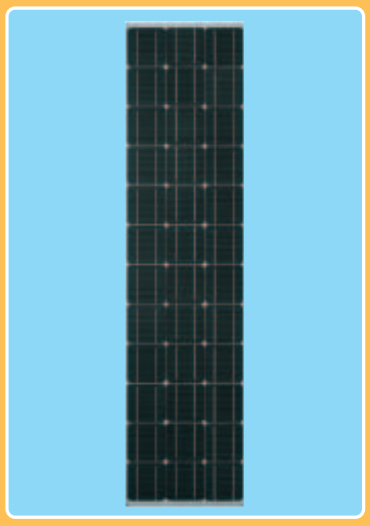

Junction Box

The junction box provides a high quality, dust protected and splash proof IP44-rated housing. The housing contains a rigid connection block with screw terminals and by-pass diodes providing "hot spot" protection for the solar cells.

ProCharger™-S Junction-Box

Maximum conductor cross-section: 4 mm²

Type of protection: IP44

Number of by-pass diodes: 2

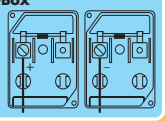

Benefits

- **PowerMax® mono-crystalline solar cells deliver maximum power output even under reduced light conditions providing more power where space is a limitation.**
- **The surface of the PowerMax® cell has a pyramidal textured surface to enable more light absorption and deliver exceptional efficiency.**
- **Highly transparent tempered glass delivers more power and ensures high impact resistance and protection against hail, snow, ice, and storms.**
- **Nearly 300MW of cumulative installed experience has been applied to the evolution of our mono-crystalline range to ensure that our products have a long and reliable service life backed by a 25 year warranty.**

ELECTRICAL EQUIPMENT, CHECK WITH YOUR INSTALLER

Due to continuous research and product improvement the specifications in this Product Information Sheet are subject to change without notice. Specifications can vary slightly. For installation and operation instructions, see the applicable manuals. No rights can be derived from this Product Information Sheet and Shell Solar assumes no liability whatsoever connected to or resulting from the use of any information contained herein.

CE

Shell SM55 Photovoltaic Solar Module

Mechanical Specifications Module

A torsion and corrosion-resistant anodized aluminium frame ensures dependable performance, even under harsh weather conditions. Pre-drilled mounting holes are provided for ease of installation.

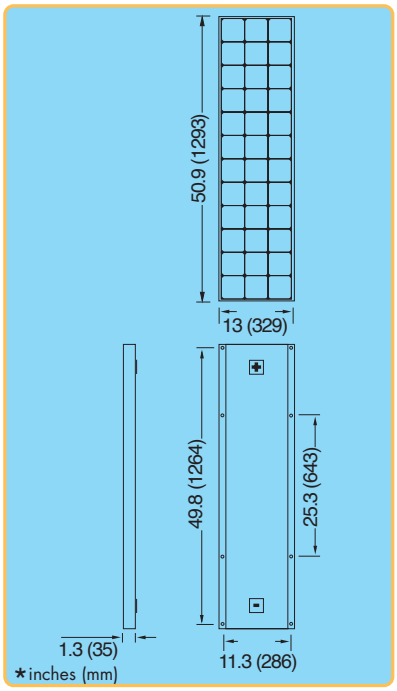

Outside dimensions (in)	50.9 x 13
Thickness (inc. junction box) (in)	1.3
Thickness (exc. junction box) (in)	1.3
Weight (lbs)	12

For installation instructions, please refer to the **Installation Manual** which is available from Shell Solar.

Electrical Characteristics

Data at Standard Test Conditions (STC)

STC: irradiance level 1000W/m², spectrum AM 1.5 and cell temperature 25°C

Rated power	P_r	55W
Peak power	P_{mpp}	55W
Peak power voltage	V_{mpp}	17.4V
Peak power current	I_{mpp}	3.15A
Open circuit voltage	V_{oc}	21.7V
Short circuit current	I_{sc}	3.45A
Series fuse rating		10A
Minimum peak power	$P_{mpp\ min}$	50W

The abbreviation 'mpp' stands for Maximum Power Point.

Typical data at Nominal Operating Cell Temperature (NOCT) conditions

NOCT: 800W/m² irradiance level, AM 1.5 spectrum, wind velocity 1m/s, T_{amb} 20°C

Temperature	T_{NOCT}	45°C
Mpp power	P_{mpp}	40W
Mpp voltage	V_{mpp}	15.9V
Open circuit voltage	V_{oc}	19.9V
Short circuit current	I_{sc}	2.8A

Typical data at low irradiance

The relative reduction of module efficiency at an irradiance of 200W/m² in relation to 1000W/m² both at 25°C cell temperature and AM 1.5 spectrum is 7%.

Temperature coefficients

αP_{mpp}	–0.45 %/°C
αV_{mpp}	–76 mV/°C
αI_{sc}	+1.4 mA/°C
αV_{oc}	–76 mV/°C

Maximum system voltage: 600 Vdc

Typical I/V Characteristics

The I/V graph below shows the typical performance of the solar module at various levels of irradiance.

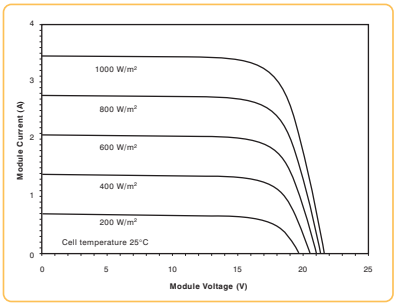

The I/V graph below shows the typical performance of the solar module at various cell temperatures.

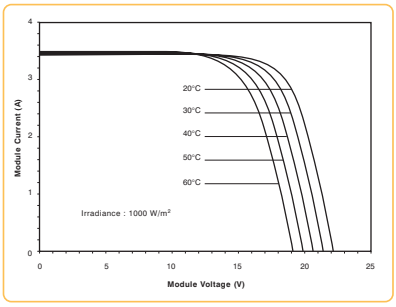

References in this Product Information Sheet to 'Shell Solar' are to companies and other organizational entities within the Royal Dutch/Shell Group of Companies that are engaged in the photovoltaic solar energy business. Shell Solar was set up in 1999 and has its principal office in Amsterdam, the Netherlands.

For further information on all Shell Solar products contact:

Shell Solar
4650 Adohr Lane, Camarillo CA 93012
805•482•6800 Fax 805•388•6511
Web www.shell.com/renewables

V2/SM55/05/02/US

A.2 SolarWorld SW255

Sunmodule® *Plus SW 250 – 255 poly*

Produced in Germany,
the center for solar technology

TUV Power controlled:
Lowest measuring tolerance in industry

Sunmodule Plus:
Positive performance tolerance

25 year linear performance warranty and
10 year product warranty

SolarWorld AG relies on Germany as its technology location, thereby ensuring sustainable product quality.

The TUV Rheinland Power controlled inspection mark guarantees that the nominal power indicated for solar modules is inspected at regular intervals and thus ensured. The deviation to TUV is maximum 2 percent.

The positive power tolerance guarantees utmost system efficiency. Only modules achieving or exceeding the designated nominal power in performance tests are dispatched. The power tolerance ranges between -0 Wp and +5 Wp.

With its linear performance warranty covering a period of 25 years, SolarWorld guarantees a maximum performance degression of 0.7% p.a., a significant added value compared to the two-phase warranties common in the industry. Therefore, the service certificate offers comprehensive protection for your investment in the long term.

www.solarworld.com

We turn sunlight into power.

Sunmodule® *Plus SW 250 – 255 poly*

PERFORMANCE UNDER STANDARD TEST CONDITIONS (STC)*

		SW 250	SW 255
Maximum power	P_{max}	250 Wp	255 Wp
Open circuit voltage	U_{oc}	37.6 V	38.0 V
Maximum power point voltage	U_{mpp}	30.5 V	30.9 V
Short circuit current	I_{sc}	8.81 A	8.88 A
Maximum power point current	I_{mpp}	8.27 A	8.32 A

Measuring tolerance (P_{max}) traceable to TUV Rheinland: +/- 2% (TUV Power controlled) *STC: 1000W/m², 25°C, AM 1.5

PERFORMANCE AT 800 W/m², NOCT, AM 1.5

		SW 250	SW 255
Maximum power	P_{max}	185.4 Wp	188.7 Wp
Open circuit voltage	U_{oc}	34.2 V	34.5 V
Maximum power point voltage	U_{mpp}	27.8 V	28.1 V
Short circuit current	I_{sc}	7.24 A	7.30 A
Maximum power point current	I_{mpp}	6.68 A	6.72 A

Minor reduction in efficiency under partial load conditions at 25°C: at 200 W/m², 100% (+/-2%) of the STC efficiency (1000 W/m²) is achieved.

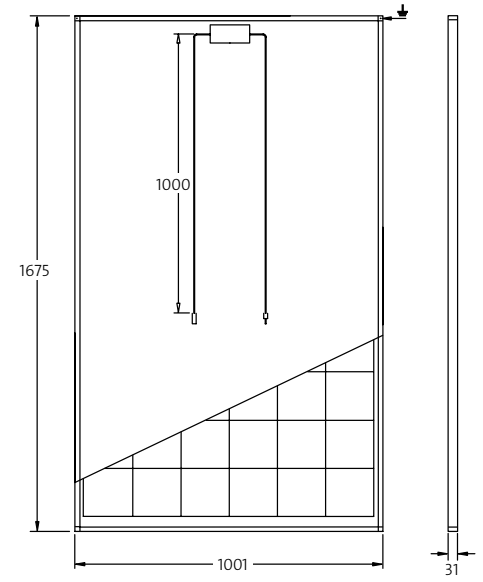

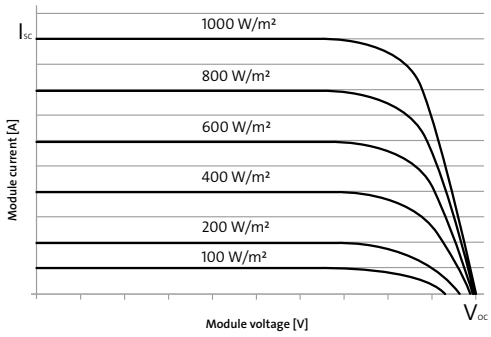

DIMENSIONS

Length	1675 mm
Width	1001 mm
Height	31 mm
Frame	Clear anodized aluminum
Weight	21.2 kg

COMPONENT MATERIALS

Cells per module	60
Cell type	Poly crystalline
Cell dimensions	156 mm x 156 mm
Front	4 mm tempered glass (EN 12150)

THERMAL CHARACTERISTICS

NOCT	46 °C
TC I_{sc}	0.051 %/K
TC U_{oc}	-0.31 %/K
TC P_{mpp}	-0.41 %/K

ADDITIONAL DATA

Power sorting	-0 Wp / +5 Wp
J-Box	IP65
Connector	MC4 / KSK4

PARAMETERS FOR OPTIMAL SYSTEM INTEGRATION

Maximum system voltage SC II	1000 V
Maximum reverse current	16 A
Load / dynamic load	5.4 / 2.4 kN/m²
Number of bypass diodes	3
Operating range	-40 °C to +85 °C

PERFORMANCE TESTED SALT MIST RESISTANT PHOTOVOLTAIC PRODUCT

Power Controlled TÜVRheinland CERTIFIED

- Qualified, IEC 61215
- Safety tested, IEC 61730
- Periodic Inspection
- Blowing sand resistant

APPROVED PRODUCT MCS

SolarWorld AG reserves the right to make specification changes without notice.
This data sheet complies with the requirements of EN 50380.

25.02.2014 EN | KB8345

A.3 BP Solar MSX60

bp solar

BP MSX 60
BP MSX 64

60-Watt and 64-Watt
Multicrystalline Photovoltaic Module

BP Solar's MSX series is a premium line of PV modules with an industry-leading 25-year performance warranty, tightly controlled electrical parameters, and labeling showing each module's tested electrical characteristics. The BP MSX 60 and BP MSX 64 provide 60 and 64 watts of peak power respectively, and are well-suited to traditional applications of photovoltaics such as telecommunications, remote villages and clinics, pumping, and land-based aids to navigation. Their attractive bronze-anodized frame and their availability as frameless laminates also suit them well for architectural applications.

Proven Materials and Construction

BP Solar's quarter-century of field experience shows in every aspect of these modules' construction and materials:

- Frame strength exceeds requirements of certifying agencies;
- 36 multicrystalline silicon solar cells configured as two 18-cell series strings;
- Cells are laminated between sheets of ethylene vinyl acetate (EVA) and high-transmissivity low-iron 3 mm tempered glass.

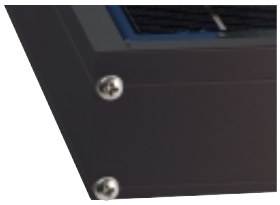

Bronze Anodized Universal Frame

High-Capacity Versatile Junction Box

The junction box is raintight (IP54 rated) and accepts PG13.5 or 1/2" nominal conduit or cable fittings. Its volume (411cc, 25 cubic inches) and 6-terminal connection block enable most system array connections (putting modules in series or parallel) to be made right in the junction box. Options include:

- blocking and bypass diodes;
- an oversize terminal block which accepts conductors up to 25mm^2 (AWG #4); standard terminals accept up to 6mm^2 (AWG #10);
- a Solarstate™ charge regulator.

Shipped in 12V configuration, modules may easily be switched to 6V configuration by moving leads in the junction box. Six-volt modules are intended to support 6V loads, and are not recommended as series elements in higher voltage arrays.

Quality and Safety

- Manufactured in ISO 9001-certified factories;
- Certified by PowerMark Corporation;
- Listed by Underwriter's Laboratories for electrical and fire safety (Class C fire rating);
- Certified by TÜV Rheinland as Class II equipment for use in systems with voltage up to 1000VDC;
- Approved by Factory Mutual Research for application in NEC Class 1, Division 2, Groups C & D hazardous locations;
- Compliant with the requirements of IEC 61215 including:
  - repetitive cycling between -40°C and 85°C at 85% relative humidity;
  - simulated impact of 25 mm (one-inch) hail at terminal velocity;
  - a "damp heat" test, consisting of 1000 hours of exposure to 85°C and 85% relative humidity;
  - a "hot-spot" test, which determines a module's ability to tolerate localized shadowing (which can cause reverse-biased operation and localized heating);
  - static loading, front and back, of 2400 pascals (50 psf); front loading (e.g. snow) of 5400 pascals (113 psf).

Limited Warranties

- Power output for 25 years;
- Freedom from defects in materials and workmanship for 5 years.

See our website or your local representative for full terms of 0these warranties.

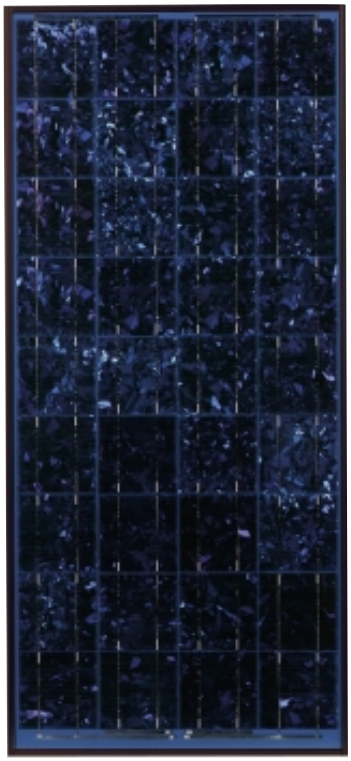

BP MSX 60

Individually Tested and Labeled

Each module tested and labeled with its actual output-voltage, current, and power at maximum power point (P_{max})–at Standard Test Conditions and Standard Operating Conditions.

UL FM APPROVED TÜV

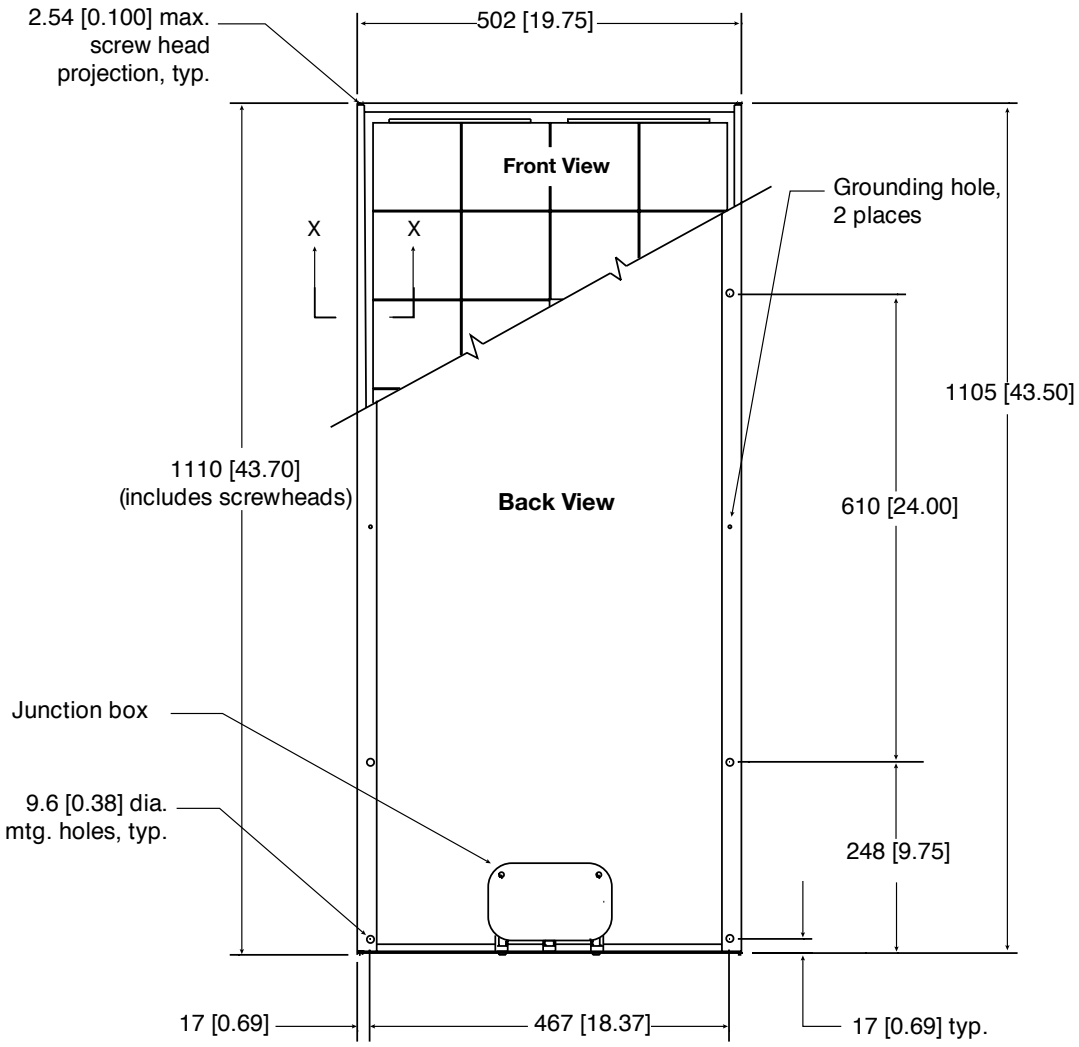

BP MSX 60, BP MSX 64

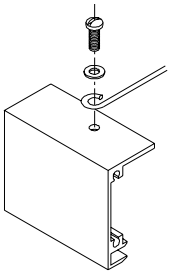

Grounding Detail

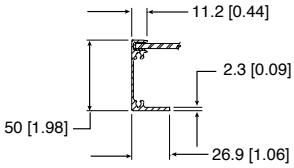

Section X-X

Dimensions

Unbracketed dimensions are in millimeters. Bracketed dimensions are in inches. Overall tolerances ±3mm (1/8")

Mechanical Characteristics

	Weight
BP MSX 60, 64	7.2 kg (15.9 pounds)

Typical Electrical Characteristics[1]	BP MSX 60	BP MSX 64
Maximum Power (P_{max})[2]	60W	64W
Voltage at P_{max} (V_{mp})	16.8W	17.5V
Current at P_{max} (Imp)	3.56A	3.66A
Warranted minimum P_{max}	58W	62W
Short-circuit current (I_{sc})	3.87A	4.0A
Open-circuit voltage (V_{oc})	21.0V	21.3V
Temperature coefficient of I_{sc}	(0.065±0.015)%/°C	
Temperature coefficient of V_{oc}	-(80±10)mV/°C	
Temperature coefficient of power	-(0.5±0.05)%/°C	
NOCT[3]	47±2°C	
Maximum system voltage[4]	600V	

Notes

1. These data represent the performance of typical BP MSX 60 and BP MSX 64 modules as measured at their output terminals, and do not include the effect of such additional equipment as diodes or cables. The data are based on measurements made in accordance with ASTM E1036-85 corrected to SRC (Standard Reporting Conditions, also known as STC or Standard Test Conditions), which are:

   • illumination of 1 kW/m² (1 sun) at spectral distribution of AM 1.5 (ASTM E892-87 global spectral irradiance);

   • cell temperature of 25°C.

2. During the stabilization process which occurs during the first few months of deployment, module power may decrease approximately 3% from typical Pmax.

3. The cells in an illuminated module operate hotter than the ambient temperature. NOCT (Nominal Operating Cell Temperature) is an indicator of this temperature differential, and is the cell temperature under Standard Operating Conditions: ambient temperature of 20°C, solar irradiation of 0.8 kW/m², and wind speed of 1 m/s.

4. U.S. NEC rating.

BP MSX 60 I-V Curves

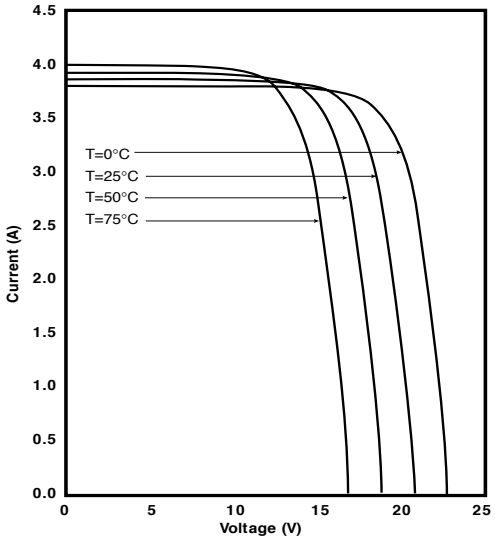

BP MSX 64 I-V Curves

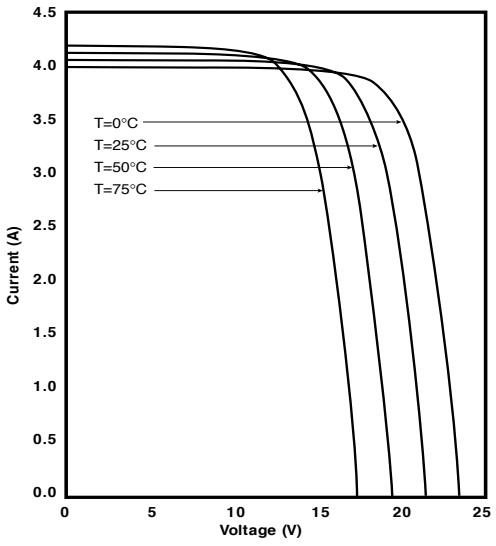

Appendix B: Calculated Values of Maximum Power, Open Circuit Voltage, and Short Circuit Current using different Equivalent Circuit Models and Datasheet.

Table B.1 Output power of the Mono-Si SM55 PV panel using various equivalent circuit models and extracted values from datasheet curves for different irradiances, T = 25 °C.

	Datasheet [W]	SSD[W]	DSD[W]	DD[W]
200 W/m²	9.88	9.4866	9.4866	9.205
400 W/m²	21.06	20.3128	20.3128	20.75
600 W/m²	32.45	31.5667	31.5837	32.29
800 W/m²	43.77	43.1	43.1122	43.67
1000 W/m²	**55.07**	**54.81**	**54.8110**	**54.81**

Table B.2 Output power of the Mono-Si SM55 PV panel using various equivalent circuit models and extracted values from datasheet curves for different temperatures, λ = 1000 W/m^2.

	Datasheet [W]	SSD[W]	DSD[W]	DD[W]
20 °C	56.01	56.1217	56.1309	56.01
30 °C	53.61	53.4847	53.4799	53.61
40 °C	51.19	50.8119	50.8119	51.19
50 °C	48.76	48.19	48.1469	48.56
60 °C	**46.31**	**45.5381**	**45.4822**	**46.01**

Table B.3 Output power of the Poly-Si MSX60 PV panel using various equivalent circuit models and extracted values from datasheet curves for different temperatures, λ = 1000 W/m^2.

	Datasheet [W]	SSD[W]	DSD[W]	DD[W]
0 °C	66.8	66.7782	66.8012	67.01
25 °C	60.52	59.8063	59.808	60.56
50 °C	54.48	52.6923	52.6745	53.82
75 °C	**47.9**	**45.4858**	**45.4506**	**46.81**

Table B.4 Open-circuit voltage of the Mono-Si SM55 PV panel using various equivalent circuit models and extracted values from datasheet curves for different irradiances, T = 25°C.

	Datasheet [V]	SSD[V]	DSD[V]	DD[V]
200 W/m²	19.69	19.091	19.111	19.978
400 W/m²	20.52	20.218	20.2303	20.728
600 W/m²	21.02	20.876	20.885	21.139
800 W/m²	21.33	21.34	21.347	21.43
1000 W/m²	**21.62**	**21.7**	**21.7**	**21.64**

Table B.5 Open-circuit voltage of the Mono-Si SM55 PV panel using various equivalent circuit models and extracted values from datasheet curves for different temperatures, λ = 1000 W/m^2.

	Datasheet [V]	SSD[V]	DSD[V]	DD[V]
20 °C	22.16	20.0976	22.0972	22.0727
30 °C	21.40	21.3167	21.3771	21.2567
40 °C	20.61	20.5308	20.5321	20.4885
50 °C	19.88	19.7404	19.7424	19.7217
60 °C	**19.1**	**18.9453**	**18.9479**	**19.9510**

Table B.6 Open-circuit voltage of the Poly-Si MSX60 PV panel using various equivalent circuit models and extracted values from datasheet curves for different temperatures, λ = 1000 W/m^2.

	Datasheet [V]	SSD[V]	DSD[V]	DD[V]
0 °C	22.72	22.947	22.944	22.95
25 °C	20.81	21.01	21.009	20.94
50 °C	18.80	19.04	19.05	18.925
75 °C	**16.82**	**17.05**	**17.06**	**16.895**

Table B.7 Short-circuit current of the Mono-Si SM55 PV panel using various equivalent circuit models and extracted values from datasheet curves for different irradiances, T = 25°C.

	Datasheet [A]	**SSD[A]**	**DSD[A]**	**DD[A]**
200 W/m²	0.683	0.69	0.689	0.6878
400 W/m²	1.377	1.38	1.379	1.375
600 W/m²	2.067	2.07	2.069	2.063
800 W/m²	2.753	2.76	2.759	2.751
1000 W/m²	**3.443**	**3.45**	**3.45**	**3.439**

Table B.8 Short-circuit current of the Mono-Si SM55 PV panel using various equivalent circuit models and extracted values from datasheet curves for different temperatures, λ = 1000 W/m^2.

	Datasheet [A]	**SSD[A]**	**DSD[A]**	**DD[A]**
20 °C	3.453	3.442	3.443	3.432
30 °C	3.459	3.458	3.457	3.446
40 °C	3.472	3.473	3.471	3.46
50 °C	3.484	3.489	3.484	3.474
60 °C	**3.497**	**3.504**	**3.498**	**3.488**

Table B.9 Short-circuit current of the Poly-Si MSX60 PV panel using various equivalent circuit models and extracted values from datasheet curves for different temperatures, λ = 1000 W/m^2.

	Datasheet [A]	**SSD[A]**	**DSD[A]**	**DD[A]**
0 °C	3.80	3.8071	3.8072	3.782
25 °C	3.859	3.87	3.8699	3.862
50 °C	3.918	3.9328	3.9327	3.942
75 °C	**3.997**	**3.9957**	**3.9956**	**4.022**

Appendix C: Derivatives of the Photovoltaic Current Equation.

The derivative of the output current of a PV cell can be written as follows:

$$\frac{\partial I_{pv}}{\partial V_{pv}} = \frac{-AI_{os}exp\left[A\left(V_{pc}+R_sI_{pv}\right)\right]-\frac{1}{R_{sh}}}{1+\frac{R_s}{R_{sh}}+R_sAI_{os}exp\left[A\left(V_{pc}+R_sI_{pv}\right)\right]} \quad \text{(C.1)}$$

We suppose that: $H = 1 + \frac{R_s}{R_{sh}} + R_sAI_{os}exp\left[A\left(V_{pc} + R_sI_{pv}\right)\right]$

$$\frac{\partial^2 I_{pv}}{\partial V_{pv}^2} = \frac{-A^2 I_{os}exp\left[A\left(V_{pc}+R_sI_{pv}\right)\right]\left(R_s\frac{\partial I_{pv}}{\partial V_{pv}}+1\right)}{H^2} \quad \text{(C.2)}$$

So, the third time derivative is presented in the following equation:

$$\frac{\partial^3 I_{pv}}{\partial V_{pv}^3} =$$

$$\frac{A^3 I_{os}exp\left[A\left(V_{pc}+R_sI_{pv}\right)\right]\left(R_s\frac{\partial Ipv}{\partial V_{pv}}+1\right)^2 - \frac{\partial^2 I_{pv}}{\partial V_{pv}^2}\left\{R_sA^2 I_{os}exp\left[A\left(V_{pc}+R_sI_{pv}\right)\right]+2A^3 I_{os}^2 R_s^2 exp^2\left[A\left(V_{pc}+R_sI_{pv}\right)\right]\left(R_s\frac{\partial I_{pv}}{\partial V_{pv}}+1\right)\right\}}{H^2}$$

(C.3)

For the time derivative of PV power and by using previous derivative of current, we can find the following equations:

$$\frac{\partial P_{pv}}{\partial V_{pv}} = I_{pv} + V_{pv}\frac{\partial I_{pv}}{\partial V_{pv}} \quad \text{(C.4)}$$

$$\frac{\partial^2 P_{pv}}{\partial V_{pv}^2} = 2\frac{\partial I_{pv}}{\partial V_{pv}} + V_{pv}\frac{\partial^2 I_{pv}}{\partial V_{pv}^2} \quad \text{(C.5)}$$

$$\frac{\partial^3 P_{pv}}{\partial V_{pv}^3} = 3\frac{\partial^2 I_{pv}}{\partial V_{pv}^2} + V_{pv}\frac{\partial^3 I_{pv}}{\partial V_{pv}^3} \quad \text{(C.6)}$$

$$\dot{y}_1 = \frac{\partial y_1}{\partial t} = \frac{\partial^2 P_{pv}}{\partial V_{pv}^2}\frac{\partial V_{pv}}{\partial t} \quad \text{(C.7)}$$

$$\ddot{y}_1 = \left(\frac{\partial^3 P_{pv}}{\partial V_{pv}^3}\right)\left(\frac{\partial V_{pv}}{\partial t}\right)^2 + \left(\frac{\partial^2 P_{pv}}{\partial V_{pv}^2}\right)\left[\frac{1}{C}\frac{\partial I_{pv}}{\partial V_{pv}}\frac{\partial V_{pv}}{\partial t} - \frac{1}{LC}\left(v_{pv} - v_{DC}\right)\right] - \boldsymbol{\alpha_1}\frac{V_{DC}}{LC}\frac{\partial^2 P_{pv}}{\partial V_{pv}^2} \quad \text{(C.8)}$$

Equation (C.8) can be rewritten as $E + \alpha_1 K$, where:

$$E = \left(\frac{\partial^3 P_{pv}}{\partial V_{pv}^3}\right)\left(\frac{\partial V_{pv}}{\partial t}\right)^2 + \left(\frac{\partial^2 P_{pv}}{\partial V_{pv}^2}\right)\left[\frac{1}{C}\frac{\partial I_{pv}}{\partial V_{pv}}\frac{\partial V_{pv}}{\partial t} - \frac{1}{LC}\left(v_{pv} - v_{DC}\right)\right] \quad \text{(C.9)}$$

$$K = \frac{V_{DC}}{LC}\frac{\partial^2 P_{pv}}{\partial V_{pv}^2} \quad \text{(C.10)}$$

Appendix D: Output AC resistance calculation

In this appendix we will demonstrate the adopted calculation of the output alternative resistance R_c. The output power of the panel (P_{pv}) is the product of the current (I_p) and the voltage (V_p):

$$P_{pv} = V_{pv} I_{pv} \tag{D.1}$$

The power (P_o) transferred to the AC load (R_c) is presented by the follow equation:

$$P_o = R_c i_o^2 \tag{D.2}$$

The output current (i_o) is a sinusoidal current presented as:

$$i_o = I_o \sin(wt) \tag{D.3}$$

Using (D.3) the average value of the output power is given by:

$$P_{pv} = \frac{1}{T/2} \int_0^{T/2} R_c i_o^2 \, dt = \frac{R_c I_o^2}{2} \tag{D.4}$$

Supposing that the transmission and the internal losses from PV panel to the load (R_c) are zero, then the hypothesis of the equality of input and output power always holds and can be expressed by:

$$P_{pv} = P_o = \frac{R_c I_o^2}{2} \tag{D.5}$$

At the MPP, the P_{pv} becomes a reference power P_{mpp} and the output current I_o corresponds to I_{ref}. assuming that the voltage at the output load is already known, we can calculate the output current and then the value of the output AC resistance at the MPP is expressed as follows:

$$R_c = \frac{2P_{mpp}}{I_{ref}^2} \tag{D.6}$$

List of symbols

$\mathbf{A_m}$	module surface [m^2]
$\mathbf{C, C_i}$	input capacitor of the DC-DC converter [F]
$\mathbf{C_o, C_{DC}}$	output capacitor of the DC-DC converter [F]
$\mathbf{E_{GO}}$	band gap [=1.22 eV]
$\mathbf{E_{pv}}$	produced energy [Wh]
$\mathbf{I, I_{pv}}$	output current of the PV module [A]
$\mathbf{I_{sol}}$	light-generated current [A]
$\mathbf{I_D}$	current of the diode [A]
$\mathbf{I_{pvg}}$	current of the PV generator [A]
$\mathbf{I_{Rsh}}$	current following in shunt resistance [A]
$\mathbf{I_{os}}$	cell saturation current [A]
$\mathbf{I_{or}}$	reverse current of the cell [A]
$\mathbf{I_{sc}}$	short-circuit current [A]
$\mathbf{i_L}$	input current of the boost converter [A]
$\mathbf{i_o}$	output current of the inverter [A]
$\mathbf{I_{ref}}$	reference current [A]
$\mathbf{I_m}$	maximal current at optimal operating point [A]
$\mathbf{k}$	Boltzmann constant [1.381 10^{-23} J/K]
$\mathbf{K_i}$	temperature coefficient of I_{sc} [A/K]
$\mathbf{K_v}$	temperature coefficient of V_{oc} [V/K]
$\mathbf{L}$	input inductance of the DC-DC converter [H]
$\mathbf{L_o}$	inductance of the output filter [H]
$\mathbf{N_{cell}}$	number of cells in series
$\mathbf{N_s}$	the number of modules in series
$\mathbf{N_p}$	the number of modules in parallel
$\mathbf{P_{MPP}}$	maximum power of the PV module [W]
$\mathbf{q}$	electron charge [=1.602 10^{-19} C]
$\mathbf{R_c}$	load resistance [Ω]
$\mathbf{R_o}$	resistance of the output filter [Ω]
$\mathbf{R_s}$	series resistance [Ω]
$\mathbf{R_{sh}}$	shunt resistance [Ω]
$\mathbf{T_a}$	ambiant temperature [K]

$\mathbf{T, T_{cell}}$	cell temperature [K]
$\mathbf{T_{NOCT}}$	nominal operating cell temperature [K]
$\mathbf{T_r}$	reference temperatures [K]
$\mathbf{V_{1,2}}$	Lyapunov function
$\mathbf{V_m}$	maximum voltage of the PV module [V]
$\mathbf{V_{oc}}$	open-circuit voltage [V]
$\mathbf{v_{DC}}$	output-voltage of the boost converter [V]
$\mathbf{V, V_{pv}}$	output voltage of the PV module [V]
$\mathbf{v_w}$	wind velocity [m/s]

List of Greek letters

$\boldsymbol{\alpha\tau}$	the transmittance-absorbance product
$\boldsymbol{\gamma}$	ideality factor
$\boldsymbol{\omega}$	the pulsation [rad/s]
$\boldsymbol{\lambda}$	solar irradiances [W/m^2]
$\boldsymbol{\lambda_{ref}}$	reference solar irradiances [= 1000 W/m^2]
$\boldsymbol{\sigma}$	sliding surface
$\boldsymbol{\eta}$	module efficiency
$\boldsymbol{\eta_{ref}}$	reference module efficiency

List of Abbreviations

AC: alternative current

DC: direct current

DDM: double diode model

IC: incremental conductance

MPP: maximum power point

MPPT: maximum power point tracking

NOCT: normal operating condition test

P&O: perturb and observe

PI: proportional integrator

PV: photovoltaic

SDM: single diode model

SMC: sliding mode control

STC: standard test conditions

Journals and Conferences Publications

Journal papers:

1. **Y. Chaibi, M. Salhi, A. Eljouni, and A. Essadki, "A new method to determine the Parameters of a photovoltaic Panel equivalent circuit," *Sol. Energy*, vol. 163, no. October 2017, pp. 376–386, 2018.**
   https://www.sciencedirect.com/science/article/pii/S0038092X18301348#
2. **Chaibi Y, Allouhi A, Malvoni M, Salhi M, Saadani R. "Solar irradiance and temperature influence on the photovoltaic cell equivalent-circuit models". *Sol Energy,* 2019, vol188:1102–10.**
   https://www.sciencedirect.com/science/article/pii/S0038092X19306590?dgcid=author

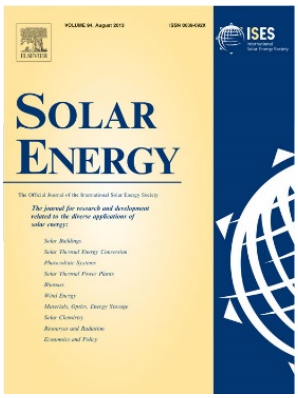

CiteScore: 5.24

Impact Factor: 4.674 (*Clarivate Analytics, 2019*)

5-Year Impact Factor: 4.807 (*Clarivate Analytics, 2019*)

Source Normalized Impact per Paper (SNIP): 1.622

SCImago Journal Rank (SJR): 1.593

3. **Y. Chaibi and M. Salhi, A . El-Jouni "Sliding Mode Controllers for Standalone PV Systems : Modeling and Approach of Control," *Int. J. Photoenergy*, no. Ic, 2019.**
   https://www.hindawi.com/journals/ijp/2019/5092078/

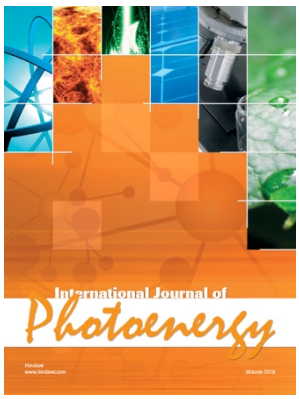

CiteScore: 1.61

Impact Factor: 2.026 (*Clarivate Analytics, 2019*)

Source Normalized Impact per Paper (SNIP): 0.683

SCImago Journal Rank (SJR): 0.377

4. **Chaibi Y, Malvoni M, Chouder A, Boussetta M, Salhi M. Simple and efficient approach to detect and diagnose electrical faults and partial shading in photovoltaic systems. *Energy Convers Manag* 2019;196:330–43. https://www.sciencedirect.com/science/article/pii/S0196890419306417?dgcid=author**

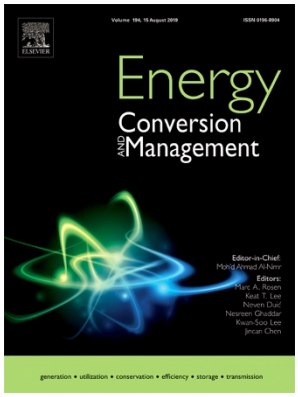

CiteScore: 7.87

Impact Factor: 7.181 (*Clarivate Analytics, 2019*)

5-Year Impact Factor: 6.722 (*Clarivate Analytics, 2019*)

Source Normalized Impact per Paper (SNIP): 2.151

SCImago Journal Rank (SJR): 2.73

5. **Chaibi Yassine, Allouhi amine, Salhi Mohamed and El-jouni Abdeslam (2018). "Annual Performance Analysis of Different Maximum Power Point Tracking Techniques used in Photovoltaic Systems ", *Protection and Control of Modern Power Systems* (In Press).**
6. **Chaibi Yassine, Maria Malvoni, Allouhi amine and Salhi Mohamed (2019). "Data on the I-V characteristics related to the SM55 monocrystalline PV module at various irradiance and temperatures". *Data in Brief* (In press).**

Conference papers

1. **Chaibi Yassine, Salhi Mohamed. (2015, Juin) ''Sur les méthodes de détermination des paramètres du schéma électrique équivalent d'un panneau photovoltaïque'', 4éme journée doctorale (JD2015). https://www.researchgate.net/publication/323015331**

2. **Chaibi Yassine, Salhi Mohammed, Abdeslam El-Jouni. (2018, February) "A robust sliding mode controllers for a standalone PV systems" International Congress on Energy and Environmental (CI2E'18). https://www.researchgate.net/publication/330040345**

3. **Ismail Chtita, Chaibi Yassine. (2018, November) "Modeling and Simulation of a Photovoltaic Panel Based on Triple Junction Cells for a Nanosatellite", International Symposium on Advanced Electrical and Communication Technologies (ISAECT'2018). https://ieeexplore.ieee.org/abstract/document/8618840**